Io's Heat Flow from Infrared Radiometry: 1983-1993

Glenn J. Veeder, Dennis L. Matson, Torrence V. Johnson, Diana L. Blaney, and Jay D. Goguen

Jet Propulsion Laboratory, California Institute of Technology, Pasadena, California

Abstract. We report the following results from a decade of infrared radiometry of Io: (1) The average global heat flow is more than ~2.5 $W m^{-2}$, (2) large warm ($\leq$200 K) volcanic regions dominate the global heat flow, (3) small high-temperature ($\geq$ 300 K) "hotspots" contribute little to the average heat flow, (4) thermal anomalies on the leading hemisphere contribute about half of the heat flow, (5) a substantial amount of heat is radiated during Io's night, (6) high-temperature ($\geq$ 600 K) "outbursts" occurred during ~4% of the nights we observed, (7) "Loki" is the brightest, persistent, infrared emission feature, and (8) some excess emission is always present at the longitude of Loki, but its intensity and other characteristics change between apparitions. Observations of 10 at M (4.8 pm), 8.7 μm, N (10 pm), and Q (20 μm) with the Infrared Telescope Facility presented here were collected during nine apparitions between 1983 and 1993. These measurements provide full longitudinal coverage as well as an eclipse observation and the detection of two outbursts, Reflected sunlight, passive thermal emission, and radiation from thermal anomalies all contribute to the observed flux densities. We find that a new thermophysical model is required to match all the data. Two key elements of this model are (1) a "thermal reservoir" unit which lowers daytime temperatures, and (2) the "thermal pedestal effect" which shifts to shorter wavelengths the spectral emission due to the reradiation of solar energy absorbed by the thermal anomalies. The thermal anomalies are modeled with a total of 10 source components at five locations. Io's heat flow is the sum of the power from these components.

1. Introduction

Thermal anomalies on the Jovian satellite Io were first recognized unambiguously in data from the Voyager 1 infrared spectrometer (IRIS) experiment [*Hanel et al.*, 1979]. Since that time, a number of ground-based techniques have been used to study Io's volcanic activity. A review of pre-Voyager infrared radiometry (including eclipse observations) showed that the signature of the volcanically heated areas was present in the older data. Furthermore, reanalysis of these data provided the first estimate of Io's large heat flow, namely, 2 ± 1 W m^{-2} [*Matson et al.*, 1981]. Subsequent observations of Io's infrared spectrum and further analysis of the Voyager IRIS data have confirmed these conclusions [Morrison *and Telesco*, 1980; Sinton, 1981; *Sinton et d., 1983; Tittemore and Sinton, 1987; McEwen et al., 1992].* Recent reviews are given by *Pearl and Sinton [1982], Nash et al. [1986],* and *McEwen* et al. [1989].

Io's heat flow results primarily from tidal interactions with Jupiter. Energy is extracted from Io's orbit and deposited as heat in the interior of Io [*Peale et al.*, 1979; *Yoder*, 1979]. Thus, the level of 10's heat flow is deter mined by the tidal dissipation properties of 10, Jupiter, and the complicated orbital mechanics of the Jovian system. These interactions make Io's heat flow a key parameter which constrains models of 10, Jupiter, and the interactions between them (see review by Greenberg [1989]).

Several observers have reported outbursts, or large temporary increases in 10's thermal emission [*Witteborn et al., 1979; Sinton, 1980;* Sinton *et al.*, 1983; *Johnson et al.*, 1988]. These

relatively rare events, associated with temperatures greater than 600 K, are quite impressive at 3.4 or 4.8 μm. However, when integrated over time, they do not contribute significantly to the average heat flow because of their relatively short durations. An additional discussion of the variability of Io is found in the. work by *Howell and Sinton [1989].*

Several Earth-breed telescopic techniques have been used to identify the locations of hotspots. These include near-infrared imaging, speckle interferometr y, occultations, and polarimetry *[Howell and McGinn, 1985; Goguen* and *Sinton*, 1985, 1988; *Sinton et al., 1988; Goguen et al., 1988; Spencer et al.*, 1990; *McLeod et al., 1991].* The locations of (positive) thermal anomalies have generally been referred to in the literature as "hotshots, " even though the range of temperatures associated with these areas includes values less than 250 K. We use the terms "thermal anomaly" and "hotspot" interchangeably in this paper.

The Voyager IRIS data and the ground-based eclipse observations provide information about hotspots for only part of Io's surface. In order to determine the distribution and variability of thermal anomalies, we initiated a program of multiwavelength radiometry of Io's thermal emission as a function of orbital phase angle, or west longitude of the sub-Earth point (see appendix note 1). These observations take advantage of the fact that hotspots of the type originally detected by IRIS will dominate the disk-integrated thermal emission from Io in the 7 to 14 μm region even though they cover only a small amount of the total surface area (see Figure 1). In contrast, the emission from 10 at 20 μm comes mainly from regions which are heated by the sun and from lower temperature thermal anomalies. At wavelengths shortward of -6 μm, an increasing fraction of the observed flux density comes from reflected sunlight. High-temperature hotspots still can make an identifiable contribution down to wavelengths as short as ~2 μm during an eclipse [*Sinton et al., 1980].*

Some observations in our 10 program have been discussed by *Johnson et al.* [1983, 1984, 1988], *Matson et al. [1993],* and *Veeder et al. [1993],* The supporting details of those measurements are all included here. Early results showed (1) the 8.7 μm emittance varies considerably with longitude, (2) the longitude of the maxima in the infrared light curves is very close to the largest anomaly observed by the Voyager IRIS (Loki Patera at 309"W and + 13°N), and (3) the 8.7 μm emittance at all longitudes is larger than expected from the reradiation of absorbed solar energy alone. We now have a relatively uniform data set for four band-passes centered at 4.8, 8.7, 10, and 20 μm obtained over the period from 1983 to 1993. In this paper we will (1) report the data acquisition and reduction methods, (2) describe a model which includes the "thermal pedestal effect" for calculating the contributions to the observed flux densities from both absorbed insolation and geothermal heat, and (3) use the results of this model to characterize the total heat flow from Io and the variations in its volcanic activity and power levels from 1983 to 1993.

2. Io Observations

The radiometric observations of 10 reported here were collected between February 18, 1983, and March 29, 1993 (UT), at the 3-m Infrared Telescope Facility (IRTF) on Mauna Kea, Hawaii, A summary of the circumstances of our Io observations is given in Table 1 (see appendix note 2). In total, we had 175 hours of photometric condition sduring 55 nights. The lRTF bolometer and data acquisition system were used with the standard filters at M (4.8 μm), N (10 μm), and Q (20 μm) as well as with the narrow-band-pass 8.7 μm filter ($\Delta\lambda \sim 1\ \mu$m). The IRTF Cassegrain system utilizes a wobbling secondary mirror to difference two fields of view on the sky. An 8 arcsec diameter aperture, a beam separation of 10 arcsec, and a frequency of 13 Hz were selected asa practical compromise to obtain accurate radiometry with adequate signal to noise ratio (SNR), sky subtraction, and scattered light rejection. The 8 arcsec aperture is much larger than the convolution of typical infrared seeing with the disk of Io, which helps to ensure accurate radiometry, since it minimizes the effect of small guiding errors. For eclipse observations, Io was acquired with a precise offset from Jupiter or another satellite. Tracking rates were updated by means of the lRTF automatic centering capability. The two telescope beams were typically oriented north-south except for observations very near the disk of Jupiter, which required that they be rotated perpendicular to the direction of the center of Jupiter's disk. This arrangement suppressed the offset which otherwise might occur from imperfect cancellation of the sky gradient due to scattered light from Jupiter.

During each night, the data stream from the IRTF bolometer system was captured in real time as an ASCII file. This tile was converted to a condensed format by means of our own semi-automatic editor (written in FORTRAN). This standardized log was checked against our handwritten notes and corrected for typographic and other errors. Logs for a few nights had to be keyed from the IRTF printout and verified by hand.

A typical observational sequence consists of four pairs of 10-s integrations at each of N, M, Q, 8.-? pm, and N. This cycle was repeated quickly (within 20 rein) relative to the rotation of Io (8.5" per hour). Measurements of 10 were alternated with cycles on appropriate standard stars to derive the atmospheric extinction and system sensitivity for each night (see also section 3).

The basic quantity determined from the observations is the magnitude of the whole disk of Io relative to Alpha Lyrae. Nearby standard stars for each night were selected from a subset of the IRTF list. These generally included at least one star before and after Jupiter in Right Ascension. Approximately one star per hour was observed throughout an observing session. Typically, three or four stars were observed two or three times each during a night at both higher and lower air mass than the range of Io. Almost all observations were made at an air mass of less than 2. A few observations of other Jovian satellites (in particular, Callisto) provided an additional

check on the stability of the IRTF system. These are especially useful for confirming the reality of infrared outbursts on 10.

The IRTF bolometer system sensitivity was monitored in real time and remained stable. throughout a night. Experience has shown that the residual, systematic change in responsivity is less than -5% between equipment setups for adjacent nights, All of our reported radiometry have relatively small statistical errors (i.e., SNR >> 10). Adjacent measurements of 10 reproduce approximately as well as or better than repeated measurements of, and the self-consistency between, the standard stars on each night (i.e., better than 5 %). The comparison of 10 data from one apparition to another is dependent on the accuracy of the whole standard star network, as the stars used slowly change with the motion of Jupiter around the sky (see also the appendix).

3. Data Reduction Procedure

The adopted standard star magnitudes are given in appendix Table A 1. This photometric system defines Alpha Lyrae as 0.0 magnitude (mag) for each wavelength. The absolute calibration of the photometric system is given in Table A2, and the monochromatic corrections are discussed in the appendix.

The system sensitivity in magnitudes was plotted for each night as a function of air mass. and a linear best tit was used to derive the extinction and average sensitivity at M, 8.7 μm, N, and Q. The typical range of values for extinction among photometric nights on Mauna Kea is 0.15-0.30 mag per air mass at 4.8, 8.7, and 10 μm and 0.3-0.50 snag per air mass at 20 μm. In addition, the system sensitivity in magnitudes was plotted for each night as a function of time at each wavelength. These plots were examined for obviously spurious events as well as for systematic trends correlated with time, seeing or humidity. Marginal weather conditions sometimes required the deletion of blocks of observations at the beginning and/or end of a given night. Useful standard star observations always bracketed those accepted for Io. In all, only a few percent of the raw Io data were rejected as nonphotometric.

The reduction of the observations to emittance is described below for each wavelength. The reduced data are given in Table 2 (4.8 pm), Table 3 (8.7 pm), Table 4 (10 pm), and Table 5 (20 μm) and are plotted in Figure 2 (4.8 μm), Figure 3 (8.7 μm), Figure 4 (10 pm), and Figure 5 (20 pm).

The reduction of Io radiometric data at 8.7 μm follows the moat straightforward procedure. The observations are sorted by universal date and time. The orbital phase angles are given in degrees (i.e., the sub-Earth west longitude or central meridian of Io). The observationally determined quantities for 10, the 8.7 μm mags and the corresponding tlux densities (F) at the Earth (above the atmosphere), are given both in Janskys and in units of 10^{-7} W cm^{-2} μm^{-1}. The spectral emittance (E) at Io's surface in units of 10^{2} W m^{-2} μm^{-1} is calculated from

$$E = \frac{F\Delta^2}{R_{Io}^2}$$

where A is the geocentric distance and R_J is the radius of 10. The 8.7 μm band-pass is relatively narrow, and therefore no monochromatic correction is necessary.

The reduction of 10 radiometric data at N (1 O μm) and Q (20 μm) is similar to the procedure for 8.7 μm data, with the exception that the wide N and Q band-passes require monochromatic corrections (see the appendix).

The reduction of 10 radiometric data at M (4.8 μm) includes the additional consideration that the M data have contributions from both reflected sunlight and thermal emission (see appendix note 3). The reflected component is about 70- 80% of the total [*Witteborn et al.*, 1979; Sin(on, 1980; *Morrison and Telesco, 1980]*. This component varies asa function of the geometric albedo distribution on the surface of lo, geocentric and heliocentric distance, and the solar phase angle. The calculated flux density (10^{-17} W cm^{-2} μm^{-1}) of the reflected and thermal components and the emittance (10^{-2} W m^{-2} μm^{-1}) of the thermal component at 10's surface arc included in Table 2.

We use a simple model to calculate the reflected flux density component for each of the observations at 4.8 μm at Io's particular geometry. An approximate value for the reflected sunlight can be determined directly by differencing the values in and out of an eclipse, We make an improved estimate of the reflected component at 4.8 μm by means of our background model, which includes the *thermal pedestal effect (see* section *4.4)*. Data from the well-observed August 3, 1986, eclipse were used to calculate this effect. Our results imply a geometric albedo for 10 of -0,7 at 4.8 μm in good agreement with $p_M = 0.72$ [*Goguen and Sinton*, 1985]. This value is similar to the albedo at 0.6 μm and consistent with the spectrum of Jo over this interval [*Clark and McCord, 1980; Cruikshank*, 1980; *McEwen et* al., 1988].

In order to derive the reflected component as a function of Io's longitude, we assume that the relative amplitude and phase of the light curve of this component at 4.8 μm is the same as for visual wavelengths as compiled by *Morrison and Morrison [1977]*. This step is justified by the small rotational color variation observed for Io between the visual and near-infrared [*Johnson*, 1971]. Similarly, the behavior with solar phase angle of the reflected component at 4.8 μm is assumed to be the same as that observed at visual and shorter infrared wavelengths which is approximated by a phase coefficient of 0,022 mag per degree (see also Figure 1 in *Sinton et al., [* 1983]). This parameter is not strongly dependent on color except in the ultraviolet [*Morrison et al.,* 1974; *Veverka, 1977]*.

The largest uncertainty in this procedure is probably introduced by the difficult eclipse observations which determine the reflected component. An error in this normalization would propagate equally "over all longitudes. Nonphysical negative values for the emittance of Jo at 4.8 μm may result if too large a value is calculated for the reflected contribution. l.Uncertainties in the phase and orbital corrections will introduce scatter in the calculated emittances between runs and possibly a small false component to the longitude variation. The absence of negative values in our data set and the presence of some apparitions showing weak longitude variation and others

with strong variations in Figure 2 suggest that such errors are not significant in this context,

A major change in the *4.8* μm albedo (for instance, due to a hemispheric-scale volcanic resurfacing event) could show up in our reduced data as a spurious longitude variation which is not due to thermal emission. However, Io's visual light curve has been remarkably constant over decades [Morrison *et al.*, 1974; *Morrison and Morrison, 1977; Veverka* et al., 1986] and current HST ultraviolet observations of Io are consistent with the overall albedo pattern seen by Voyager [*Sartoretti et al.*, 1992].

The Io radiometric data from Tables 2, 3, 4, and *5* are binned by apparition and plotted against decreasing west longitude in Figures 2, 3, 4, and 5. These data directly show spatial and temporal changes in the thermal emission from Io. The general shape of these infrared light curves does not vary greatly from year to year, but the amplitude does vary, It is obvious that the distribution of hotspots on Io is not uniform. The Loki source (see appendix note 4) dominates Io's thermal emission at short wavelengths in the trailing hemisphere (1 80°- 360°W). As a result of the changing viewing geometry, Loki produces a distinctive, approximately cosine, peak near 309"W in the plots. By contrast, the leading hemisphere (O" - 180°W) usually shows relatively little variation with longitude. Further discussion on the variability in the light curves is given in section 5.1, in the context of our model for thermal emission,

4. Thermal Emission Model

Thermal models of airless planetary bodies generally fall into one of two categories: (1) those dealing with thermal, emission from the body as an idealized whole, and (2) those dealing with the details of temperature distribution as a function of position on the surface. The latter distributions include variations in thermophysical properties and time of day (so-called diurnal models). Disk-averaged models similar to those used in asteroid radiometry [e.g., *Matron et al., 1978; Morrison and Lebofsky*, 1979; *Lebofsky and Spencer, 1989; Veeder et al., 1989]* have usually been used to analyze telescopic, disk-integrated Io data [e.g., Morrison *et* al., 1972; *Motion and Cruikshank*, 1973; *Mornson and Telesco*, 1980; Matson *et al,*, 1981; *Sinton*, 1981; *Johnson et al., 1984, 1988].* When dealing with Voyager data and combinations of spacecraft data and ground-based telescopic measurements, both approaches have been used [e. g., *McEwen et al., 1988; Simonelli and Veverka, 1988].* To date, no model has been successful in explaining all aspects of Jo's thermal properties.

Our approach in this paper is to use versions of 'slow" and "fast" rotating whole-disk models (see appendix notes 5 and 6) modified to meet Voyager-derived hemispheric albedos (see also sections 4.1 and 4.2). In addition, volcanic thermal anomalies or hotspots are included. This has enabled a number of new insights into the type of model required to match 10 infrared data and has allowed us to interpret most of Jo's observed characteristics. Our model is not unique, however,

and much work remains to be done to achieve a full thermophysical, time dependent description for this satellite.

To understand the motivation for the characteristics of our model, it is important to note the problems with previous approaches (both ours and those of other workers). In the past, Iong-wavelength (e.g., 10 and 20 μm) observations of 10 have been analyzed in terms of absorbed solar energy using a thermal model appropriate for airless, slowly rotating bodies with very low thermal inertia. Previous models assumed that the anomalies had such high temperatures that the contribution from absorbed insolation was negligible at short wavelengths (i.e., less than 4.8 μm). Eclipse results were viewed as due to a combination of two components: (1) the rapidly cooling background regions whose heat was only due to absorbed insolation, and (2) the hotspots whose temperatures were controlled by volcanic processes and remained constant on the timescale of an eclipse.

Such models have been recognized as failing to satisfy completely either the details of eclipse observations [*Sinton and Kaminski*, 1988] or the absolute level of Io's 20 μm emittance [*McEwen et al.*, 1988]. The large size of this discrepancy can be seen by direct comparison with tbe eclipse of August 3, 1986. The observations of Io at 4.8, 8.7, and 20 μm before and after immersion are plotted in Figure 6a. A first-order attempt to use a "standard" model (see appendix note 5) in instantaneous equilibrium with solar insolation for the background emission of Io fails (see also section 4.1). The expected emittance from such a sphere with a bolometric Bond albedo of 0.44 (Table 8 for longitude 340°W) is shown by the dashed line. It predicts too much emission at 20 μm and too little at 8.7 μm. In contrast, an analogous "standard" model fits similar data for Callisto quite well.

Since this "standard" model (see appendix note 5) only accounts for background emission, it is easy to understand why it yields too little emittance at 8.7 pm. The shortfall can be fixed easily by including some contribution from hotspots. However, this approach fails because the predicted model emission at 20 μm increases even further above the observations. The key question is, Why is *the 20 μm emittance of Io* so low?

Bolometric albedos for Io high enough to match the 20 μm data (e.g., 0.7) were deemed reasonable before the detailed analysis of Voyager photometry. Then, it became evident that Io's Bond albedo was significantly lower: an average of 0.5 from *Simonelli and Veverka [1984];* hemispheric averages of 0.45-0.52 from *McEwen [1988]* and *McEwen et al. [1988];* and 0.6-0.8 for the brightest regions from *Simonelli and Veverka [1988].* These improved albedo estimates result in a factor of 2 more absorbed power compared to older values. One of the suggestions of *McEwen et al. [1988]* was that the 20pm emittance levels, combined with Voyager albedo maps, might require a wavelength-dependent emissivity, with the value near 20 μm being about 15% lower than elsewhere. However, continued analysis of the Voyager IRIS data has ruled out any significantly lower emissivity at 20 μm [*McEwen et al.*, 1992; J.C. Pearl and A.S. McEwen, private communications, 1993].

Another possible wavelength-dependent effect results from polarization. Polarization is not normally considered when interpreting radiometry of airless, particulate surfaces. 10 is unusual, and thermal radiation from hotspots has been shown to be polarized [*Goguen and Sinton*, 1985]. Because both surface. temperature and emissivity decrease with distance from the center of Io*s disk, the contribution of long-wavelength radiation will be reduced compared to that expected from a unit emissivity model. However, our calculation of this effect for a smooth surface with the index of refraction (1.5 at 4.8 μm) determined by *Goguen and Sinton [1985]* shows that emissivity would change by less than 1 % between 4.8 and 20 μm for a slow-rotator temperature distribution. Furthermore, the smooth surface represents a worst case calculation in the sense that it would produce the largest polarization effect.

Sinton and Kaminski [1988] encountered a related problem in analyzing the heating and cooling of Io during eclipses from their data set. They consider a range of models which illustrate the need for a mixture of regions with very different thermal inertia values (cf. the equilibrium and reservoir units in sections 4.1 and 4.2). However, even their best model (i. e., number 5) did not match the Voyager bolometric Bond albedo for Io, and they assumed that the thermal anomalies remained at constant temperatures.

Possible evidence for failure of the "standard" model for Io was also noted by *Simonelli and Veverka [1988]*. They pointed out that the limited Voyager IRIS observations of the nightside of Jo suggested temperatures about 35 K higher than calculated from a "normal" thermophysical model. The Voyager nighttime observations unfortunately suffered from low spatial resolution and poor pointing knowledge, leading to an uncertainty in whether the elevated temperatures resulted from multiple unresolved hotspots or were a true measure of nighttime "passive" emission [*Pearl and Sinton, 1982; McEwen et* al., 1992; J.C. Pearl, persona} communication, 1993], Nevertheless, *Simonelli and Veverka [1988]* suggested that the discrepancy might be an indication that heat was being transported from the dayside to the nightside of Io, possibly by a solid-state greenhouse effect [*Brown and Matson, 1987]*.

Our strategy is to construct a simple model consistent with Io's known properties and including hotspot thermal emission from both geothermal emission and the reradiation of absorbed sunlight. We then apply this model to a well-observed eclipse to constrain several key parameters. Our thermal emission model for 10 involves three types of surface units: (1) a low-albedo unit which is in instantaneous equilibrium with sunlight to provide for the falloff in emission when 10 enters eclipse, (2) a high-albedo thermal reservoir unit to allow for more thermal emission in the antisolar direction and thus lower the observed 20 μm flux density, and (3) the thermal anomalies. An essential step is to account properly for the heating of the anomalies by sunlight (i.e., the thermal pedestal effect defined in section 4.4), These thermal units produce five spectral components: the emission due to radiation of absorbed sunlight for each of the three units, the emission due to heat flow, and reflected sunlight at 4.8 μm (see appendix note 7). The equilibrium and reservoir thermal units are assumed to be

interspaced uniformly over 10's disk (except for [he sites of thermal anomalies). The anomalies, which are at specific locations, occupy several percent of the surface.

4,1. Equilibrium Thermal Unit

The equilibrium thermal unit is a passive background unit which is heated only by sunlight. It has a low thermal inertia such that it is in instantaneous equilibrium. Its emissivity is taken as 0.9. Later, we will find that it has a bolometric Bond albedo of 0.29 and that its areal coverage is about 20% of the surface of 10. This is similar in extent to the darker *regions* seen in the Voyager pictures. For the purpose of comparing with disk-integrated radiometry, the equilibrium unit is treated as a nonrotating sphere (see appendix note 5) whose surface temperature is a function of the Sun's zenith angle z (i.e., the angular distance from the sub-solar point). There is a small (geometrically) projected defect of illumination (from which there is no emission) due to the solar phase angle. Thus, for the daytime hemisphere

$$T_z = T_{subsolar} \cos^{1/4} z$$

$$T_{subsolar} = \left[\frac{S_\odot}{r^2} \frac{1 - A}{\epsilon \sigma} \right]^{1/4}$$

where So is the solar constant (1 .388 x 10^6 erg $cm^{-2} s^{-1}$ AU"*), *A* is the bolometric Bond albedo, ϵ is the emissivity, σ is the Stefan-Boltzmann constant (5.669 x 10^{-5} erg $cm^{-2} s^{-1}$ T"), and *r* is the heliocentric distance in AU.

4,2. Thermal Reservoir Unit

A heat storage unit is the key to solving many of the problems that limit the approach of the "standard" model as defined in section 4.1 (see also appendix note 5). This passive background unit absorbs heat during the daytime but reradiates it *at night* as well as during the day. The emission in the direction of the Earth is reduced compared to that of an analogous equilibrium unit. The emissivity of the reservoir unit is taken as 0.9. Later, we will find that its bolometric Bond albedo ranges from 0.58 to 0.70 and that its area! extent is -80% of the surface of 10. This unit may correspond to the. bright, higher albedos seen in the Voyager images. "Computationally, the reservoir unit is treated as a rapidly rotating sphere (see appendix note 6) with a large thermal inertia whose surface temperature is a function of latitude ϕ. In this case no correction for defect of illumination is required. The temperature distribution is given by

$$T_\phi = T_{equatorial} \cos^{1/4} \varphi$$

$$T_{\bullet\ quatOddl} \left[\frac{S_\odot}{r^2} \frac{1 - A}{\pi \epsilon \sigma} \right]^{-1/4}$$

The nature of the reservoir unit is not further constrained by our present analysis. There are several processes that could operate on Io to provide the needed heat storage. The thermal inertia of the surface, alone, is an obvious candidate for carrying heat to the nightside. The fast rotator (see appendix note 6) may appear to be an unrealistic assumption. However, models developed by *Spencer et al. [* 1989] indicate that, for Io's rotation period and heliocentric distance and with a thermal inertia similar to other Galilean satellites, the calculated diurnal temperature variations are relatively small and thus closer to a fast rotator than an equilibrium model.

If significant sublimation occurs, then the latent heat of volatiles could help provide the characteristics needed for the mode.]. Another possibility is a solid-state greenhouse in which sunlight is absorbed within the upper few centimeters *or more* of the surface. Such deep deposition increases the timescale for conduction to the surface. and heat is carried onto the nightside of Io [*Brown and Matson*, 1987].

4.3. Thermal Anomaly Unit

This unit consists of all of the thermal anomalies or hotspots. Each anomaly is assigned a particular location (latitude and longitude). Later their temperatures and areas are adjusted as needed to tit the orbital phase data. We find that this unit typically occupies -2 % of the surface. The anomalies are modeled as gray-body radiators with an emissivity of 0.9 (for all of our band-passes). In particular, their emissivity is not constrained by the 4.8 μm geometric albedo of Io which we determined in section 3. We assume that the anomalies may have significantly different properties from the disk average values.

Hotspot albedos were assigned following the general correlation between measured temperatures and albedos by *McEwen et al. [1985]*. For hotspots identified by IRIS, higher temperature anomalies have lower albedos (see appendix note 8), For the anomalies in our model which correspond to the Voyager hotspots, we have adopted the *McEwen et al. [1985],* albedos as listed in Table 6. These are normal albedos in the Voyager orange filter (-0.6 μm) but given the uncertainties in the scattering laws from these anomalous surfaces, we have used them as reasonable estimates of the biometric Bond albedos for the purpose of the calculation of the thermal pedestal effect (see section 4.4). For the non-Voyager locations, we have assigned small warm components an albedo of 0.15, typical of observed spots with temperatures greater than 300 K, and the larger, cooler components an albedo of 0.5, typical of observed areas with temperatures of less than 200 K [see *McEwen et al., 1985]*. The only exception was the third component required for Loki, where we used 0.3, close to the value for the warm unit (Loki 2) observed by *McEwen et al. [1985]. The* albedos and locations are tabulated in Table 6. They are used later in sections 5.1 and 6.1, where we adjust their temperatures and areas to fit the infrared light curves.

4.4, Thermal Pedestal Effect

The fourth spectral component is one which is due entirely to sunlight absorbed by the thermal anomalies themselves. Previously, this background component had been assumed to be negligible, since the anomalies occupy a small percentage of the surface and because their temperature was viewed as being regulated only by 10's heat flow. In terms of total power, this absorbed insolation is a small percentage. What has been overlooked, however, is that the anomalies provide a way to spectrally redistribute emission due to absorbed sunlight, resulting, in a significant effect at the wavelengths of our observations. We find that a key element in fitting the data is recognizing that the *solar heating and cooling of even volcanically heated regions* must be taken into account, especially for the lower temperature anomalies.

The *thermal pedestal effect* is the spectral blue shift which occurs in the background spectrum when sunlight is absorbed on a thermal anomaly caused by heat flow. Recognition of this effect leads to the separate concepts of *active* and *passive* components of the background spectrum. Passive components (i.e., the equilibrium and *reservoir* units) can be calculated a priori, while the active components cannot be computed until after the geothermal temperatures of the anomalies are specified. In practice, the active background is calculated simultaneously with the fit of thermal anomalies to the data. See Figure 7 for illustrations of the pedestal effect (see appendix note 9).

The solar energy absorbed by the anomalies elevates their temperatures during the day. If $\epsilon \sigma T_{geo}^4$ is the geothermal heat flow at an anomaly and $\epsilon \sigma T_{abs}^4$ *is the* absorbed solar power which is governed by the albedo, then the observed daytime temperature is obtained from

$$T_{obs} = \left(T_{geo}^4 + T_{abs}^4\right)^{1/4}$$

In our model, T_{geo} is specified for each anomaly and then T_{obs} is calculated. As our nomenclature indicates, the warming due to sunlight is superimposed upon a geothermally-supported temperature pedestal. The amount of warming and the spectral distribution of the reradiated solar power are both functions of the temperature of the anomaly, Another complexity is that this effect is a function of the zenith angle of the sun at each anomaly. Thus, latitude and time of day must be considered (in addition to heliocentric distance).

The pedestal effect has a temporal signature which should be evident during Io's eclipses, when the sun is eclipsed, the solar energy absorbed on hotspots is radiated away much more rapidly than for the cooler, passive background elements. In eclipse, the hotspot temperature drops quickly to T_{geo}, the level supported by geothermal heat flow alone, Previous analyses of eclipse data have not taken the thermal pedestal effect into account, This omission yields an apparent thermal inertia for Io which is too low.

4.5. Determination of Background Parameters

An accounting of the number of model parameters quickly shows that they exceed the constraints from daytime whole-disk observations alone. Observations both in and out of Jovian eclipse are necessary to solve for all of the parameters. For this purpose, we have chosen from our data set a well-observed eclipse disappearance on August 3, 1986 (see Tables 2, 3, and 5). The observed daytime and eclipse emittances at 10 ($W\ m^{-2}\ \mu m^{-1}$) for 4.8, 8.7, and 20 μm are summarized at the bottom of Table 7.

Since Io rotates -10° during an eclipse disappearance, we assume that we are seeing the same (or equivalent) *passive* surface units both before and after entry into eclipse. For the thermal anomalies in general, and for the strong, discrete Loki source in particular, we allow for the change in geometric foreshortening over this time interval.

From our eclipse radiometry, we have two data points at each of three wavelengths (Figure 6a) for a total of six constraints on the model as well as information on the area of Io's disk, the bolometric Bond albedo estimated from the Voyager photometry, and the relationship between the bolometric Bond albedo and the total background power radiated from Io. In addition to the general properties of our model previously discussed, there are nine model parameters to be determined. The passive background includes five of them, namely, the bolometric Bond al bedos and areas for the equilibrium and reservoir units; and the Bond albedo of Io at 4.8 pm. A reasonable fit to the eclipse data requires the use of two hotspot components at Loki, each defined by a temperature and an area. Since, at this stage, we are solving for the passive background only, we are not now concerned about the distribution of the hotspots. Later, when the longitude data are taken into account, we shall see that a further adjustment in the thermal anomalies is required.

The particular values and components of the model spectral emittances ($W\ m^{-2}\ \mu m^{-1}$) which are consistent with both the daytime and the eclipse data are given in Table 7. The model emittance in eclipse is the simplest. The 20 μm emission has two components. Slightly more than half is due to the thermal reservoir unit. The remainder is from the thermal anomalies. At 8.7 μm almost all of the signal is from the anomalies. At 4.8 μm, only a trace of the emittance is from the passive background,

The daytime spectral distribution (i.e., before eclipse) has more components. The chief surprise is the size of the thermal pedestal effect at 8.7 μm, which accounts for almost 30% of the observed radiation. At 4.8 μm the thermal pedestal effect is -13%! The recognition of this component is important because previously it has been generally assumed that there was *no* significant background radiation at such short wavelengths. The sum of all the background units is more than 45% of the emittance at 8.7 μm. At 20 μm, the background is -75 % of the total. Here, the 25% due to emission from the thermal anomalies is significant because it corrects the earlier assumption that hotspot emission was negligible at this wavelength. The percentages due to the pedestal effect depend on

the model albedos assigned to the hotspots.

Data at particular wavelengths constrain some model parameters more than others. The equilibrium unit is constrained by the daytime 8.7 and 20 μm emission. 'l'he reservoir unit is constrained by the eclipse 8.7 μm data and even more by the eclipse 20 μm data. The pedestal effect is determined from daytime 4.8 and 8.7 μm emission. In general, cooler regions are more constrained by the longer wavelength data, and hotter regions more by the 4.8 μm data,

'I'he areal combination of the smaller, dark equilibrium unit with the larger, bright reservoir unit results in lowering the physical temperature of much of 10's daytime surface to well below the values that would be expected based on rapid equilibrium with absorbed insolation. This effect is what allows the low observed values of 20 μm emittance to be modeled successfully. The subsolar temperature of the equilibrium unit is -167 K whereas the equatorial temperature of the reservoir unit is -109 K (see Table 7). The latter does vary slightly with longitude as a function of its albedo (see discussion of background parameters below and also Table 8). Both temperatures also vary slightly with the heliocentric distance of Jupiter.

Figure 6b shows the different background models discussed for 10. The "standard" model (see appendix note 5) has a bolometric Bond albedo of 0.44. The eclipse model contains emission solely from the reservoir unit. The daytime model includes emission from the equilibrium unit as well. These passive backgrounds were then combined with the thermal anomalies to fit the daytime and eclipse data.

4.6. Thermal Model as a Function of Longitude

The previous discussion yields an average bolometric Bond albedo of -0.53 for Io which only applies for a narrow range of orbital longitude near 340" W (see Table 7). To interpret our infrared data, it is necessary to extend the model of the background to other longitudes. We have done this by utilizing the form of the albedo versus longitude curve labeled "solar" from Figure 8 of *McEwen et al.* [1988]. Table 8 lists the longitudinal values of the bolometric Bond albedo averaged over 10"W longitude bins. These albedos have been scaled to match the albedo of our eclipse model at longitude 340"W. This scaling will be discussed again later in section 4.7.

The albedo of the equilibrium unit is taken to be 0.29 at all longitudes. This unit occupies -20% of the surface. We then derive the albedo for the reservoir unit as a function of longitude as given in Table 8. The reservoir unit occupies -80% of the surface of Io.

At least five locations with a total of 10 temperature components are needed to match the shape of the corresponding parts of the infrared light curves (at all three wavelengths simultaneously). The model hotspot designations, albedos, longitudes (°W), and latitudes are listed in Table 6 (see also Table 7 and section 6.1). Since the Voyager IRIS experiment identified several major hotspots on the trailing hemisphere, we began with the locations of the most prominent ones, in the spirit of Occam's Razor. On the leading hemisphere, our

model includes additional thermal anomalies at two locations, each with two components. These are needed to match the shape of the corresponding parts of the infrared light curves (again, at all three wavelengths simultaneously). We locate these new hotspots at 170° and 80" W longitude, but at 0° latitude. This choice of latitude minimizes their heat flow contribution, If any of the. actual hotspots on this part of 10 are. at higher latitudes, they would have larger surface areas (due to foreshortening) and thus produce even more heat flow than our model predicts. We find for all the spots that although their characteristics change from apparition to apparition, the data are well fit, assuming that the locations remain unchanged.

For the Loki region, it is necessary to consider three active components to match the peak in emittance near 300-320"W at all three wavelengths simultaneously. We have approximated tire distribution of temperature and area in this region with (1) a small hotspot (~450 K and radius -22 km), (2) a warm area (-245 K and radius ~140 km), and (3) a large cool area (- 180 K and radius -300 km). The Pele region contains two components which are hotter but much smaller (-654 K and radius -6 km; -350 K and radius -180 km). A more subtle feature which appears in our data is near the longitude of the Voyager source Colchis. A model component at this position is necessary to match the asymmetry and broadness of the (composite) trailing side emittance peak (see also section 6. 1).

4.7. Caveats

The model presented in this paper should be viewed as the first in an evolutionary sequence. It is the first thermal emission model which is consistent with the known properties of Io, resolving large discrepancies between previous models and the Earth-based observations. It is a simple model which provides an accurate way to calculate the background emission and determine the basic characteristics of the thermal anomalies which are responsible for Io's heat flow, but it is not yet a complete description of Io's thermophysical properties. We arrived at the adopted model parameters by manual iteration after making appropriate range checks. A discussion of limitations of our model follows.

1. Our model conserves energy but it does not attempt to model the transient response of the surface either diurnally or in eclipse. Additional information remains to be determined about the thermal inertia of the equilibrium and reservoir units, characteristics of a possible solid-state greenhouse, and/or latent heat as well as possible effects due to atmospheric transport.

2. The passive background units in our model are distributed uniformly over the surface of 10 in a manner analogous to a tine "checkerboard. " Since the poles a.. well as the midlatitudes of Io are darker than the equator, an obvious improvement would be to include the albedo distribution seen by Voyager at an appropriate resolution.

3. There is an offset of 0.09 between the Voyager bolometric Bond albedo of 0.44 at 340"W [*McEwen et* al., 1988] and the value of 0.53 in our model. The Voyager

albedo weighs all parts of the projected disk equally. In contrast, our model is most sensitive to the infrared emittance from warm low latitudes. The difference in albedo between the equatorial regions and higher latitudes is sufficient to explain the direction and size of this offset. Considering uncertainties in the calculation of Io's phase integral, we regard the level of agreement as satisfactory for this stage of analysis.

4. The approximation of the thermal anomalies as flat disks has obvious restrictions with respect to the large, cool regions. An improvement would be to represent them as elements on a spherical surface and to associate them, where possible, with identifiable surface albedo features in the Voyager (and eventually Galileo) images.

5. Thermal Emission Variability

Our infrared data set provides the first relatively uniform, long-term overview of 10's thermal characteristics. The basic nature of Io's thermal emission has remained relatively stable throughout 1983-1993. Nevertheless, there are significant variations between apparitions. Dramatic outbursts at 4.8 μm from relatively hot sources (greater than 600 K) can vary rapidly on timescales of hours to days and occasionally reach very high levels of thermal emission.

5.1. Orbital Infrared Light Curves

The thermal emission model discussed in the previous section was used to match the infrared data as a function of Longitude for each apparition. First, the passive background is adjusted to account for the relatively small changes in absorbed sunlight due to heliocentric distance variation. Then, each thermal anomaly is assigned a "geothermal temperature, " radius, and location. The active background, due to the pedestal effect, is calculated from the physical temperature of the hotspot in sunlight. We attempt to make a minimum number of changes, from year to year, in anomaly temperatures and sizes, consistent with producing a good match to the emittance versus longitude data. It does not appear to be necessary to change the model locations of any of. the thermal anomalies to produce good fits, suggesting that at least the average longitude distribution of thermally active areas on Io has remained approximately constant throughout the last decade.

The radius and temperature for each of the 10 model thermal anomalies (at five locations) are listed in Table 9 for each apparition. The model tits to the data at 4.8, 8.7, and 20pm during each apparition are shown plotted as the curves in Figures 2, 3, and 5. The 10 μm data are not modeled because of the wide bandwidth of this filter which causes the effective wavelength to change, depending on the temperatures of the thermal anomalies. The model radii and temperatures vary from year to year, with the largest changes generally in the higher temperature components required to match the 4.8 μm emission. One way of visualizing both the variation in Io's emittance by year and the models required to match the

data is to overlay the model emittance curves at each wavelength for all apparitions as in Figure 8 (see also section 6,1).

As seen in previous studies, there is more variation at 4.8 μm than at longer wavelengths (8.7 and 20 μm). For most years the thermal emission at all wavelengths is very similar in intensity and shape from apparition to apparition. The thermal emission from the trailing hemisphere is roughly consistent with that expected from the hotspots detected by Voyager [*Johnson et al.*, 1984].

However, there are several exceptions to this broad generalization. Most obvious are the outbursts which will be discussed below in section 5.2. Other exceptions result from general increases in emission levels. On the leading hemisphere (O"- 1800), the 1987 apparition had more than twice the ernittance at 4.8 μm than the other apparitions. Emittances at 8.7 and 20 μm were also elevated. Emittance at 4,8 μm from the trailing hemisphere (dominated by Loki) appears to have two modes. One mode peaks at less than 0,05 W m^{-2} μm^{-1} and is representative of most apparitions. The other mode peaks at greater than 0.07 W m^{-2} μm^{-1} and occurred during the 1983, 1984, and 1989-1990 apparitions. This bimodal activity is much less distinct at 8.7 μm, but the 1989-1990 and the 1984 model fits do have higher emittances than other apparitions. At 20 μm the variation in emittance at Loki forms a continuum, with 1984 and 1989-1990 data showing the highest emittances.

5.2. Outburst Activity

Outbursts on Io are characterized by a large increase in the 4.8 μm emission over a short period of time (i.e., hours to days). The first report of such an event was the pre-Voyager 5 μm enhancement reported by *Witteborn et al.* [1979]. Other events were subsequently observed, including one during the interval between Voyager encounters in 1979, which was apparently connected with a change in the appearance of the feature Surt [*Sinton*, 1980].

We have observed two well-characterized events of this sort, one on August 7, 1986, the second on January 9, 1990 (see appendix note 10). Both events were observed for several hours during the course of a single night. Our current data set includes observations from 175 hours over 55 nights. We conclude that such events are occurring -4% of the time during our program, This appears to be consistent with the number of other reports, but we do not have enough information concerning the total time other observers could have detected outbursts to calculate a more precise frequency.

These two outbursts have similar emission characteristics. The August 7, 1986 (leading hemisphere), outburst is quite large. The emittance at 4.8 μm increased by over a factor of 10 from -0.02 to greater than 0.3 W m^{-2} μm^{-1}! At 8.7 μm it almost doubled. On January 9, 1990, the. emission from Io increased by a factor of 2.5 at 4.8 μm and also 20% at 8.7 μm. This event occurred on the trailing hemisphere near the same longitude as Loki (309°W longitude), Since we have data at each of our wavelengths during the outbursts, it is possible to characterize the sizes and temperatures of the sources responsible.

Preliminary analysis of the January 9, 1990, outburst on the trailing hemisphere is illustrated in Figure 9. This suggests a small (-5.6 km radius) high-temperature (~ 1200 K) source at the beginning of the event, and also indicates that the model source required at the end of the event is significantly cooler (-700 K) and larger (-13 km radius). While the latter size is large by terrestrial standards, it is only -0.2% of the area of Loki Patera. These characteristics are consistent with a high eruption rate silicate lava flow and the suggestion that 10's heat flow is coming from an ensemble of volcanic features with differing emplacement histories and temperatures [*Carr, 1986; McEwen et of.,* 1992]. These temperatures are consistent with liquidus temperatures of basaltic magmas (1550-1600 K [cf. *Lofgren et al.,* 1981]).

The August 7, 1986, outburst was discussed by *Johnson et al.[1988],* who reported that a model temperature of 900 K and a radius of 15 km were required to account for the flux density increases at each of the wavelengths. They further concluded that such high temperatures were strong evidence for the source being a silicate lava rather than a sulfur melt (whose STP boiling point is 715 K).

The earlier analysis of the 1986 event did not attempt to match the characteristics of the event in detail. Rather, the maximum emittance excesses at 4.8 and 8.7 μm were used to produce an estimate of the required high-temperature source. Since the 4.8 μm flux density decreased rapidly over the course of about 2.5 hours, it was clear that more detailed modeling would either require a different hotspot location, a changing source emittance, or both. Using our model for the anomaly characteristics required to match the rest of the apparition's data, we find that an even higher temperature source (- 1550 K and ~8 km radius) at a longitude of -35" W best fits the observations at both wavelengths during the outburst (see Figure 9). This is consistent with the location of a persistent source imaged by *Spencer et al. [1990].* The fit is not perfect, and it is probable that this source changed both temperature and size during the observing session. However, there are not enough 4.8 μm data during the early hours of the night, nor enough 8.7 μm data late in the night, to obtain simultaneous solutions at both wavelengths and constrain a time variable model of the type used for the 1990 event.

6. Heat Flow

The heat flow from thermal anomalies on 10 IS calculated from the sum of nonbackground power radiated by each of the hotspots needed to match the infrared light curves. The heat flow power P for each model thermal anomaly IS

$$P = \pi \epsilon \sigma T_{geo}^4 R^2$$

where ϵ is the emissivity, σ is the Stefan-Boltzmann constant, T_{geo} is the geothermal temperature, and R is the radius of the

anomaly. The hotspot radii and temperatures are given in Table 9, and the resulting heat flow is listed in Table 10.

6.1. Active Regions

Figure 10 shows the variations in power for the different temperature components in the five model regions: Loki, Pele, Colchis, Leading Hemisphere (170°W), and Leading Hemisphere (80° W). We will discuss the behavior of these regions and then turn to a discussion of the global heat flow from 10.

Loki. Loki is one of the best characterized volcanic features on Io. It was easily recognized in the Voyager IRIS data because of its temperature and size and the favorable geometry during the Voyager flyby [*Hanel et al., 1979; Pearl and Sinton, 1982]*. Loki has also proved to be the most easily detected thermal feature from Earth by a number of techniques, including our initial fill-disk radiometry [e. g., *Johnson et al., 1984]*. Other known or suspected anomalies, such as Pele and Babbar Patera, may contribute to the emittance near the longitude of Loki (see appendix note 4). The signature of the Loki region in our data is usually a prominent peak near 3090W longitude which falls off on either side more or less as expected from the change in projected area with rotation. In detail, the shape of the Loki feature is asymmetric and requires smaller sources to the east of 309"W to match the infrared data (see discussion of Pele, Colchis, and the leading hemisphere below),

The Io thermal model for Loki includes three temperature components which are probably closely grouped and whose variation with apparition is shown in Figure 10a. Pele is modeled separately (see below and Figure 10h). Our model values of Loki's characteristics are not constrained strictly by the physical size of the albedo feature at Loki or the IRIS derived temperature and area components, but rather are a composite of temperatures and areas which could in fact be distributed among-a number of sites near the same longitude. Based on the lines of evidence cited earlier, Loki itself has been the major contributor to the infrared emittance in this region throughout the decade.

The data in Tables 2, 3, 4, and 5 show that the volcanic activity in the Loki region has been continuous during the course of our study. The intensity of this source at 4.8 μm has varied considerably due to changes in the moderate- and high-temperature components. Thus, in the 1988-1989 apparition, sources with temperatures greater than 200 K contributed much less emission than in 1983, 1984, or 1989-1990. In particular, the high-temperature component was near its lowest level at the time of the Ulysses flyby in 1992 as well as during the 1993 apparition.

Pele. Pele is about 50" east of Loki and was the site of one of the largest eruptive plumes seen by Voyager [*Smith et al.*, 1979]. It had one of the highest temperature anomalies detected by IRIS [*Hanel et al.*, 1979]. The 10 thermal model includes a small high-temperature region similar to the Voyager-derived values [*Pearl and Sinton, 1982]* and, in addition, a larger but lower temperature component to match our data at longer wavelengths (see Figure 10b). The time history for Pele is qualitatively similar to Loki, with the bigh-

temperature component model area changing by an order of magnitude (essentially disappearing during three apparitions) and the larger low-temperature region area varying by a factor of 4 at most. This region and Colchis, discussed next, do not produce a clear separate "signature" in our data, in contrast to Loki, but together provide infrared emission at longitudes east of Loki required to match the shape of the emittance versus longitude data.

Colchis. Colchis was also identified as a thermal anomaly in IRIS data [*Hanel et al., 1979]*. It is approximately 50° east of Pele. This is a transition region in the infrared data between the peak due to Loki and the relatively constant emittance levels seen on the leading hemisphere at most wavelengths. The 10 thermal model includes a source with a single temperature component greater than *350* K which affects primarily the 8,7 and 4.8 μm emittance (see Figure 10c). The area and temperature of the Colchis model are relatively constant for most apparitions. The major exceptions are the 1989-1990 apparition, when the required area increased about a factor of 10, and 1993, when the area is similar to other apparitions, but a model temperature of 700 K is required to match the data.

170°W and 80°W. The 170°W and 80°W. regions on the leading hemisphere are not tied directly to Voyager observations. Voyager did not acquire high-resolution imaging or IRIS data on this hemisphere. The relatively constant emittance level with longitude over this hemisphere requires that sources of volcanic activity here not be concentrated in a single relatively small region, such as Loki, but rather be more uniformly distributed over Io's surface. Qualitatively this is in agreement with lower resolution imaging data from Voyager which show no large albedo feature or caldera structures analogous to Loki. Occultations reveal no evidence for any strong concentrated source on the leading hemisphere [*Goguen et al.,* 1988].

The Io thermal model includes two relatively large sources in the leading hemisphere with two temperature components each, separated by 90" (see Figures 10d and 10e). These are sufficient to provide good matches to the observed longitude variations in the data. They should not be interpreted literally as specific volcanic localities but rather as parameterized "stand-ins" for what may be an ensemble of surface features having a similar combined area and temperature distribution. Partial confirmation of the. validity of the general characteristics of the 170°W source comes from recent analyses of IRIS data by *McEwen et al.* [1992], who find that a whole-disk spectrum from Voyager centered on 1550 W is matched by a thermal anomaly with a temperature of 169 K and a radius of 769 km. The lower temperature source at 170°W in our model varies from 140 K to 180 K and from 420 km to 760 krn in radius.

The characteristics of all these model sources are relatively constant during the decade, the only major change being observed in 1987, where emittance from the leading hemisphere at all wavelengths was higher than normal. This required increased areas for the lower temperature components and higher temperatures for the high-temperature components. It may be significant that this higher emission level occurs the

year following the high-temperature outburst event in 1986 [*Johnson et* al., 1988]. If that event represented lava flow activity for some significant duration, elevated temperatures from cooling flows could still be releasing significant heat a year later [*Carr*, 1986].

6.2. Global Heat Flow

The model fits to the data at each apparition can be used to estimate the heat flow coming from the thermal anomalies, and thus the variation of the geothermal power with time and location on Io. Total heat flow power for a given apparition is calculated simply by summing the contributions from each of the anomalies.

Table 11 compares the total power (10" W) and heat flow ($W m^{-2}$) for Io during each apparition with the model contributions from the larger, cooler regions and the smaller, hotter regions. Clearly, the bulk of the power is coming from regions with a surface temperature of less than 200 K. Figure 1 la shows the history of power output from the thermal anomalies in our model. As expected from the larger variability of the 4.8 μm emittance compared with other wavelengths, the small amount of power from the hotter components tends to vary considerably from apparition to apparition. Total power tends to be less variable, however, since most of the power comes from the larger, cooler, and less variable anomalies which affect the 20 μm emittance the most, This implies that the activity in such regions is long lived.

In a similar manner, Table 12 compares the total power and heat flow with the model sources located on the leading and trailing (i.e., Loki) hemispheres. Approximately *equal* amounts of power come from each hemisphere. Figure 1 lb shows these powers and the total as a function of apparition. Both hemispheric and total power values are relatively constant, with an average total power of 1.05 x 10^{14} W (2.5 W m^{-2}). This value is considerably larger than most previous estimates, but consistent with the even higher value of 3.2 $\pm$ 1.0 W m^{-2} [*McEwen et al.*, 1992; A.S. McEwen, personal communication, 1993].

Note that conduction through the crust of 10 for the more than -95 % of the surface that has no detectable thermal anomalies is not considered in the present model [see also *Stevenson and McNamara, 1988]*. As noted in previous discussions of volcanic power from Io, the power radiated by hotspot anomalies is a *lower limit* to the total, globally averaged heat flow [e.g., *Johnson et al.*, 1984]. Figure 12a illustrates the key characteristics of the model spots for each apparition; it plots the area of each model component versus the temperature. Lines of constant power output are also shown, This plot clearly shows the dominant contribution of the large area, low-temperature anomalies to the total heat flow, as well as the larger variation of modeled area and temperature for the hotter components of the model.

The characteristics of our model anomalies for the past decade can be compared with what was observed by the IRIS instrument during the Voyager flyby. *McEwen et al. [1992]* have recently refined the pointing knowledge for Voyager and

reanalyzed the IRIS data. This permits the recognition and modeling of lower temperature anomalies than were previously possible [e.g., *Pearl and Sinton*, 1982]. In Figure 12b, the IRIS thermal anomalies identified by *McEwen et al.* [1992] are compared with our data binned in 100 K increments. We find very good agreement between these and our model thermal anomalies. The trend between area and temperature from our results and those of *McEwen et al.* [1992] is qualitatively what is expected for a surface with multiple, cooling lava flows of different ages, as pointed out for sulfur models by *Sinton* [1982] and for silicate models by *Carr* [1986] and *McEwen et al.* [1992].

The consistency of our results with the IRIS analyses is particularly important for evaluating the new class of anomalies with temperatures less than 200 K. In our thermal model, these anomalies are a consequence of the new background model required to match our disk-integrated radiometry including eclipse observations. These anomalies are identified directly in the IRIS analysis of small Voyager regions [*McEwen et al.*, 1992; A.S. McEwen, personal communication, 1993]. Lower daytime and higher nighttime background temperatures in agreement with our conclusions are also implied by the interpretation of IRIS data by *McEwen et al. [1992]*. The IRIS observations are an independent data set with respect to instrumentation (i. e., Fourier transform spectroscopy versus filter radiometry), observational resolution (i.e., disk-resolved versus disk-integrated), and calibration techniques. The agreement of these two independent approaches lends considerable support both to the conclusion that higher heat flows result from the lower temperature anomalies and to the necessity of improved thermophysical models for Io's passive background.

Figure 13 compares various estimates of observed and calculated heat flow with constraints from tidal heating and orbital evolution. Both our present estimate and that of *McEwen et al. [1992]* increase the previously noted disc repancy between the geothermal output from Io and theoretical limits on the total amount of power dissipated in Io due to tides. A number of possible explanations have been proposed which include time variations in 10's internal properties, variations in the dynamical state of the system and variations in Jupiter's dissipation over the last 4.5 Gyr. It is not the purpose of this paper to explore this problem in detail (see *Greenberg [1989]* for a recent review). We note only that models of the dynamics of the system including tidal dissipation must now cope with even higher values of Io heat flow observed over the past decade. Accurate measurement of the change in Io's orbit during the current epoch from spacecraft observations and/or improved astrometry or else a better understanding of Jupiter's interior may be necessary to resolve this issue (see also *Peale et al. [1979]*, *Yoder* [*1979]*, *Yoder and Peale [198 1]*, *Cassen et al. [1982]*, *Ojakangas and Stevenson [1986]*, *Segatz et al.* [1988], *Fischer and Spohn [1990]*, and *Ross et al.* [1990]).

7. Summary and Conclusions

A new view of 10 can be synthesized from our multi-wavelength observations made over more than a decade (nine apparitions). This data set defines the characteristic states of 10's thermal emission as a function of orbital phase angle. It allows anomalous conditions to be recognized and compared with other times, The probability of observing a large variation, or outburst, on any given observing night is about 4%. We observed two such outbursts and both had high temperatures typical of silicate lavas.

10's flux density at 20 μm is curiously low compared to 8.7 μm. From this, we have inferred that 10 is radiating a large part of its thermal emission at nighttime. We suggest three possible mechanisms which may be involved: (1) high thermal inertia (e.g., rock), (2) solid-state greenhouse, and (3) atmospheric transport (e.g., latent heat).

The *thermal pedestal effect is* an important aspect of physics which must be included in modeling Jo's thermal anomalies. This blue shift of the background spectrum for the reradiation of absorbed sunlight can lead to emittance components as large as 30% at 8.7 μm and 13% (of the thermal emission component) at 4.8 μm. The thermal pedestal effect gives rise to the concepts of active and passive background thermal emission. The spectrum for an active background cannot be calculated until the geothermally supported temperature of the underlying anomaly is specified, The thermal pedestal effect also has a temporal signature when 10 goes into eclipse, The solar energy absorbed on hotspots is radiated away more rapidly than for analogous, passive surfaces.

We have developed a new thermal emission model for 10 which has three types of surface units: a dark albedo equilibrium thermophysical unit, a high albedo thermal reservoir, and a set of thermal anomalies. The equilibrium unit covers about 20% of the surface. The thermal reservoir unit greatly increases thermal emission in the antisolar hemisphere by carrying significant heat into Io's nightside. This unit occupies about 80% of the surface. The area] combination of the smaller, dark equilibrium unit with the larger, bright reservoir unit results in lowering the 'physical temperature of much of , 10's daytime surface to well below the values that would be expected based on rapid thermal equilibrium with absorbed sunlight. The thermal anomalies are located at five positions, and the data for each apparition are modeled by varying the areas and temperature of 10 components. The area] coverage of the thermal anomalies is ~2%.

The thermal emission model allows us to compute accurately the daytime emission and thereby isolate the reflected component at 4.8 pm. The geometric albedo of 10 at 4.8 μm is about 0.7. A model for the orbital phase/longitude dependence of the passive background and the 4.8 μm albedo was synthesized by comparison with Io's visual light curve. The contributions due to individual hotspots were identified and tracked. Thus, individual histories for Loki, Pele, Colchis, and the behavior of anomalies on the leading side at longitudes of 170" and 80°W can be studied. The temperature versus area plot for our hotspots is similar to that predicted for a surface with multiple,

cooling lava flows of different ages. The anomalies may include overturning of crusts on lava lakes as well as lava flows. At least for the high-temperature outbursts, the lava must involve silicates.

The total heat flow is calculated by summing the radiated power from all of the anomalies. We find that 10's heat flow is greater than 2.5 W m^{-2}. Most of the beat flow comes from the large, persistent, low-temperature (less than 200 K) anomalies. Short-lived outbursts, despite their high temperatures., contribute very little to heat tlow due to their small sizes and short durations. Since we are not sensitive to conductive heat flow through the crust of the passive areas (most of Io's surface), our heat flow values are formal lower bounds on the actual heat flow. Nevertheless, this value alone is so high that tidal dissipation in 10 remains the only viable mechanism. The heat flow is large enough to rule out existing steady state models for dissipation in Jo. All of this suggests there may be further complexities in the Jupiter-1o tidal interactions and in the volcanic activity of Io.

Appendix

Magnitude

"For each observing night, standard stars were selected from a subset of the IRTF list. These generally included at least one star before and after Jupiter in RA. The Bright Star catalog number (BS) and the magnitudes are listed in Table A 1. These magnitudes have been adopted from *Hanner et al. [1984], Tokunaga [1984], Hanner and Tokunaga [1991],* and *Hanner et al. [1992]. This* network is expected to be self-consistent to within 0.05 msg. The value for p Gem at 8.7 μm was developed as a secondary standard from comparisons with other stars within our own data set,

Absolute Calibration

The IRTF photometric system defines a Lyrae as 0.0 mag at each wavelength. The absolute calibrations at M (4.8 μm), 8.7 μm, N (10 pm), and Q (20 μm) as listed in Table A2 have been adopted from *Beckwith et al. [1976]* and *Hanner et al. [* 1984]. These values are expected to be more accurate than *1o%. Calibration issues at particular wavelengths are discussed by *Campins et al.* [1985], *Rieke et al.* [1985], and *Tokunaga et al.* [1986]. other photometric systems that have been used for Jo are discussed by *Morrison and Lebofsky [1979], Sinton and Tittemore [1984], Campins et al. [1985], Rieke et al.* [1985], and *Tokunaga et al. [*1986].

Monochromatic Correction

A monochromatic correction factor is required for measurements of 10 with the N (10 μm) and Q (20 μm) filters. Over the width of these band-passes, the spectral flux density distribution of the Galilean satellites is significantly different from that for the standard stars used. There are a number of contributions which affect the correction which must be made to the observed (instrumental) magnitude (or flux density) to

obtain the equivalent monochromatic value which would have been measured with a very narrow band-pass at the effective wavelength. The factor Y is defined by

$$\frac{B(\lambda_*,T_\circ)}{B(\lambda_*,T_*)} = Y \frac{\int B(\lambda,T_\circ) r_\lambda \, d\lambda}{\int B(\lambda,T_*) r_\lambda \, d\lambda}$$

where the integrals are taken over the band-pass of interest, $B(\lambda,T)$ is the Planck function, $T_\circ$ is the effective temperature of the object, T_* is the effective temperature of the reference star, and λ_* is the reference wavelength, The system response function, r, as a function of wavelength is defined by

$$r = aft$$

where a is the atmospheric transmission function, f is the filter transmission function, and t is the combined detector and telescope response function. For the purposes here, we have taken t as constant over the filter band-pass, which is a reasonable approximation for a bolometer used with a reflecting telescope at N and Q, The relevant standard star temperature was taken as 10,000 K (i.e., approximating a Lyrae). The results are not very sensitive to the exact value adopted for T_* above effective temperatures of -3500 K.

Atmospheric absorption from water vapor within the N (10 μm) band-pass is approximately constant with wavelength. At N the measured flux density of 10 includes a significant hot volcanic component with an inferred color temperature of approximately 600 K and a cool "background" surface component with an estimated color temperature of perhaps 120 K at noon on the equator (depending upon the local albedo and also the heliocentric distance) as well as a range of various warm components with interrnediate color temperatures. Over the N filter we use an effective temperature of -170 K for Jo due to the average volcanic flux contribution. This yields the value used in Table 4 for Y (10 μm) of 0.95 (i.e., -0.05 mag).

The column density of water in the atmosphere affects the calculation for the Q (20 μm) band-pass since the long-wavelength portion of the band-paw is effectively controlled by H_20 absorption. The theoretical atmospheric absorption as a function of wavelength and H_2O column density was calculated by V, Kunde (personal communication, 1993). However, we found in practice that assuming a constant factor produced less scatter over many nights than calculating the effective wavelength of Q based on our estimate of the H_2O column density for each night. Thus, a 3-mm column water abundance and a T_{eff} at Q of -170 K yields the value used in Table 5 for Y (20 μm) of 1,08 (i.e., 0.08 mag). Again, the effective temperature is higher than the expected physical temperature of Io of ~120 K due to the contribution from volcanic emission. Since this value for Y (20 μm) may vary by up to 20% between a very dry and a marginal night at the IRTF, our reported 20 μm measurements in principle could have a

systematic error of up to this amount, However, the consistency of our observations from night to night and from apparition to apparition suggests that relative errors between nights are typically less than 10% (i.e., less than O. 1 mag).

Notes

1. Numerically, this longitude. has the same value as the orbital phase angle. Plots with west longitude decreasing to the right can be compared directly with U.S. Geological Survey maps of 10.

2. Data at 8.7 μm are not available for April 12, 1980, and March 19, 1982, and so these dates are not considered further.

3. One approach that has been taken to this problem is to define a "pseudo-geometric albedo," p', from the total 4.8 μm flux density which is thus larger than the physical albedo [*Sinton*, 1980]. This quantity can show changes in the hotspot activity of Io over a few days; but comparisons at different longitudes, and especially at different epochs, are confused by the different angular and heliocentric distance dependencies of the reflected and emitted components,

4. The association with Loki Patera is established by comparison of the Voyager observations from IRIS [*Hanel et al.*, 1979; *McEwen et al.*, 1985] with occultation, speckle, imaging and polarization observations which have resolved Loki [*Goguen et al.*, 1988; *Howell and McGinn*, 1985; *Spencer et al.*, 1990; *McLeod et al., 1991; Goguen and Sinton, 1985,* 1988]. Strictly speaking, our data only require that there be a source at the same longitude as Loki.

5.' The treatment in section 4.1 is the same as for the "standard" asteroid thermal emission model but with the empirical beaming factor (which is not used in our Io model) set to unity [cf. *Matson et al., 1978; Morrison and Lebofsky*, 1979; *Lebofsky and Spencer,* 1989; *Veeder et al.,* 1989].

6. The treatment in section 4.2 is the same as for one of the "nonstandard" asteroid thermal emission models with an empirical beaming factor of unity [cf. *Matson et al., 1978; Morrison and Lebofsky, 1979; Lebofsky and Spencer, 1989; Veeder et al.,* 1989].

7. For an emissivity of 0.9, the reflected component at 8.7 μm is -1 % of the observed emission. The reflected component is even less at 20 μm.

8. *Goguen et al. [* 1988] occultation results confirm that the lowest albedo regions at Loki had the highest temperatures, which strengthens this relationship.

9, Calculations of the intrinsic luminosity of Jovian planets involve the same physics as the thermal pedestal effect. For example, see Figures 1-4 of *Hubbard [1980].*

10. Data for the night March 11, 1983, plot well above the leading hemisphere measurements collected on July 19 and 21 at all wavelengths, including 20 μm. Rechecking the photometry indicates that while this is not an outstanding night, it is good enough and has no obvious problems that could immediately call the data into question. Given the highly variable nature of Io, we are including the data for completeness. However, observational concerns such as north/south differences in the sky could have caused the discrepancy. Addition-

ally, the intensity of the emission level at 4.8 μm is consistent with other nonoutburst measurements during other apparitions. We therefore do not consider this measurement an outburst.

Acknowledgments. I'he authors arc visiting astronomers at the Infrared Telescope Facility which is operated by the Institute for Astronomy of the University of Hawaii under contract from the National Aeronautics and Space Administration. The authors would like to thank their many colleagues who have participated over the years in various aspects of the data collection for this program. Those participating directly on specific observing runs arc named in Table 1. Many others generously shared their data, their expertise, and even their telescope time! David Morrison (NASA/ARC) was instrumental in helping develop the original plan for this long-term program. We have also benefited from many fruitful discussions with John Pearl (NASA/GSFC), Alfred McEwen (USGS Flagstaff), William Sinton (Lowell), John Spencer (Lowell), Robert H. Brown (JPL), and Damon Simonelli (Cornell). The calibration of our 8.7pm band-pass data was greatly facilitated by the work of Martha Hanner (JPL). We also appreciate the efforts of two very helpful and thoughtful JGR reviewers, Their comments and suggestions have, wc hope, significantly improved the paper. Remaining errors and oversights are, of course, still our responsibility. Donald Hunten (University of Arizona) pointed out the parallel between our thermal pedestal effect development and work on the luminosity of giant planets. This research was carried out at the Jet Propulsion laboratory, California Institute of Technology under a contract from NASA. This paper is IOG Contribution No. 42.

References

Beckwith, S., N.J. Evans, E.E. Becklin, and G. Neugebauer, Infrared observations of Monoceros R2, *Astrophys. J., 208,* 390-395, 1976.

Brown, R. H., and D .L. Matson, Thermal effects of insolation propagation into the regoliths of airless bodies, *Icarus,* 72, 84-94, 1987.

Campins, H., G.H. Rieke, and M.J. Lebofsky, Absolute calibration of photometry at 1 through 5 μm, *Astron. J., 90,* 896-906, , 1985.

Carr, M. H., Silicate volcanism on 10, *J. Geophys. Res.* ,91, 3521-3532, 1986.

Cassen, P. M., S.J. Peale and R. T.' Reynolds, Structure and thermal evolution of the Galilean satellites, in *The Satellites of Jupiter,* edited by D. Morrison, pp. 93-128, University of Arizona Press, Tucson, 1982.

Cruikshank, D. P., Infrared spectrum of 10, 2.8-5.2μm, *Icarus,* 41, 240-245, 1980.

Clark, R. N., and T.B. McCord, The Galilean satellites: New near-infrared reflectance measurements (0.65-2.5μm) and a 0.325-5pm summary, *Icarus,* 41, 323-339, 1980.

Fischer, H.-J., and T. Spohn, Thermal-orbital histories of viscoelastic models of Io (J1), *Icarus,* 83, 39-65, 1990.

Goguen, J. D., and W.M. Sinton, Characterization of 10's volcanic activity by infrared polarimetry, Science, 230, 65-69, 1985.

Goguen, J. D., and W.M. Sinton, 10 hot spots: IR polarization measurements in 1987, *Bull. Am. Astron. Sot,, 20, 817, 1988.*

Goguen, J. D., W.M. Sinton, D.L. Matson, R.R. Howell, H.M. Dyck, T.V. Johnson, R.}{. Brown, G.J. Veeder, A.L. Lane, R.M. Nelson and R.A. McLaren, 10 hot spots: Infrared photometry of satellite occultations, *Icarus, 76, 465-484, 1988.*

Goldreich, P., and S. Soter, Q in the solar system, *Icarus, 5, 375-389, 1966.*

Greenberg, R., Galilean satellites: Evolutionary paths in deep resonance, *Icarus, 70, 334-337, 1987.*

Greenberg, R., Time-varying orbits and tidal heating of the Galilean satellites, in Time-Variable Phenomena in the Jovian System, edited by M.J.S. Belton, R.A. West, and J. Rahe, *NASA Spec. Publ., SP-494*, 100-115, 1989.

Hanel, R., and the Voyager IRIS Team, Infrared observations of the Jovian system from Voyager 1, Science, 204, 972-976, 1979.

Hanner, M. S., and A.T. Tokunaga, Infrared techniques for comet observations, in *Comets in the Post-Halley Era,* edited by R.L. Newburn Jr., M. Neugebauer, and J. Rahe, vol. 1, pp. 67-91, Kluwer Academic, Nor-well, Mass., 1991.

Hanner, M. S., A.T. Tokunaga, G.J. Veeder, and M. F. A'Hearn, Infrared photometry of the dust in comets, *Astron. J.*, 89, 162-169, 1984.

Hanner, M.S., G.J. Veeder, and A.T. Tokunaga, The dust coma of comet P/Giacobini-Zinner in the infrared, *Astron. J., 104,* 386-393, 1992.

Howell, R. R., and M.T. McGinn, Infrared speckle observations of 10: An eruption in the Loki region, *Science, 230, 63-64, 1985.*

Howell, R. R., and W.M. Sinton, 10 and Europa: The observational evidence for variability, in Time-Variable Phenomena in the Jovian System, edited by M.J.S. Belton, R.A. West, and J. Rahe, NASA *Spec. Publ., SP-494, 47-62,* 1989.

Hubbard, W. B., Intrinsic luminosities of the Jovian planets, *Rev. Geophys. and Space Phys., 18,* 1-9, 1980.

Johnson, T. V., Galilean satellites: Narrowband photometry 0.30-1.10 microns, *Icarus, 14, 94-111,* 1971.

Johnson, T. V., D.L. Matson, G.J. Veeder, D. Morrison and R.H. Brown, Spatial distribution of hot spots on 10: Implications for heat flow, *Eos Trans.* AGU, 64, 746, 1983.

Johnson, T. V., D. Morrison, D.L. Matson, G.J. Veeder, R.H. Brown, and R.M. Nelson, 10 volcanic hotspots: Stability and longitudinal distribution, Science, 226, 134-137, 1984.

Johnson, T. V., G.J. Veeder, D.L. Matson, R.H. Brown, R.M. Nelson and D. Morrison, 10: Evidence for silicate volcanism in 1986, *Science,* 242, 1280-1283, 1988.

Lebofsky, L. A., and J .R. Spencer, Radiometry and thermal modeling of asteroids, in *Asteroids II,* edited by R. Binzel, T. Gehrels, and M. Matthews, pp. 128-147, University of Arizona Press, Tucson, 1989.

Lieske, J. H., Galilean satellite evolution: Observational evidence for secular change its the mean motion, A.wren. *Astrophys.*, 176, 146-158, 1987.

Lofgren, G. E., and Team 1, Petrology and chemistry of terrestrial, lunar and meteoritic basalts, Basaltic Volcanism Study Project, in *Basaltic Volcanism on the Terrestrial Planets,* pp. 179, Pergamon, New York, 1981.

McEwen, A. S., Global color and albedo variations on 10, *Icarus,* 73, 385-426, 1988.

McEwcn, A. S., N.R.Isbell, K. E.. Edwards, and J.C. Pearl, New Voyager 1 hot spot identifications and the heat flow of 10, *Bull. Am. AsIron. Sot., 24, 935, 1992.*

McEwen, AS., T.V. Johnson, D.L. Matson, and L.A. Soderblom, The global distribution, abundance, and stability of SO_2 on 10, *Icarus, 75, 450-478, 1988.*

McEwen, AS., J.I.Lunine, and M.H. Carr, Dynamic geophysics of 10, in Time-Variable Phenomena in the Jovian System, edited by M.J.S.Belton,R.A. West, and J. Rahe, *NASA Spec.Publ., SP-494, 11-46, 1989.*

McEwcn, A. S., D.L. Matson, T.V. Johnson, and L.A. Soderblom, Volcanic hot spots on 10: Correlation with low-albedo calderas, *J. Geophys. Res., 90,* 12,345-12,379, 1985.

McLeod, B. A., D.W. McCarthy, and J.D. Freeman, Global high-resolution imaging of hotspots on Io, *Astron. J.,* 102, 1485, 1991.

Matson, D. L., G.Ransford, and T.V. Johnson, Heat flow from 10 (J 1), (abstract), *Lunar Planet. Sci., Xl, 686687,* 1980.

Matson, D. L., G. Ransford, and T.V. Johnson, Heat flow from 10, *J. Geophys. Res.,* 86, 1664-1672, 1981.

Matson, D. L., G.J. Veeder, T.V. Johnson, D. I.. Blaney, and J.D. Goguen, A decade's overview of 10's volcanic activity, (abstract), *Lunar Planet.* Sci., *XXIV,* 939-940, 1993.

Matson, D. L., G.J. Veeder and L.A. Lebofsky, Infrared observations of asteroids from Earth and space, in *Asteroids: An Exploration Assessment,* edited by D. Morrison and W.C. Wells, NASA *Conf.Publ., 2053, 127-144, 1978.*

Morrison, D., and D.P. Cruikshank, Thermal properties of the Galilean satellites, *Icarus,* 18, 224-236, 1973.

Morrison, D., D.P. Cruikshank, and R.E. Murphy, Temperatures of Titan and the Galilean satellites at 20p, *Astrophys. J., 173,* L143-L146, 1972.

Morrison, D., and L.A. Lebofsky, Asteroid radiometry, in *Asteroids,* edited by T. Gehrels, pp. 184205, University of Arizona Press, Tucson, 1979.

Morrison, D., and N.D. Morrison, Photometry of the Galilean satellites, in *Planetary* Satellites, edited by J .A. Burns, pp. 363-378, University of Arizona Press, Tucson, 1977.

Morrison, D., N.D. Morrison, and A.R.Lazarewicz, Four-color photometry of the Galilean satellites, Icarus, 23, 399-416, 1974.

Morrison, D., and C.M. Telesco, 10: Observational constraints on internal energy and thermophysics of the surface, *Icarus,* 44, 226-233, 1980.

Nash, D. B., M.H. Carr, J. Gradie, D.M. Hunten, and C.F. Yoder, 10, in *Satellites,* edited by J .A. Bums and M.S. Matthews, pp. 629-688, University of Arizona Press, Tucson, 1986.

Ojakangas, G.W. and D.J. Stevenson, Episodic volcanism of tidally heated satellites with application to Io, *Icarus,* 66, 341-358, 1986.

Peale, S. J., P. Cassen and R.T. Reynolds, Melting of 10 by tidal dissipation, Science, 203, 892-894, 1979.

Pearl, J .C., and W.M. Sinton, Hot spots of 10, in *Satellites of Jupiter,* edited by D. Morrison, pp. 724-755, University of Arizona Press, Tucson, 1982.

Rieke, G. H., M.J.Lebofsky, and F.J. Low, An absolute photometric system at 10 and 20 pm, *Astron. J., 90,* 900-906, *1985.*

Ross, M.M., G. Schubert, T'. Spohn, and R.W.Gaskell, Internal structure of Io and the global distribution of its topography, Icarus, 85, 309-325, 1990.

Sartoretti, P., F. Paresce, M.A. McGrath, V, Dols, and J.-C. Gerard, Imaging of 10 with the faint object camera on HST, International Workshop on Variable Phenomena in Jovian Planetary Systems, Annapolis, Md, 1992.

Segatz, M., T. Spohn, M.N. Ross, and G. Schubert, Tidal dissipation, surface heat flow, and figure of viscoelastic models of 10, *Icarus,* 75, 187-206, 1988.

Simonelli, D. P., and J. Veverka, Voyager disk-integrated photometry of Io, *Icarus, 59, 406-425, 1984.*

Simonelli, D, P., and J. Veverka, Bolometric albedos and diurnal temperatures of the brightest regions on 10, *Icarus, 74, 240-261,* 1988.

Sinton, W.M., 10's 5-μm variability, *Astrophys. J., 2.?5, L49-L51, 1980.*

Sinton, W, M., The thermal emission spectrum of Io and a determination of the heat flux from its hot spots, *J. Geophys. Res.,* 86, 3122-3128, 1981.

Sinton, W. M., Io: A volcanic flow model for the hot spot emission spectrum and a thermostatic mechanism, *Icarus, 51, 563-773,* 1982.

Sinton, W. M., J.D. Goguen, T. Nagata, H.B. Ellis and M. Werner, Infrared polarization measurements of 10 in 1986, *Astron. J., 96, 1095-1105, 1988.*

Sinton, W. M., and C. Kaminski, Infrared observations of eclipses of Io, its thermophysical parameters, and the thermal radiation of the Loki volcano and environs, *Icarus,* 75, '207-232, 1988.

Sinton, W. M., D. Lindwall, F. Cheigh, and W.C. Tittemore, 10: The near-infrared monitoring program, 1979-1981, *Icarus,* 54, 133-157, 1983.

Sinton, W. M., and W.C. Tittemore, Photometric standard stars for L' and M filter bands, *Astron. J., 89, 13661370, 1984.*

Sinton, W. M., A.T. Tokunaga, E.E. Becklin, 1. Gatley, T.J. Lee and C.J. Lonsdale, 10: Ground-based observations of hot spots, Science, 210, 1015-1017, 1980.

Smith, B. A., and the Voyager Imaging Team, The Galilean satellites and Jupiter: Voyager 2 imaging science results, *Science,* 206, 927-950, 1979.

Spencer, J. R., L.A. Lebofsky, and M.V. Sykes, Systematic biases in radiometric diameter determinations, *Icarus, 78, 337-354, 1989.*

Spencer, J. R., M.A. Shure, M.E. Ressler, J. D. Goguen, W.M. Sinton, D.W. Toomey, A. Denault, and J. Westfall, Discovery of hot spots on 10 using disk resolved infrared imaging, *Nature, 348, 618-621, 1990.*

Stevenson, D. J., and S.C. McNamara, Background heatflow on hotspot planets: 10 and Venus, *Geophys. Res. Lett., 15,* 1455-1458, 1988.

Tittemore, W. C., and W.M. Sinton, Near-infrared photometry of the Galilean satellites, *Icarus,* 77, 82-97, 1987.

Tokunaga, A. T., A revaluation of the 20-μm magnitude system, *Astron. J.,* 89, 172, 1984.

Tokunaga, A. T., W.F. Golisch, D.M. Griep, C.D. Kaminski, and M.S. Hanner, The NASA infrared telescope facility comet Halley monitoring program, 1, Preperihelion results, *Astron. J., 92, 1183-1190, 1986.*

Veeder, G. J., D.L. Blaney, D. I.. Matson, T.V. Johnson, and J.D. Goguen, Infrared radiometry of 10: Thermal anomalies and heat flow for the past decade, *Io: An International Conference,* Capistrano Conf. No. 3, San Juan Capistrano Research Institute, San Juan Capistrano, Calif., 115-116, 1993.

Veeder, G, J., M.S.Hanner, D.L. Matson, E.F.Tedesco, L.A. Lebofsky, and A.T. Tokunaga, Radiometry of near-Earth asteroids, A.wren, J., 97, 1211-1219, 1989.

Veverka, J., Photometry of satellite surfaces, in *Planetary Satellites*, edited by J.A. Burns, pp. 171-209, University of Arizona Press, Tucson, 1977.

Veverka, J., T, V. Johnson, D.L. Matson, and K.Housen, The physical characteristics of satellite surfaces, in *Satellites*, edited by J. A. Burns and M S. Matthews, pp. 342-402, University of Arizona Press, Tucson, 1986.

Witteborn, F, C., J.D.Bregman and J.B.Pollack, 10: An intense brightening near 5 micrometers, *Science, 203*, 643-646, 1979.

Yoder, C. F., How tidal heating in Io drives the Galilean orbital resonance locks, *Nature*, 279, 767-770, 1979.

Yoder, C. F., and S.J. Peale, The tides of 10, *Icarus, 47, 1-35, 1981.*

D.L. Blaney, J.D. Goguen, T.V. Johnson, D.L. Matson, and G.J. Veeder, Mail Stop 183-501, Jet Propulsion Laboratory, 4800 Oak Grove Drive, Pasadena, CA 91109-8099.

(Received June 28, 1993; revised February 23, 1994; accepted March 8, 1994.)

Paper number 94JE00637.
01 48-0227 /94/94JE-O0637$05 .00

Figure 1. Io's infrared spectral components. The "hotspot" and "background" curves are from our model for August 3, 1986 (UT), with Loki on the central meridian (309°W). The background curve contains only the passive background component. The reflected solar component (which dominates at short wavelengths) corresponds to an albedo of 0.44. Detailed spectral features, such as SO_2 frost absorption, are not shown. The thermal anomaly emission (including the active background) peaks near 13 pm. Passive background emission dominates at long wavelengths, but emission from thermal anomalies remains significant.

Figure 2. Io's 4.8 μm (M) emittance (W m^{-2} μm^{-1}) versus west longitude (of the sub-Earth point) for apparitions from 1983 to 1993, Reflected sunlight has been subtracted. The longitude scale spans 1.5 revolutions. Consequently, the observations from Table 2 between O" and 180°W are plotted twice. Two large outbursta are evident: the first on August 7, 1986 (UT) (seen near 90°W), and the second on January 9, 1990 (UT) (seen near 330°W). The solid curve is our model fit. Temperatures and areas for the model hotspots are listed in Table 9. Model curves calculated for the outbursts are shown in Figure 9.

Figure 3. 10's 8.7 μm emittance ($W m^{-2} \mu m^{-1}$) versus west longitude. The outbursts during August 7, 1986 (UT) (seen near 90" W), and during January 9, 1990 (UT) (seen near 330 °W), are not as strong as at 4.8 μm (Figure 2). The upper solid curve is our model fit. The lower solid curve (just above the bottom of the frame) is the passive background caused by the heating the surface by insolation. (See also caption for Figure 2).

Figure 4. Io's 10 μm (N) emittance ($W m^{-2} \mu m^{-1}$) versus west longitude. The outbursts during August 7, 1986 (UT) (seen near 90" W), and during January 9, 1990 (UT) (seen near 3300 W), are only barely noticeable. (See also caption for Figure 2).

Figure S. 10's 20 μm (Q) emittance ($W m^{-2} \mu m^{-1}$) versus west longitude. The upper solid curve is our model fit. The lower solid curve is the model passive background which is caused by the heating of the surface by insolation. 10's albedo distribution controls the variation with longitude of the passive background which is the largest component of the 20 μm emission. (See also caption for Figure 2).

Figure 6. Jo's emittance spectra for August 3, 1986 (UT). (a) The data are shown as solid circles (daytime) and open triangles (in eclipse). The solid and dotted curves are our model fits. The components of the model at each wavelength are given in Table 7. The dashed curve is a "standard" thermophysical model (see appendix note 5) based on the bolometric Bond albedo of 0.44 from Voyager data at 340°W longitude [*McEwen et al.*, 1988] (see also section 4. 1). This curve illustrates the problem of attempting to match the 20 μm data with conventional models. (b) Comparison of passive background model spectra with the standard model from Figure 6a.

Figure 7. Emittance spectra illustrating the thermal pedestal effect. (a) An example of a hotspot with a nighttime temperature of 32S K and a (higher) daytime temperature of331 K due to heating by sunlight. The spectrum of the active background is the difference between these two curves. (b) The active background components for a hotspot with a bolometric Bond albedo of 0.29 (and emissivity of 0.9) as a function of its nighttime geothermal and daytime temperatures. Note that the power is the same for each curve, even though the spectral distribution is different, The lowest spectrum is the degenerate case without any thermal anomaly (in this case, the geothermal temperature is identically O K and the temperature at equilibrium with insolation is 140 K). Thus, the spectrum of the absorbed solar power is blue shifted from the longer wavelengths expected for a passive reradiation spectrum.

Figure 8. Overlay of all the 10 models for the 1983-1993 apparitions. The curves include both the anomaly and the background emittance for 4.8, 8.7, and 20 μm. These plots show both the *general* stability of the shape of the light curves, the locations of the thermal anomalies, and their variation in intensity. The variation at 4.8 μm is significantly larger than at longer wavelengths,

Figure 9. Emittance versus longitude of the sub-Earth point for the outbursts of August 7, 1986, and January 9, 1990 (UT), compared with model calculations at 4.8 and 8.7 μm. (Note that for a given event time. increases towards the left). Available "nonoutburst" data for these apparitions are also included, The thermal emission at 4.8 μm is plotted after removal of the reflected component. The curves labeled "model" correspond to our fits for the entire apparition. The curves for the passive background at 8.7 μm are labeled as "background." The differences between the model and background curves are due to the emission from the hotspots including the pedestal effect. The curves labeled with values for T and r show the result of adding the thermal emittance from a hotspot of the indicated temperature and radius to the model for the apparition. For the 1986 outburst, the model hotspot was placed on the equator. For 1990, the event was assumed to be located at Loki.

Figure 10. Heat flow histories of the thermal anomalies for the 1983-1993 apparitions. In addition to the total, power levels are also binned by temperature as indicated (see also Table 10).

Figure 11. Io heat flow during the 1983-1993 apparitions. (a) In addition to the total, power levels are also binned by temperature as indicated (see also Table 11). (b) Leading and trailing (i.e., Loki) hemispheres compared to the total (see also Table 11).

Figure 12. Surface area versus temperature log-log plot for Io's hotspots. The diagonal lines are contours of constant emitted power (10^9 to 10^{14} W). (a) All of the thermal anomalies for the 1983-1993 apparitions. (b) Hotspots for each apparition binned by 100 K increments compared with results from *McEwen et al. [1992].*

Figure 13. Comparison of Io's heat flow determinations with calculations of tidal dissipation and other power values from the literature. The heat flow for two values of Q_{Io} (50 and 100) and the upper limit from the orbital evolution are from *Cassen* et al. [1982] following the method of *Goldreich and Sorer [1966].* The upper limit from the rate of orbital acceleration for tbe last 300 years is from *Greenberg's [1987]* analysis of data from *Lieske* [1987]. These estimates all are significantly lower than the observed heat flow values determined from thermal emission. Heating by the decay of radiogenic elements and heating by electrical induction are 2 orders of magnitude smaller and plot off scale.

Figure 1. 10's infrared spectral components. The "hotspot" and "background" curves are from our model for August 3, 1986 (UT), with Loki cm the central meridian (309" W). The background curve contains only the passive background component. The reflected solar component (which dominates at short wavelengths) corresponds to an albedo of 0.44. Detailed spectral features, such as SO_2 frost absorption, are not shown. The thermal anomaly emission (including the active background) peaks near 13 μm. Passive background emission dominates at long wavelengths, but emission from thermal anomalies remains significant.

Figure 2. 10's 4.8 μm (M) emittance (W m^{-2} μm^{-1}) versus west longitude (of the sub-Earth point) for apparitions from 1983 to 1993. Reflected sunlight has been subtracted. The longitude scale spans 1.5 revolutions. Consequently, the observations from Table 2 between 0° and 180°W are plotted twice. 'I'wo large outbursts are evident: the. first on August 7, 1986 (UT) (seen near 90°W), and the second on January 9, 1990 (UT) (seen near 330°W). The solid curve is our model fit. Temperatures and areas for the model hotspots are listed in Table 9. Model curves calculated for the outbursts are shown in Figure 9.

Figure 3. Io's 8.7 μm emittance (W m^{-2} μm^{-1}) versus west longitude. The outbursts during August 7, 1986 (UT) (seen near 90°W), and during January 9, 1990 (UT) (seen near 330°W), are not as strong as at 4.8 μm (Figure 2). The upper solid curve is our model fit. The lower solid curve (just above the bottom of the frame) is the passive background caused by the heating the surface by insolation. (See also caption for Figure 2).

Figure 4. Io's 10pm (N) emittance (W m^{-2} μm^{-1}) versus west longitude. Tbe outbursts during August 7, 1986 (UT) (seen near 90°W), and during January 9, 1990 (UT) (seen near 330°W), are only barely noticeable. (See also caption for Figure 2).

Figure 5. Io's 20pm (Q) emittance (W m^{-2} pm^{-1}) versus west longitude. The upper solid curve is our model tit. The lower solid curve is tbe model passive background which is caused by the heating of the surface by insolation. Io's albedo distribution controls the variation with longitude of the passive background which is the largest component of the 20 μm emission. (See also caption for Figure 2).

Figure 6. Io's emittance spectra for August 3, 1986 (UT). (a) Tbe data are shown as solid circles (daytime) and open triangles (in eclipse). The solid and dotted curves are our model fits. The components of the model at each wavelength are given in Table 7. The dashed curve is a "standard" thermophysical model (see appendix note 5) breed on tJre bolometric Bond albedo of 0.44 from Voyager data at 340° W longitude [*McEwen et al., 1988] (see* also section 4. 1). This curve illustrates the problem of attempting to match the 20 μm data with conventional models. (b) Comparison of passive background model spectra with the standard model from Figure 6a.'

Figure 7. Emittance spectra illustrating the thermal pedestal effect. (a) An example of a hotspot with a nighttime temperature of 325 K and a (higher) daytime temperature of 331 K due to heating by sunlight. The spectrum of the active background is the difference between these two curves. (b) The active background components for a hotspot with a bolometric Bond albedo of 0.29 (and emissivity of 0.9) as a function of its nighttime geothermal and daytime temperatures. Note that the power is the same for each curve, even though the spectral distribution is different. Tbe lowest spectrum is the degenerate case without any thermal anomaly (in this case, the geothermal temperature is identically O K and the temperature at equilibrium with in.solatlon is 140 K). Thus, the spectrum of the absorbed solar power is blue shifted from the longer wavelengths expected for a passive reradiation spectrum.

Figure 8. Overlay of all the 10 models for the 1983-1993 apparitions. The curves include both the anomaly and the background emittance for 4.8, 8.7, and 20 pm. These plots show both the general stability of the shape of the light curves, the locations of the thermal anomalies, and their variation in intensity. The variation at 4.8 μm is significantly larger than at longer wavelengths.

Figure 9. Emittance versus longitude of the sub-Earth point for the outbursts of August 7, 1986, and January 9, 1990 (UT), compared with model calculations at 4.8 and 8.7 μm. (Note that for a given event time increases towards the left). Available "nonoutburst" data for these apparitions are also included. The thermal emission at 4.8 μm is plotted after removal of the reflected component. The curves labeled "model" correspond to our fits for the entire apparition. The curves for the passive background at 8.7 μm are labeled as "background." The differences between the model and background curves are due to the emission from the hotspots including the pedestal effect. The curves labeled with values for T and r show the result of adding the thermal emittance from a hotspot of the indicated temperature and radius to the model for the apparition. For the 1986 outburst, the model hotspot was placed on the equator. For 1990, the event was assumed to be located at Loki.

Figure 10. Heat flow histories of the thermal anomalies for the 1983-1993 apparitions. In addition to the total, power levels are also binned by temperature as indicated (see also Table 10).

Figure 11. Io heat flow during the 1983-1993 apparitions. (a) In addition to the total, power levels are also binned by temperature as indicated (see also Table 11). (b) Leading and trailing (i.e., Loki) hemispheres compared to the total (see also Table 11).

Figure 12. Surface area versus temperature log-log plot for Io's hotspots. The diagonal lines are contours of constant emitted power (10^9 to 10^{14} W). (a) All of the thermal anomalies for the 1983-1993 apparitions. (b) Hotspots for each apparition binned by 100 K increments compared with results from *McEwen et al. [1992].*

Figure 13. Comparison of Io's heat flow determinations with calculations of tidal dissipation and other power values from the literature. The heat flow for two values of Q_{Io} (50 and 100) and the upper limit from the orbital evolution are from *Cassen et al. [1982]* following the method of *Goldreich and Soter* [1966]. The upper limit from the rate of orbital acceleration for the last 300 years is from *Greenberg's* [1987] analysis of data from *Lieske [* 1987]. These estimates all are significantly lower than the observed heat flow values determined from thermal emission. Heating by the decay of radiogenic elements and heating by electrical induction are 2 orders of magnitude smaller and plot off scale.

Date (UT)	Solar Phase Angle (deg)	r (AU)	Δ (AU)	Longitude Range (deg West)	Observers[1] and Operators[2]
80/04/12	8 4	5 40	4.72	20-35	DM
82/03/19	7 0	5 44	4 66	342-343	WS
83/02/18	10 4	5 38	5.46	326-344	AT, RN
83/03/06	10 6	5 38	5 20	339-340	GV, ET, CK, LL
83/03/11	10 5	5.38	5 12	101-103	GV, ET, LL, CK
83/04/24	6 4	5 36	4 57	36	WS
83/07/19	8 9	5 34	4 68	50 64	RB, TJ
83/07/20	9 0	5 34	4 70	234-271	GV, DM, CK
83/07/21	9 1	5.34	4 71	73-111	GV, DM, DG
83/08/07	10 4	5 33	4 94	316-328	GV, MH, JH
83/08/27	10 9	5.33	5 25	24-27	WS
84/05/08	9 1	5.24	4.60	113-130	GV, ET, WG
84/06/27	0 6	5.22	4 21	194	RB
84/07/19	4 0	5.22	4 25	322-336	DLM, GV, M
84/08/19	9 0	5 21	4 53	151-168	DLM, TJ, DM, M
84/08/20	9 1	5 20	4 54	347-20	DLM, TJ, DM, M
85/06/06	10.1	5.10	4.54	325-335	GV, RB, WG
85/06/07	10 0	5 10	4.53	162 164	GV, RB, WG, RN, AL,DLM
85/06/08	9 9	5 10	4 51	20 35	GV, RN, AL, DLM, WG
85/06/09	9 8	5 10	4 50	212-231	GV, RN, AL, DLM, WG
85/06/10	9 7	5.10	4 49	60-69	GV, WG, DLM
85/07/09	5 5	5 09	4 17	198-200	DLM, TJ, GV, WG
85/07/10	5 2	5 09	4 16	21-68	GV, WG, DLM, TJ
85/07/11	5 1	5 09	4.16	226-284	GV, DM, WG
85/07/12	4 9	5 09	4 15	70 99	GV, DM, WG
85/09/12	7 6	5 06	4 26	76-88	LL, GV, MH, AT, DG
86/06/25	11 6	4.99	4 70	312-323	DLM, JG
86/07/02	11 2	4 99	4 60	302-320	GV, LL, CK
86/08/03	7 8	4 99	4.18	311-346	GV, RB, DG
86/08/04	7 6	4 99	4.17	148-156	GV, RB, DG
86/08/05	7 5	4 98	4 16	16 42	GV, RB, CK
86/08/06	7.3	4 98	4.15	201-243	GV, RB, DLM, CK
86/08/07	7 1	4 98	4.14	48 89	GV, DLM, CK
86/08/08	7 0	4 98	4 13	259-260	GV, DLM, CK
87/09/28	4 5	4 95	4 02	281-309	GV DLM, TJ, DG
87/11/23	7.2	4 96	4 55	115-160	DLM, GV, TJ, RN, DG
87/11/25	7 6	4 96	4 58	152-207	DLM, GV, TJ, RN, WG
87/11/26	7 8	4 96	4 59	19-47	DLM, GV, WG
88/11/16	1 6	5 02	4 04	49 81	RB, RD
89/01/18	9 9	5 04	4 50	286 310	DLM, GV, DG
89/12/12	3 4	5.14	4 20	36-93	GV, DLM, CK
89/12/14	3 0	5.14	4 19	69-141	DLM, GV, JG, DG
89/12/15	2 7	5 14	4.19	319-344	DLM, GV, WG
89/12/16	2 5	5 15	4 18	115-147	DLM, GV, HH, WG
90/01/06	2 0	5 15	4 18	71-121	DLM, CK
90/01/07	2 3	5.15	4 19	266 334	DLM, GV, CK
90/01/08	2 5	5 15	4 19	111-168	DLM, GV, CK
90/01/09	2 7	5 15	4 20	324-249	DLM, GV, CK
90/01/10	2 9	5 15	4 20	164-223	DLM, GV, CK
92/02/04	5 0	5 40	4 51	58-71	JG, DB, GV, DG
92/02/05	4 8	5 40	4 50	246-275	JG, DB, GJ, DG, WG
92/02/07	4 4	5 40	4 49	280-339	JG, DB, GV, WG
92/02/08	4 2	5 40	4 49	125-148	JG, DB, GV, WG
93/03/25	1 2	5 45	4 46	195-255	JG, DB, GV, DG
93/03/26	1 0	5 45	4 46	33-100	JG, DB, GV, DG
93/03/27	0 8	5 45	4 46	236-305	JG, DB, GV, WG
93/03/28	0 4	5 45	4 46	79-139	JG, DB, GV, WG
93/03/29	0 1	5 45	4 46	283-347	JG, DB, GV, WG

The tabulated columns are the UT date, solar phase angle in degrees, heliocentric distance in AU, geocentric distance in AU the range of orbital phase covered in °W longitude, and the observers and telescope operators. The observers and operators are designated by their initials and are presented below.

1. Telescope Observers:

AL = Arthur Lane
AT = Alan Tokunaga
DB = Diana Blaney
DM = Dave Morrison
DLM = Dennis Matson
ET = Edward Tedesco
GV = Glenn Veeder
JG = Jay Goguen
HH = Heidi Hammel
LL = Larry Lebofsky
MH = Martha Hanner
RB = Robert Brown
RD = Richard Dailey
RN = Robert Nelson
TJ = Torrence Johnson
WS = William Sinton

2. Telescope Operators:

CK = Charlie Kaminski
DG = Dave Griep
JH = John Hamilton
M = Miller
WG = William Golish

Table 2. M (4.8 μm) Photometry of Io (J1).

Date (UT)	Time (UT)	Orbital Phase Angle (deg.)	Observed			Calculated Flux Densities		Spectral Emittance (10^{-2} Wm$^{-2}\mu$m^{-1})
			Magnitude	Flux (Jy)	Flux (10^{-17} W m$^{-2}\mu$m^{-1})	Reflected Sunlight (10^{-17} W m$^{-2}\mu$m^{-1})	Thermal Emission (10^{-17} W m$^{-2}\mu$m^{-1})	
80/04/12		20	3.05	9.26	12.0	4.95	7.10	10.7
83/02/18		327	3.62	5.48	7.13	3.36	3.77	7.64
83/02/18		333	3.66	5.28	6.87	3.36	3.51	7.11
83/02/18		337	3.63	5.42	7.06	3.36	3.70	7.50
83/02/18		339	3.63	5.42	7.06	3.36	3.70	7.50
83/02/18		342	4.53	2.37	3.08	0.00	3.08	6.24
83/02/18		343	4.53	2.37	3.08	0.00	3.08	6.24
83/02/18		344	4.41	2.64	3.44	0.00	3.44	6.97
83/03/11	1502	101	3.40	6.70	8.73	4.42	4.31	7.66
83/03/11	1513	103	3.43	6.52	8.48	4.42	4.06	7.23
83/03/11	1515	103	3.38	6.80	8.86	4.42	4.43	7.89
83/07/19	825	52	3.58	5.68	7.40	5.32	2.08	3.10
83/07/19	835	53	3.57	5.73	7.47	5.32	2.15	3.20
83/07/19	902	58	3.61	5.53	7.19	5.32	1.88	2.80
83/07/19	916	60	3.60	5.58	7.26	5.39	1.88	2.79
83/07/19	940	63	3.60	5.58	7.26	.39	1.88	2.79
83/07/20	557	234	3.52	6.00	7.82	16	2.65	3.97
83/07/20	559	235	3.52	6.00	7.82	5 16	2.65	3.97
83/07/20	610	237	3.48	6.23	8.11	5 16	2.95	4.41
83/07/20	757	252	3.47	6.29	8.19	5.10	3.09	4.62
83/07/20	813	254	3.46	6.34	8.26	5.10	3.16	4.74
83/07/20	844	259	3.41	6.64	8.65	5.10	3.55	5.32
83/07/20	858	261	3.41	6.64	8.65	5.05	3.60	5.39
83/07/20	921	265	3.40	6.70	8.73	5.05	3.68	5.51
83/07/20	936	266	3.43	6.52	8.49	5.05	3.44	5.15
83/07/20	956	269	3.38	6.83	8.89	5.05	3.84	5.75
83/07/20	1009	271	3.32	7.22	9.40	4.99	4.40	6.59
83/07/21	522	73	3.44	5.89	7.67	5.40	2.28	3.43
83/07/21	531	74	3.44	5.89	7.67	5.40	2.28	3.43
83/07/21	554	78	3.44	5.89	7.67	5.40	2.28	3.43
83/07/21	615	81	3.59	5.63	7.33	5.47	1.86	2.80
83/07/21	704	88	3.50	6.11	7.96	5.47	2.50	3.76
83/07/21	734	92	3.54	5.89	7.67	5.49	2.19	3.29
83/07/21	755	95	3.51	6.06	7.89	5.49	2.40	3.62
83/07/21	933	109	3.55	5.84	7.60	5.46	2.15	3.23
83/07/21	941	111	3.54	5.99	7.67	5.39	2.29	3.44
83/08/07	814	317	3.49	6.17	8.04	4.19	3.84	6.37
83/08/07	830	319	3.43	6.52	8.49	4.19	4.30	7.13
83/08/07	842	321	3.50	6.11	7.96	4.17	3.79	6.29
83/08/07	854	324	3.54	5.89	7.67	4.17	3.50	5.81

Table 2. M (4.8 μm) Photometry of Io (J1) (continued).

Date (UT)	Time (UT)	Orbital Phase Angle (deg.)	Observed			Calculated Flux Densities		Spectral Emittance (10^{-2} Wm$^{-2}\mu$m^{-1})
			Magnitude	Flux (Jy)	Flux (10^{-17} W m$^{-2}\mu$m^{-1})	Reflected Sunlight (10^{-17} W m$^{-2}\mu$m^{-1})	Thermal Emission (10^{-17} W m$^{-2}\mu$m^{-1})	
83/08/07	907	326	3.43	6.52	8.49	4.17	4.32	7.17
84/06/27		194	3.11	8.80	11.5	8.08	3.38	4.06
84/07/19	659	323	2.98	9.90	12.9	6.71	6.19	7.59
84/07/19	721	326	3.00	9.72	12.7	6.71	5.95	7.31
84/07/19	804	332	2.97	10.0	13.0	6.72	6.30	7.73
84/07/19	817	334	2.97	9.94	12.9	6.72	6.22	7.63
84/08/19	653	153	3.48	6.23	8.11	5.97	2.14	2.99
84/08/19	728	158	3.38	6.83	8.89	5.97	2.93	4.08
84/08/19	814	164	3.40	6.70	8.73	5.95	2.78	3.87
84/08/19	823	165	3.41	6.64	8.65	5.95	2.70	3.75
84/08/19	837	167	3.39	6.77	8.81	5.95	2.86	3.98
84/08/20		16	4.61	2.20	2.86	0.00	2.86	4.01
84/08/20	1016	20	3.37	6.89	8.97	5.68	3.29	4.61
85/06/06	1148	325	3.71	5.04	6.56	5.44	1.13	1.58
85/06/06	1159	327	3.67	5.23	6.81	5.44	1.37	1.92
85/06/06	1239	332	3.43	6.52	8.49	5.45	3.05	4.26
85/06/06	1247	334	3.44	6.46	8.41	5.45	2.97	4.15
85/06/06	1257	335	3.49	6.17	8.04	5.45	2.59	3.62
85/06/07	1103	162	3.40	6.70	8.73	6.09	2.64	3.67
85/06/07	1104	163	3.39	6.77	8.81	6.09	2.72	3.78
85/06/08	1246	21	3.46	6.34	8.26	5.89	2.37	3.27
85/06/08	1316	25	3.46	6.34	8.26	5.89	2.37	3.27
85/06/08	1359	31	3.45	6.40	8.34	5.97	2.37	3.27
85/06/08	1423	35	3.44	6.46	8.41	5.97	2.44	3.38
85/06/09	1125	213	3.40	6.70	8.73	6.10	2.63	3.62
85/06/09	1208	219	3.39	6.77	8.81	6.10	2.71	3.73
85/06/09	1227	221	3.38	6.83	8.89	6.08	2.81	3.86
85/06/09	1245	224	3.37	6.89	8.97	6.08	2.89	3.97
85/06/09	1254	225	3.35	7.02	9.14	6.08	3.06	4.20
85/06/09	1303	226	3.36	6.96	9.06	6.08	2.97	4.08
85/06/10	1154	60	3.43	6.52	8.49	6.33	2.16	2.95
85/06/10	1203	62	3.42	6.58	8.57	6.33	2.24	3.06
85/06/10	1213	63	3.45	6.40	8.34	6.33	2.01	2.74
85/06/10	1227	65	3.36	6.96	9.06	6.33	2.73	3.72
85/06/10	1236	66	3.37	6.89	8.97	6.33	2.64	3.61
85/06/10	1246	68	3.39	6.77	8.81	6.33	2.48	3.39
85/06/10	1256	69	3.38	6.83	8.89	6.33	2.56	3.50
85/07/09	1117	198	3.27	7.56	9.84	7.83	2.01	2.38
85/07/10	855	22	3.27	7.56	9.84	7.64	2.20	2.58
85/07/10	1019	34	3.23	7.84	10.2	7.74	2.47	2.90
85/07/10	1142	46	3.20	8.06	10.5	7.84	2.65	3.12

Table 2. M (4.8 μm) Photometry of Io (J1) (continued).

Date (UT)	Time (UT)	Orbital Phase Angle (deg.)	Observed			Calculated Flux Densities		Spectral Emittance (10^{-2} $Wm^{-2}\mu m^{-1}$)
			Magnitude	Flux		Reflected Sunlight (10^{-17} $Wcm^{-2}\mu m^{-1}$)	Thermal Emission (10^{-17} $Wcm^{-2}\mu m^{-1}$)	
				(Jy)	(10^{-17} $Wcm^{-2}\mu m^{-1}$)			
85/07/10	1403	91	3.15	8.22	11.0	8.08	2.91	3.43
85/07/10	1414	67	3.16	8.36	11.09	8.08	2.91	3.43
85/07/11	900	232	3.27	7.56	9.84	7.87	1.97	2.31
85/07/11	947	233	3.26	7.63	9.90	7.85	2.09	2.45
85/07/11	1016	237	3.22	7.91	10.3	7.85	2.46	2.89
85/07/11	1036	240	3.22	7.91	10.3	7.85	2.46	2.89
85/07/11	1046	241	3.23	7.84	10.2	7.82	2.39	2.81
85/07/11	1207	253	3.19	8.14	10.6	7.70	2.85	3.34
85/07/11	1226	255	3.18	8.21	10.7	7.74	2.95	3.46
85/07/11	1249	258	3.17	8.29	10.8	7.70	3.05	3.57
85/07/11	1312	262	3.18	8.21	10.7	7.67	3.02	3.54
85/07/11	1352	267	3.17	8.29	10.8	7.67	3.12	3.66
85/07/11	1434	273	3.16	8.36	10.9	7.59	3.30	3.87
85/07/11	1456	277	3.18	8.21	10.7	7.59	3.01	3.64
85/07/11	1531	281	3.20	8.06	10.5	7.49	3.00	3.52
85/07/11	1541	283	3.16	8.36	10.9	7.49	3.40	3.99
85/07/11	1548	284	3.12	8.52	11.1	7.49	3.60	4.22
85/07/12	905	70	3.28	7.49	9.75	8.32	1.29	1.67
85/07/12	953	71	3.17	8.29	10.8	8.32	2.47	2.89
85/07/12	1004	72	3.17	8.29	10.8	8.32	2.47	2.89
85/07/12	1046	85	3.09	8.92	11.6	8.43	3.19	3.72
85/07/12	1109	88	3.10	8.80	11.5	8.43	3.08	3.60
85/07/12	1230	99	3.18	8.21	10.7	8.46	2.23	2.61
85/09/12	712	78	3.23	7.86	10.2	7.52	2.71	3.36
85/09/12	815	87	3.22	7.94	10.3	7.62	2.72	3.36
86/06/25	1208	312	3.65	5.31	6.92	5.17	1.75	2.62
86/06/25	1221	314	3.59	5.63	7.33	5.17	2.16	3.16
86/06/25	1250	318	3.63	5.42	7.05	5.17	1.88	2.83
86/06/25	1315	322	3.62	5.47	7.12	5.14	1.96	2.97
86/07/02	1251	302	3.46	6.30	8.19	5.50	2.76	3.96
86/07/02	1259	304	3.45	6.40	8.34	5.50	2.84	4.07
86/07/02	1324	307	3.46	6.34	8.26	5.50	2.76	3.96
86/07/02	1336	309	3.44	6.46	8.42	5.50	2.92	4.18
86/07/02	1424	316	3.49	6.17	8.04	5.45	2.59	3.71
86/07/02	1434	318	3.45	6.40	8.34	5.45	2.89	4.14
86/07/02	1446	319	3.46	6.34	8.26	5.45	2.81	4.03
86/08/03	1003	311	3.25	7.71	10.0	7.07	2.97	3.51
86/08/03	1023	314	3.25	7.71	10.0	7.07	2.96	3.51
86/08/03	1043	317	3.24	7.79	10.1	7.07	3.07	3.65
86/08/03	1136	324	3.26	7.69	9.96	7.03	2.92	3.47
86/08/03	1139	325	3.25	7.73	10.1	7.03	3.03	3.60

Table Z, M(4.8μm)Photometryof Io(J1)(continued).

Date (UT)	Time (UT)	Orbital Phase Angle (deg.)	Observed			Calculated Flux Densities		Spectral Emittance (10^{-2} $Wm^{-2}\mu m^{-1}$)
			Magnitude	Flux		Reflected Sunlight (10^{-17} $Wcm^{-2}\mu m^{-1}$)	Thermal Emission (10^{-17} $Wcm^{-2}\mu m^{-1}$)	
				(Jy)	(10^{-17} $Wcm^{-2}\mu m^{-1}$)			
6/08/03	1222	331	3.24	7.80	10.2	7.05	3.11	3.70
6/08/03	1251	336	3.25	7.69	10.0	7.05	2.97	3.53
6/08/03	1318	339	3.25	7.68	10.0	7.05	2.95	3.51
6/08/03	1351	341	3.63	5.43	7.07	0.00	7.07	8.39
6/08/03	1408	346	3.98	1.57	2.05	0.00	2.05	2.43
6/08/04	916	148	3.08	8.98	11.7	7.92	3.77	4.46
6/08/04	926	150	3.12	8.68	11.3	7.92	3.38	3.99
6/08/04	945	152	3.14	8.49	11.1	7.89	3.16	3.73
6/08/04	956	154	3.15	8.42	10.9	7.89	3.08	3.63
6/08/05	1218	18	3.29	7.39	9.65	7.53	2.10	2.47
6/08/05	1234	20	3.29	7.41	9.65	7.62	2.03	2.38
6/08/05	1248	22	3.29	7.44	9.69	7.62	2.07	2.43
6/08/05	1325	27	3.30	7.58	9.86	7.62	2.24	2.63
6/08/05	1340	29	3.30	7.60	9.90	7.62	2.28	2.68
6/08/05	1356	32	3.26	7.95	9.96	7.72	2.24	2.63
6/08/05	1431	37	3.25	7.81	10.0	7.72	2.31	2.72
6/08/05	1446	39	3.25	7.70	10.0	7.72	2.30	2.71
6/08/05	1459	41	3.30	7.80	10.1	7.82	2.25	2.65
6/08/06	1004	202	3.18	8.18	10.7	7.91	2.74	3.21
6/08/06	1201	205	3.17	8.30	10.8	7.91	2.89	3.38
6/08/06	1216	207	3.18	8.22	10.7	7.91	2.80	3.27
6/08/06	1412	237	3.17	8.26	10.7	7.84	2.91	3.41
6/08/06	1443	242	3.16	8.33	10.9	7.81	3.04	3.55
6/08/07	1211	67	1.69	32.43	42.2	8.79	34.0	39.6
6/08/07	1333	79	1.85	27.9	36.4	8.32	28.0	32.7
6/08/07	1350	81	1.88	27.23	35.5	8.32	27.0	31.5
6/08/07	1422	86	1.94	25.62	33.0	8.43	24.9	29.0
6/08/07	1436	88	1.96	25.23	32.9	8.43	24.4	28.4
6/08/08	1501	260	3.12	8.71	11.3	7.87	3.47	4.03
87/09/28	1205	283	2.99	9.80	12.8	8.58	4.18	4.58
87/09/28	1227	286	2.99	9.76	12.7	8.58	4.14	4.53
87/09/28	1305	292	3.00	9.65	12.6	8.57	4.11	4.50
87/09/28	1419	302	2.97	9.96	13.0	8.07	4.60	5.03
87/09/28	1454	307	3.02	9.55	12.4	8.37	4.06	4.45
87/09/28	1505	308	3.03	9.42	12.3	8.37	3.90	4.27
87/11/23	654	121	3.03	9.42	12.3	6.93	5.34	7.49
87/11/23	742	127	3.06	9.43	12.3	6.93	5.34	7.50
87/11/23	818	133	3.08	9.27	12.1	6.88	5.18	7.28
87/11/23	832	135	3.05	9.30	12.1	6.88	5.22	7.33
87/11/23	926	147	3.10	8.86	11.5	6.79	4.74	6.66
87/11/23	1054	154	3.10	8.83	11.5	6.77	4.73	6.64
87/11/23	1125	159	3.05	9.30	12.1	6.77	5.34	7.49
87/11/25	506	153	3.14	8.53	11.1	6.63	4.48	6.37
87/11/25	538	157	3.10	8.50	11.1	6.69	4.44	6.31
87/11/25	612	162	3.11	8.72	11.4	6.69	4.75	6.75
87/11/25	627	164	3.10	8.87	11.6	6.61	4.94	7.02
87/11/25	642	166	3.04	9.38	12.2	6.69	5.60	7.96

Table 2. M (4.8 μm) Photometry of Io (J1) (continued)

Date (UT)	Time (UT)	Orbital Phase Angle (deg.)	Observed			Calculated Flux Densities		Spectral Emittance (10^{-2} $Wm^{-2}\mu m^{-1}$)
			Magnitude	Flux		Reflected Sunlight (10^{-17} $Wcm^{-2}\mu m^{-1}$)	Thermal Emission (10^{-17} $Wcm^{-2}\mu m^{-1}$)	
				(Jy)	(10^{-17} $Wcm^{-2}\mu m^{-1}$)			
87/11/25	1037	199	3.24	7.75	10.1	6.56	3.52	5.01
87/11/25	1051	201	3.24	7.78	10.1	6.54	3.59	5.11
87/11/25	1122	206	3.22	7.93	10.3	6.54	3.78	5.37
87/11/26	756	20	3.26	7.60	9.89	6.28	3.61	5.17
87/11/26	810	22	3.22	7.89	10.3	6.28	3.99	5.72
87/11/26	930	33	3.23	7.85	10.2	6.36	3.86	5.53
87/11/26	948	36	3.24	7.76	10.1	6.36	3.74	5.36
87/11/26	1100	46	3.17	8.31	10.8	6.45	4.37	6.26
88/11/16	806	51	3.04	9.34	12.2	9.38	2.78	3.08
88/11/16	807	51	3.05	9.27	12.1	9.38	2.70	2.99
88/11/16	834	54	3.03	9.39	12.2	9.38	2.85	3.16
88/11/16	836	55	3.03	9.42	12.3	9.38	2.89	3.19
88/11/16	837	55	3.04	9.36	12.2	9.38	2.82	3.12
88/11/16	851	57	3.02	9.47	12.3	9.38	2.96	3.27
88/11/16	852	57	3.02	9.53	12.4	9.38	3.03	3.35
88/11/16	956	66	3.06	9.15	11.9	9.50	2.42	2.68
88/11/16	957	66	3.04	9.36	12.2	9.50	2.68	2.97
88/11/16	1011	68	3.01	9.61	12.5	9.50	3.02	3.34
88/11/16	1012	68	3.01	9.61	12.5	9.50	3.01	3.33
88/11/16	1025	70	3.01	9.64	12.6	9.66	2.90	3.21
88/11/16	1026	70	3.03	9.40	12.2	9.66	2.58	2.85
88/11/16	1125	79	3.00	9.65	12.6	9.66	2.91	3.22
88/11/16	1127	79	3.01	9.58	12.5	9.66	2.81	3.11
88/11/16	1141	81	2.99	9.74	12.7	9.78	2.90	3.21
88/11/16	1142	81	2.98	9.89	12.9	9.78	3.09	3.42
89/01/18	809	288	3.34	7.07	9.21	5.93	3.27	4.49
89/01/18	839	292	3.32	7.24	9.42	5.85	3.57	4.27
89/01/18	921	298	3.29	7.42	9.66	5.85	3.81	4.55
89/01/18	935	300	3.30	7.35	9.57	5.85	3.72	4.43
89/01/18	950	302	3.31	7.26	9.45	5.79	3.66	4.35
89/01/18	1018	306	3.25	7.71	10.0	5.79	4.25	5.04
89/01/18	1034	308	3.21	7.96	10.4	5.79	4.58	6.28
89/12/12	848	36	3.28	7.50	9.76	7.74	2.02	2.41
89/12/12	923	41	3.25	7.70	10.0	7.84	2.18	2.61
89/12/12	1014	48	3.21	8.01	10.4	7.84	2.58	3.09
89/12/12	1115	57	3.17	8.32	10.8	7.97	2.86	3.42
89/12/12	1241	69	3.09	8.90	11.6	8.08	3.51	4.19
89/12/12	1256	71	3.07	9.09	11.8	8.21	3.63	4.34
89/12/12	1339	77	3.04	9.30	12.1	8.21	3.90	4.66
89/12/12	1424	84	3.01	9.58	12.5	8.32	4.16	4.97
89/12/14	705	69	3.19	8.16	10.6	8.17	2.46	2.92
89/12/14	727	72	3.16	8.33	10.8	8.31	2.54	3.03
89/12/14	846	83	3.19	8.13	10.6	8.42	2.17	2.59
89/12/14	903	86	3.35	7.04	9.17	8.42	0.75	0.89
89/12/14	905	86	3.15	8.42	11.0	8.42	2.55	3.03
89/12/14	1003	94	3.14	8.51	11.1	8.45	2.63	3.13

Table 2. M (4.8 μm) Photometry of Io (J1) (continued).

Date (UT)	Time (UT)	Orbital Phase Angle (deg.)	Observed			Calculated Flux Densities		Spectral Emittance (10^{-2} $Wm^{-2}\mu m^{-1}$)
			Magnitude	Flux		Reflected Sunlight (10^{-17} $Wcm^{-2}\mu m^{-1}$)	Thermal Emission (10^{-17} $Wcm^{-2}\mu m^{-1}$)	
				(Jy)	(10^{-17} $Wcm^{-2}\mu m^{-1}$)			
89/12/14	1020	97	3.14	8.49	11.1	8.45	2.61	3.11
89/12/14	1112	104	3.11	8.72	11.4	8.40	2.95	3.52
89/12/15	1237	319	2.94	10.2	13.3	7.35	5.99	7.12
89/12/15	1402	332	2.94	10.2	13.3	7.32	6.01	7.14
89/12/15	1445	338	2.94	10.2	13.3	7.32	5.99	7.12
89/12/15	1503	340	2.92	10.4	13.6	7.32	6.27	7.45
89/12/15	1522	343	3.00	9.65	12.6	7.39	5.18	6.15
89/12/16	659	115	3.08	8.98	11.7	8.40	3.29	3.90
89/12/16	720	118	3.17	8.29	10.8	8.40	2.39	2.84
89/12/16	915	135	3.21	7.98	10.4	8.31	2.08	2.47
90/01/06	655	71	3.13	8.62	11.2	8.48	2.75	3.27
90/01/06	709	73	3.11	8.76	11.4	8.48	2.93	3.48
90/01/06	746	78	3.08	8.99	11.7	8.48	3.22	3.83
90/01/06	823	83	3.04	9.36	12.2	8.59	3.61	4.30
90/01/06	1156	114	3.12	8.65	11.3	8.46	2.80	3.35
90/01/06	1238	119	3.09	8.92	11.6	8.46	3.16	3.75
90/01/07	559	266	2.91	10.6	13.7	7.81	5.93	7.05
90/01/07	614	269	2.91	10.5	13.7	7.81	5.85	6.96
90/01/07	710	277	2.87	10.9	14.2	7.73	6.47	7.70
90/01/07	725	279	2.86	11.1	14.4	7.73	6.66	7.92
90/01/07	809	285	2.85	11.1	14.5	7.63	6.87	8.17
90/01/07	823	287	2.85	11.1	14.4	7.63	6.82	8.12
90/01/07	910	293	2.79	11.7	15.3	7.52	7.74	9.20
90/01/07	924	295	2.78	11.8	15.4	7.52	7.88	9.38
90/01/07	1055	308	2.81	11.5	15.0	7.45	7.53	8.96
90/01/07	1109	310	2.83	11.3	14.7	7.38	7.36	8.76
90/01/07	1145	315	2.84	11.3	14.7	7.38	7.30	8.68
90/01/07	1242	323	2.83	11.3	14.8	7.34	7.42	8.83
90/01/07	1317	328	2.83	11.3	14.8	7.34	7.43	8.83
90/01/07	1331	330	2.83	11.4	14.8	7.35	7.42	8.83
90/01/07	1345	332	2.84	11.2	14.6	7.35	7.23	8.60
90/01/08	613	112	3.13	8.63	11.2	8.36	2.87	3.42
90/01/08	626	114	3.13	8.56	11.1	8.36	2.79	3.32
90/01/08	742	125	3.13	8.61	11.2	8.33	2.89	3.43
90/01/08	757	127	3.13	8.63	11.2	8.33	2.91	3.46
90/01/08	851	134	3.13	8.60	11.2	8.27	2.94	3.49
90/01/08	904	136	3.13	8.62	11.2	8.27	2.96	3.52
90/01/08	944	142	3.09	8.92	11.6	8.16	3.46	4.11
90/01/08	1020	147	3.11	8.78	11.4	8.16	3.28	3.90
90/01/08	1054	152	3.14	8.52	11.1	8.13	2.96	3.53
90/01/08	1139	158	3.18	8.22	10.7	8.13	2.58	3.07
90/01/08	1215	163	3.19	8.15	10.6	8.12	2.49	2.96
90/01/08	1231	166	3.19	8.15	10.6	8.12	2.50	2.97
90/01/08	1246	168	3.25	7.73	10.1	8.12	1.95	2.32
90/01/09	717	325	2.35	17.7	23.0	7.25	15.8	18.8
90/01/09	730	327	2.37	17.4	22.6	7.25	15.4	18.3
90/01/09	808	332	2.43	16.3	21.3	7.26	14.0	16.7

Table 2. M (4.8 μm) Photometry of Io (J1) (continued).

Date (UT)	Time (UT)	Orbital Phase Angle (deg.)	Observed			Calculated Flux Densities		Spectral Emittance (10^{-2} Wm$^{-2}\mu$m^{-1})
			Magnitude	Flux		Reflected Sunlight (10^{-17} Wcm$^{-2}\mu$m^{-1})	Thermal Emission (10^{-17} Wcm$^{-2}\mu$m^{-1})	
				(Jy)	(10^{-17} Wcm$^{-2}\mu$m^{-1})			
90/01/09	906	339	2.51	15.2	19.8	7.26	12.2	15.0
90/01/09	916	342	2.53	15.0	19.5	7.33	12.2	15.0
90/01/09	932	346	2.55	14.6	19.0	7.33	11.7	14.0
90/01/09	948	346	2.56	14.5	18.9	7.33	11.6	13.8
90/01/09	1001	348	2.54	14.9	19.4	7.33	12.0	14.0
90/01/10	651	165	3.24	7.80	10.2	8.00	2.16	2.58
90/01/10	710	167	3.27	7.55	9.83	8.00	1.83	2.19
90/01/10	1037	197	3.31	7.10	9.51	7.94	1.51	1.87
90/01/10	1052	199	3.27	7.59	9.88	7.94	1.94	2.32
90/01/10	1136	202	3.26	7.65	9.96	7.91	2.04	2.44
90/01/10	1151	207	3.19	8.10	10.6	7.91	2.64	3.16
90/01/10	1232	213	3.22	7.93	10.3	7.88	2.44	2.92
90/01/10	1249	215	3.21	8.02	10.4	7.88	2.52	3.02
90/01/10	1301	221	3.18	8.21	10.7	7.87	2.82	3.38
92/02/04	1225	58	3.49	6.15	8.00	6.08	1.93	2.66
92/02/04	1302	63	3.47	6.27	8.16	6.16	2.01	2.77
92/02/04	1341	69	3.47	6.50	8.21	6.16	2.05	2.83
92/02/05	1037	246	3.49	6.18	8.05	5.97	2.08	2.86
92/02/05	1313	268	3.44	6.48	8.43	5.86	2.58	3.54
92/02/05	1351	274	3.45	6.39	8.32	5.79	2.53	3.47
92/02/07	905	280	3.46	6.33	8.24	5.80	2.44	3.34
92/02/07	953	287	3.47	6.31	8.21	5.80	2.41	3.29
92/02/07	1127	300	3.42	6.55	8.53	5.66	2.87	3.92
92/02/07	1226	309	3.48	6.25	8.14	5.66	2.48	3.39
92/02/07	1321	317	3.51	6.08	7.91	5.61	2.30	3.14
92/02/07	1503	331	3.52	6.02	7.84	5.59	2.25	3.08
92/02/07	1518	333	3.54	5.88	7.65	5.59	2.06	2.82
92/02/07	1541	336	3.59	5.65	7.36	5.59	1.77	2.41
92/02/08	916	125	3.33	7.15	9.31	6.40	2.91	3.96
92/02/08	1143	146	3.33	7.18	9.34	6.28	3.07	4.18
93/03/25	723	195	3.43	6.51	8.48	6.51	1.97	2.66
93/03/25	737	197	3.42	6.57	8.55	6.51	2.04	2.76
93/03/25	751	199	3.42	6.58	8.57	6.51	2.06	2.78
93/03/25	837	206	3.40	6.69	8.71	6.49	2.23	3.01
93/03/25	854	208	3.40	6.70	8.73	6.49	2.24	3.03
93/03/25	1001	218	3.41	6.64	8.65	6.46	2.19	2.95
93/03/25	1013	220	3.41	6.64	8.65	6.46	2.19	2.95
93/03/25		236	3.43	6.51	8.47	6.30	2.05	2.76
93/03/25	1223	238	3.43	6.54	8.52	6.43	2.09	2.82
93/03/25	1318	246	3.50	6.09	7.93	6.40	1.53	2.06
93/03/25	1333	248	3.52	6.00	7.82	6.40	1.41	1.91
93/03/25	1414	254	3.54	5.86	7.63	6.34	1.35	1.82
93/03/25	1427	255	3.55	5.84	7.61	6.34	1.26	1.70
93/03/26	644	34	3.40	6.72	8.75	6.41	2.33	3.15
93/03/26	702	36	3.39	6.79	8.84	6.41	2.43	3.27
93/03/26	716	38	3.39	6.78	8.83	6.41	2.42	3.26
93/03/26	729	40	3.33	7.17	9.33	6.41	2.92	3.94

Table 2. M (4.8 μm) Photometry of Io (J1) (continued).

Date (UT)	Time (UT)	Orbital Phase Angle (deg.)	Observed			Calculated Flux Densities		Spectral Emittance (10^{-2} Wm$^{-2}\mu$m^{-1})
			Magnitude	Flux		Reflected Sunlight (10^{-17} Wcm$^{-2}\mu$m^{-1})	Thermal Emission (10^{-17} Wcm$^{-2}\mu$m^{-1})	
				(Jy)	(10^{-17} Wcm$^{-2}\mu$m^{-1})			
93/03/26	743	42	3.30	7.35	9.57	6.69	2.07	2.14
93/03/26	828	48	3.25	7.71	10.0	6.49	3.55	4.79
93/03/26	838	50	3.26	7.62	9.92	6.49	3.42	4.62
93/03/26	926	56	3.27	7.58	9.87	6.60	3.26	4.40
93/03/26	1029	65	3.28	7.51	9.78	6.69	3.09	4.17
93/03/26	1135	75	3.24	7.75	10.1	6.80	3.29	4.44
93/03/26	1247	85	3.27	7.53	9.80	6.89	2.91	3.93
93/03/26	1301	87	3.29	7.40	9.64	6.89	2.75	3.71
93/03/26	1342	93	3.27	7.56	9.85	6.91	2.93	3.96
93/03/26	1413	97	3.29	7.44	9.69	6.91	2.78	3.74
93/03/26	1428	99	3.35	7.03	9.16	6.91	2.25	3.03
93/03/27	636	252	3.32	7.20	9.38	6.49	2.89	3.89
93/03/27	649	238	3.35	6.99	9.10	6.49	2.61	3.52
93/03/27	707	240	3.37	6.91	9.00	6.46	2.53	3.42
93/03/27	722	243	3.37	6.91	8.99	6.46	2.53	3.41
93/03/27	755	247	3.31	7.28	9.48	6.46	3.01	4.06
93/03/27	846	254	3.35	7.05	9.18	6.41	2.77	3.74
93/03/27	859	256	3.34	7.07	9.21	6.41	2.80	3.78
93/03/27	933	261	3.30	7.15	9.31	6.35	2.97	4.00
93/03/27	1024	268	3.35	7.02	9.14	6.35	2.79	3.76
93/03/27	1038	270	3.33	7.16	9.32	6.28	3.04	4.10
93/03/27	1157	281	3.35	6.99	9.11	6.20	2.91	3.92
93/03/27	1210	283	3.37	6.89	8.97	6.20	2.78	3.74
93/03/27	1259	290	3.39	6.78	8.83	6.19	2.70	3.64
93/03/27	1324	296	3.41	6.67	8.69	6.11	2.58	3.48
93/03/27	1337	296	3.42	6.57	8.55	6.19	2.36	3.20
93/03/27		300	3.43	6.51	8.47	6.11	2.37	3.19
93/03/27	1431	302	3.40	6.69	8.72	6.09	2.67	3.59
93/03/27	1433	304	3.38	6.83	8.90	6.05	2.85	
93/03/28	607	80	3.28	7.48	9.74	6.89	2.84	3.83
93/03/28	749	82	3.41	6.64	8.65	6.98	1.67	2.25
93/03/28	759	82	3.28	7.49	9.76	6.98	2.78	3.74
93/03/28	807	84	3.30	7.32	9.54	6.98	2.55	3.44
93/03/28	739	89	3.29	7.41	9.65	6.98	2.67	3.59
93/03/28	752	90	3.29	7.43	9.68	7.01	2.67	3.60
93/03/28	820	94	3.28	7.51	9.78	7.01	2.78	3.74
93/03/28	833	96	3.27	7.55	9.83	7.01	2.83	3.81
93/03/28	900	100	3.26	7.62	9.92	6.97	2.95	3.97
93/03/28	958	108	3.30	7.09	9.26	6.97	2.27	3.06
93/03/28	1011	110	3.32	7.19	9.36	6.88	2.48	3.34
93/03/28	1201	126	3.28	7.49	9.75	6.85	2.90	3.91
93/03/28	1214	127	3.36	6.98	9.09	6.85	2.24	3.01
93/03/28	1303	134	3.37	6.88	8.96	6.80	2.15	2.90
93/03/28	1316	136	3.39	6.78	8.83	6.80	2.03	2.73
93/03/28	1337	139	3.36	6.91	9.02	6.80	2.22	2.99
93/03/29	606	283	3.44	6.48	8.44	6.29	2.15	2.90

Table 2. M (4.8 μm) Photometry of Io (J1) (continued).

Date (UT)	Time (UT)	Orbital Phase Angle (deg.)	Observed			Calculated Flux Densities		Spectral Emittance (10^{-17} Wm$^{-2}\mu$m^{-1})
			Magnitude	Flux		Reflected Sunlight (10^{-17} Wcm$^{-2}\mu$m^{-1})	Thermal Emission (10^{-17} Wcm$^{-2}\mu$m^{-1})	
				(Jy)	(10^{-17} Wcm$^{-2}\mu$m^{-1})			
93/03/29	650	285	3.38	6.80	8.91	6.29	2.62	9.53
93/03/29	705	287	3.42	6.57	8.61	6.29	2.32	8.65
93/03/29	736	292	3.36	6.97	9.07	6.29	2.87	10.87
93/03/29	749	294	3.40	7.09	9.30	6.20	3.04	11.09
93/03/29	801	300	3.31	7.30	9.51	6.14	3.37	12.53
93/03/29	854	303	3.31	7.29	9.49	6.14	3.35	12.51
93/03/29	942	310	3.30	7.36	9.60	6.14	3.46	12.95
93/03/29	954	311	3.29	7.39	9.63	6.09	3.54	13.27
93/03/29	1053	320	3.26	7.62	9.92	6.09	3.84	14.47
93/03/29	1112	322	3.31	7.32	9.53	6.08	3.48	13.18
93/03/29	1144	327	3.28	7.46	9.71	6.09	3.66	13.93
93/03/29	1157	329	3.31	7.31	9.52	6.05	3.47	13.17
93/03/29	1242	335	3.34	7.08	9.22	6.06	3.16	11.96
93/03/29	1254	337	3.33	7.10	9.28	6.06	3.22	12.34
93/03/29	1308	339	3.36	6.97	9.08	6.06	3.02	11.56
93/03/29	1321	341	3.37	6.90	8.99	6.12	2.87	10.86
93/03/29	1340	343	3.33	7.15	9.31	6.12	3.20	12.30
93/03/29	1354	345	3.41	6.64	8.64	6.12	2.52	9.40
93/03/29	1408	347	3.39	6.79	8.84	6.12	2.72	10.26

Table 3. Photometry of Io (J1) at 8.7 μm.

Date (UT)	Time (UT)	Orbital Phase Angle (deg.)	Observed			Spectral Emittance (10^{-2} Wm$^{-2}\mu$m^{-1})
			Magnitude	Flux Density		
				(Jy)	(10^{-17} Wcm$^{-2}\mu$m^{-1})	
83/03/29		340	1.03	196	775	102
83/07/19	822	51	1.59	11.7	4.62	6.88
83/07/19	833	53	1.54	12.2	4.84	7.21
83/07/19	900	61	1.56	12.0	4.75	7.08
83/07/19	914	63	1.54	12.2	4.84	7.21
83/07/19	937	61	1.53	12.3	4.89	7.27
83/07/20	603	235	1.11	18.2	7.19	10.8
83/07/20	604	236	1.08	18.7	7.40	11.1
83/07/20	755	253	1.09	21.8	8.65	12.9
83/07/20	808	254	1.09	21.8	8.65	12.9
83/07/20	849	258	0.97	22.7	8.97	13.4
83/07/20	854	260	0.96	22.9	9.06	13.6
83/07/20	926	266	0.81	23.9	9.48	14.2
83/07/20	931	267	0.78	24.6	9.75	14.6
83/07/20	1000	269	0.77	24.8	9.84	14.7
83/07/20	1004	270	0.75	25.3	10.0	15.0
83/07/21	526	74	1.40	10.9	5.51	8.29
83/07/21	535	75	1.42	10.7	5.42	8.16
83/07/21	558	79	1.40	10.9	5.51	8.29
83/07/21	619	82	1.39	14.0	5.56	8.37
83/07/21	705	89	1.28	15.5	6.15	9.26
83/07/21	738	92	1.31	15.1	5.98	9.01
83/07/21	759	96	1.28	15.5	6.15	9.26
83/07/21	806	101	1.30	14.8	5.88	8.84
83/07/21	945	111	1.31	15.1	5.98	9.01
83/08/07	820	318	0.97	28.5	11.3	16.9
83/08/07	833	320	0.96	28.5	11.3	16.9
83/08/07	845	322	0.61	28.8	11.4	17.1
83/08/07	858	325	0.61	28.3	11.2	16.8
83/08/07	911	327	0.64	28.0	11.1	16.6
83/08/27		10	1.71	10.5	4.14	7.73
83/08/27		27	1.77	9.9	3.92	7.32
84/05/09	1245	113	1.28	15.6	6.18	8.87
84/05/09	1255	114	1.24	16.1	6.36	9.13
84/05/08	1303	115	1.26	15.8	6.24	8.96
84/05/08	1334	120	1.26	15.9	6.30	9.04
84/05/08	1348	122	1.25	16.0	6.33	9.09
84/05/08	1425	127	1.28	15.5	6.16	8.84
84/05/08	1438	129	1.27	15.7	6.20	8.91
84/06/17	814	299	-0.02	51.3	20.4	24.7
84/06/17	856	305	0.17	43.0	17.0	20.7
84/06/17	910	307	0.20	41.8	16.6	20.1
84/06/17	946	312	0.50	38.3	15.2	18.5
84/06/17	1015	316	0.37	35.9	14.2	17.3
84/06/17	1046	320	0.43	34.0	13.5	16.4
84/06/17	1117	324	0.48	32.5	12.9	15.6

Table 3. (J1) at 8.7 μm (continued).

Date (UT)	Time (UT)	Orbital Phase Angle (deg.)	Observed			Spectral Emittance (10^{-2} Wm$^{-2}\mu$m^{-1})
			Magnitude	Flux Density		
				(Jy)	(10^{-17} Wcm$^{-2}\mu$m^{-1})	
84/06/17	1145	328	0.52	31.3	12.4	15.1
84/06/17	1158	330	0.56	30.0	11.9	14.5
84/06/17	1209	332	0.56	30.2	12.0	14.5
84/07/19	707	324	0.31	38.1	15.1	18.5
84/07/19	727	327	0.34	37.1	14.7	18.0
84/07/19	811	333	0.33	37.3	14.8	18.1
84/07/19	813	333	0.33	37.3	14.8	18.1
84/08/19	648	152	1.24	16.1	6.38	8.89
84/08/19	723	157	1.17	17.2	6.81	9.48
84/08/19	812	164	1.15	17.5	6.93	9.66
84/08/19	820	165	1.15	17.5	6.93	9.66
84/08/19	830	166	1.19	16.9	6.68	9.31
84/08/19	844	168	1.15	17.5	6.93	9.66
84/08/20	537	347	0.58	29.6	11.7	16.4
84/08/20	1011	20	1.40	13.9	5.51	7.71
85/06/06	1153	326	0.93	21.5	8.52	11.9
85/06/06	1202	327	0.89	22.3	8.84	12.4
85/06/06	1242	333	0.79	24.4	9.66	13.5
85/06/06	1249	334	0.79	24.4	9.66	13.5
85/06/06	1254	335	0.79	24.4	9.66	13.5
85/06/07	1101	162	0.99	20.3	8.04	11.2
85/06/07	1107	163	0.99	20.3	8.04	11.2
85/06/08	1323	25	1.31	15.1	5.98	8.27
85/06/08	1402	31	1.33	14.8	5.88	8.12
	1426	34	1.36	14.4	5.72	7.90
85/06/09	1128	213	1.12	18.0	7.13	9.79
85/06/09	1213	219	1.01	19.9	7.89	10.8
85/06/09	1230	222	1.01	19.9	7.89	10.8
85/06/09	1247	224	0.98	20.4	8.09	11.1
85/06/09	1256	225	0.98	20.4	8.10	11.1
85/06/09	1305	227	0.97	20.7	8.21	11.3
85/06/09	1130	231	1.07	18.8	7.47	10.3
85/06/10	1157	61	1.30	15.3	6.04	8.25
85/06/10	1207	62	1.27	15.7	6.21	8.48
85/06/10	1229	65	1.18	17.0	6.75	9.21
85/06/10	1239	67	1.18	17.0	6.75	9.21
85/06/10	1249	68	1.19	16.9	6.68	9.13
85/06/10	1259	69	1.16	17.3	6.87	9.38
85/07/09	1122	199	0.93	21.4	8.48	10.0
85/07/10	858	22	1.17	17.2	6.81	8.01
85/07/10	907	24	1.17	17.2	6.81	8.01
85/07/10	1022	34	1.20	16.7	6.62	7.79
85/07/10	1134	44	1.15	17.5	6.93	8.16
85/07/10	1359	65	1.04	19.4	7.67	9.03
85/07/10	1417	67	1.06	19.0	7.53	8.86
85/07/10	1423	68	1.04	19.4	7.67	9.03

Table 3. Photometry of Io (J1) at 8.7 μm ued

Date (UT)	Time (UT)	Orbital Phase Angle (deg.)	Observed			Spectral Emittance (10^{-2} Wm$^{-2}\mu$m^{-1})
			Magnitude	Flux Density		
				(Jy)	(10^{-17} Wcm$^{-2}\mu$m^{-1})	
85/07/11	903	227	0.88	22.6	8.93	10.5
85/07/11	950	233	0.83	23.6	9.35	11.0
85/07/11	1019	237	0.79	24.5	9.70	11.4
85/07/11	1038	240	0.76	25.0	9.90	11.6
85/07/11	1049	242	0.75	25.3	10.0	11.8
85/07/11	1210	253	0.66	27.5	10.9	12.8
85/07/11	1228	256	0.64	28.0	11.1	13.0
85/07/11	1252	259	0.62	28.6	11.3	13.3
85/07/11	1315	262	0.60	29.1	11.5	13.5
85/07/11	1354	268	0.58	29.7	11.8	13.8
85/07/11	1436	274	0.56	30.1	11.9	14.0
85/07/11	1459	277	0.56	30.1	11.9	14.0
85/07/11	1533	282	0.55	30.4	12.0	14.1
85/07/11	1543	283	0.54	30.7	12.2	14.3
85/07/11	1551	284	0.55	30.5	12.1	14.2
85/07/12	908	71	1.12	18.0	7.13	8.34
85/07/12	956	78	1.01	19.9	7.89	9.22
85/07/12	1006	79	0.99	20.2	8.01	9.37
85/07/12	1049	85	0.91	21.8	8.63	10.1
85/07/12	1111	88	0.90	22.0	8.71	10.2
85/09/12	709	78	1.03	19.6	7.76	9.52
85/09/12	812	86	1.00	20.2	7.99	9.66
86/06/25	1218	314	0.63	28.3	11.2	16.8
86/06/25	1229	315	0.62	28.6	11.3	17.0
86/06/25	1258	319	0.75	25.3	10.0	15.1
86/06/25	1322	323	0.66	27.4	10.9	16.3
86/07/02	1255	302	0.69	26.8	10.6	15.2
86/07/02	1304	304	0.69	26.7	10.6	15.1
86/07/02	1329	308	0.69	26.8	10.6	15.2
86/07/02	1342	310	0.69	26.8	10.6	15.2
86/07/02	1430	316	0.70	26.5	10.5	15.0
86/07/02	1441	318	0.75	25.3	10.0	14.4
86/07/02	1453	320	0.71	26.2	10.4	14.9
86/07/02	1457	320	0.72	26.1	10.3	14.8
86/08/03	1010	312	0.41	34.7	13.7	16.3
86/08/03	1030	315	0.42	34.3	13.6	16.1
86/08/03	1049	318	0.42	34.2	13.5	16.1
86/08/03	1207	329	0.47	32.7	12.9	15.4
86/08/03	1229	332	0.49	32.1	12.7	15.1
86/08/03	1308	337	0.53	31.1	12.3	14.6
86/08/03	1329	340	0.53	31.1	12.3	14.6
86/08/03	1351	344	1.28	15.5	6.13	7.27
86/08/03	1402	345	1.33	14.8	5.86	6.95
86/08/04	917	148	0.60	29.1	11.5	13.6
86/08/04	935	151	0.61	28.8	11.4	13.5
86/08/04	951	153	0.61	28.7	11.4	13.4

Table 3. Photometry of Io (J1) at 8.7 μm (continued).

Date (UT)	Time (UT)	Orbital Phase Angle (deg)	Observed			Spectral Emittance (10^{-2} Wm$^{-2}\mu$m^{-1})
			Magnitude	Flux Density		
				(Jy)	(10^{-17} Wcm$^{-2}\mu$m^{-1})	
86/08/05	1225	19	0.90	21.2	8.69	10.2
86/08/05	1241	21	1.60	21.8	8.65	10.2
86/08/05	1256	23	0.92	21.7	8.58	10.1
86/08/05	1333	28	1.60	21.2	8.51	10.0
86/08/05	1348	31	0.93	21.0	8.49	9.99
86/08/05	1403	33	0.94	21.2	8.41	9.89
86/08/05	1438	K	0.94	21.2	8.40	9.88
86/08/05	1453	40	1.60	21.0	8.49	9.98
86/08/05	1505	41	0.92	21.7	8.59	10.1
86/08/06	1011	202	0.75	25.4	10.1	11.8
86/08/06	1029	206	0.74	25.5	10.1	11.8
86/08/06	1045	208	0.74	25.5	10.1	11.8
86/08/06	1418	238	1.60	28.3	11.2	13.1
86/08/06	1434	243	0.60	29.1	11.5	13.5
86/08/07	1008	50	0.28	39.1	15.5	18.0
86/08/07	1039	54	0.27	39.4	15.6	18.1
86/08/07	1052	56	0.27	39.5	15.6	18.2
86/08/07	1340	80	0.24	40.6	16.1	18.7
86/08/07	1356	82	0.24	40.5	16.0	18.7
86/08/07	1428	87	0.26	39.7	15.7	18.3
86/08/07	1442	89	0.26	39.7	15.7	18.3
87/09/28	1200	282	0.28	39.1	15.5	17.9
87/09/28	1235	287	0.28	38.9	15.4	17.9
87/09/28	1314	293	0.30	38.6	15.2	17.6
87/09/28	1336	301	0.27	39.5	15.7	18.1
87/09/28	1502	308	0.31	37.9	15.0	17.4
87/09/28	1521	309	0.31	38.0	15.1	17.5
87/11/23	613	115	1.38	14.2	5.63	16.2
87/11/23	629	117	0.69	23.2	9.20	26.4
87/11/23	646	122	0.68	27.0	10.7	30.9
87/11/23	749	128	0.69	23.2	9.20	26.4
87/11/23	825	134	0.69	26.8	10.6	30.4
87/11/23	840	136	0.69	26.2	10.4	29.8
87/11/23	948	145	0.70	24.2	9.61	27.5
87/11/23	1058	155	0.70	24.2	9.61	27.5
87/11/23	1132	160	0.70	25.2	10.0	28.6
87/11/25	513	154	0.71	26.2	10.4	29.8
87/11/25	545	158	0.70	26.6	10.5	30.2
87/11/25	619	163	0.68	27.1	10.7	30.7
87/11/25	634	591	0.67	27.2	10.8	30.9
87/11/25	1044	002	080	24.2	9.55	27.1
87/11/25	1101	202	080	24.2	9.55	27.1
87/11/25	1129	207	0.83	23.4	9.28	26.2
87/11/26	747	19	1.14	17.7	7.01	20.1
87/11/26	803	21	1.05	19.0	7.63	21.7
87/11/26	818	23	1.00	20.2	7.99	22.7

Table 3. Photometry of Io (J1) at 8.7 μm (continued).

Date (UT)	Time (UT)	Orbital Phase Angle (deg.)	Observed			Spectral Emittance (10^{-2} Wm$^{-2}\mu$m^{-1})
			Magnitude	Flux Density		
				(Jy)	(10^{-17} Wcm$^{-2}\mu$m^{-1})	
87/11/26	939	35	0.99	20.3	8.01	11.5
87/11/26	954	37	1.00	20.2	7.93	11.4
87/11/26	1109	47	0.97	20.7	8.19	11.7
88/11/16	755	49	0.85	23.1	9.15	10.1
88/11/16	756	49	0.85	23.1	9.17	10.1
88/11/16	855	57	0.79	24.4	9.66	10.7
88/11/16	858	58	0.80	24.2	9.60	10.6
88/11/16	941	W	0.80	24.8	9.84	10.8
88/11/16	942	W	MO	24.2	9.58	10.6
88/11/16	944	64	0, W	24.1	9.56	10.6
88/11/16	1000	67	0.75	25.2	9.98	11.0
88/11/16	1001	67	0.76	25.1	9.94	11.0
88/11/16	1018	69	0.75	25.0	10.1	11.1
88/11/16	1016	64	SL 0	25.3	0.01	11.1
88/11/16	1136	W	0.74	25.2	10.1	11.2
88/11/16	1138	80	0.76	25.2	9.95	11.0
89/01/18	906	275	1.00	28.2	11.1	15.2
89/01/18	830	291	1.00	28.8	11.0	13.6
89/01/18	928	662	CL 0	25.2	10.2	12.1
89/01/18	936	301	0.67	27.3	10.8	12.9
89/01/18	1028	307	0.62	28.5	11.3	14.1
89/01/18	1041	309	0.69	26.4	10.6	12.6
89/12/12	900	38	1.33	14.9	5.91	20.1
89/12/12	916	40	1.08	18.6	7.38	25.1
89/12/12	1004	47	1.00	20.0	8.09	26.2
89/12/12	1020	49	1.00	20.2	7.99	26.8
89/12/12	1122	58	0.94	22.4	8.89	29.1
89/12/12	1142	70	0.78	19.2	7.62	25.7
89/12/12	1301	72	0.79	24.0	9.66	32.1
89/12/12	1344	78	0.74	25.5	10.1	33.7
89/12/12	1430	85	0.72	26.0	10.3	34.2
89/12/14	712	70	0.97	20.7	8.18	26.9
89/12/14	733	73	0.97	20.6	8.17	26.9
89/12/14	851	84	1.01	20.1	7.97	26.5
89/12/14	911	87	0.89	22.2	8.79	29.0
89/12/14	1008	95	0.85	25.2	9.10	30.0
89/12/14	1026	97	0.80	24.2	9.57	31.4
89/12/15	1111	105	0.79	24.3	9.61	31.7
89/12/15	1243	320	0.08	47.1	18.6	62.2
89/12/15	1408	332	0.14	44.3	17.6	58.2
89/12/15	1451	338	0.20	42.0	16.6	54.8
89/12/15	1514	341	0.19	41.2	16.2	53.3
89/12/15	1525	343	0.20	39.7	15.6	51.4
89/12/16	801	116	0.69	27.2	10.8	35.8
89/12/16	822	119	1.00	20.0	7.93	26.1
89/12/16	836	120	0.72	25.8	10.2	33.7

Table 3. Photometry of Io (J1) at 8.7 μm (continued).

Date (UT)	Time (UT)	Orbital Phase Angle (deg.)	Observed			Spectral Emittance (10^{-2} Wm$^{-2}\mu$m^{-1})
			Magnitude	Flux Density		
				(Jy)	(10^{-17} Wcm$^{-2}\mu$m^{-1})	
89/12/16	921	135	0 11	6CZ	9 47	11 z
91/21/6S	1037	146	0 79	24 ●	9 68	11.5
90/01/06	658	7L	0 81	6CZ	9 47	11 2
90/01/06	712	CL	0 82	23 7	9 38	11.2
90/01/06	7*9	6L	0.79	00Z	9.68	s 11
90/01 /06	825	84	O 74	25 5	101	121
90/01/06	1158	114	O 87	9ZZ	8 96	L 01
90/01/06	1241	120	O 78	24 7	9 U	11 6
90/01 /O7	602	267	0.24	40.7	16.1	2 61
90/01/07	617	692	CZO	o I*	z 91	19.3
90/01/07	712	277	O 15	43 9	17 4	LOZ
90/01/07	728	279	O 10	44.9	17.8	z 21
XCIOIOIO7	811	285	0 08	46 9	18 6	122
90/01 /07	826	287	0 11	45 7	18 1	21 5
90/01/07	841	289	LOO	47 ●	18 8	22 0
90/01/07	16 ●	294	OOZ	49 ●	19.6	23 0
90/01/07	9Z6	96Z	OOZ	+96	196	23 0
90/01/07	1058	60S	0 04	48 8	C 61	OCZ
90/01/07	i 112	311	0 02	9 62	961	23 4
90/01/07	1147	316	LOO	47 4	18 8	22 3
90/01/07	1154	317	0 04	48 8	19 3	23 0
90/01 /07	1245	0Z ●	0 09	46.7	18 5	22 0
90/01 /07	1320	329	0 / ●	44 5	17 6	21 0
90/01 /07	1 334	1cc	0.17	43 i	17 1	20.3
90/01/07	WC 1	ccc	6i 0	42 5	16 8	OOZ
90/01/08	619	112	0 84	C R	23 6	011
90/01 /08	629 W/	● //	0 84	23 2	9.20	601
90/01/08	S*7	125	0 82 o	23 i	9 42	11 2
90/01/08	800	127	0 82 o	23 8	9 42	11 z
90/01/08	SS ●	5C1	0 82	23 8	9 43	11.2
90/01 /08	606	137	0 81	6 a	9 46	11 0
90/01/08	947	I *Z	O10	10Z	SS 6	11.4
90/01/08	1023	147	6LO	?0Z	9 65	11.5
90/01 /W	1057	152	0 81	6 23	9.48	11 3
90/01/08	Z* I i	65I	0 82 o	23 8	9.44	11.2
90/01/08	6121	W/	0 84	c 23	CZ6	0 11
90/01 /08	1235	166	0 83 o	9CZ	CC 6	1 11
90/01/09	719	325	10 W	8 05	1 02	0 2
90/01/09	733	LZC	0 00	90S	OOZ	6CZ
90/01/09	810	332	0 02	96V	961	S 23
90/01 /09	905	340	1 0 0	46 7	s 81	1 22
90/01/09	126	342	0 11	45 8	18 1	21.7
90/01/09	9C6	344	cl 0	44 9	17 1	1.12
90/01 /09	952	347\	cl 0	44 9	17 8	C12
90/01/09	C001	348 /	0.16	43 6	CL/	902

Table 3. Photometry of Io (J1) at 8.7 μm (continued)

Date (UT)	Time (UT)	Orbital Phase Angle (deg.)	Observed			Spectral Emittance (10^{-2} Wm$^{-2}\mu$m^{-1})
			Magnitude	Flux Density		
				(Jy)	(10^{-17} Wcm$^{-2}\mu$m^{-1})	
90/01/10	6S*,	165	016	23.2	9.20	011
90/01/10	713	IM	0.82	23.8	9.41	11.3
90/01/10	1041	197	016	22.8	9.02	10.8
90/01/10	1055	199	0.86	6'22	9.06	10.8
90/01/10	1139	205	O 83	23.4	9.27	1'11
90/01/10	1155	208	016	23 0	9.09	601
90/01/10	1235	213	016	6"ZZ	9.06	1'01
90/01/10	1252	216	O 87	22.8	106	10.8
90/01/10	1329	221	0.84	23 2	9, 61	011
90/01/10	1344	223	1.48	13 o	5.j ●	6, 15
92/02/04	1233	6S	1.28	15.6	6.18	8.52
92/02/04	1309	W	1.23	Z-91	6.43	8 87
92/02/04	I 347	69	1.22	16.4	6,"S0	8 97
92/02/04	1351	70	1 21	991	6,"S6	9.05
92/02/05	1044	247	1.08	18.6	7.37	10.1
92/02/05	1321	69Z	O 9]	21.8	8.63	11.9
92/02/05	1359	275	090	22.1	8.75	021
92/02/07	916	282	090	22.1	8.74	119
92/02/07	1001	288	0 83	23 5	9 32	12 7
92/02/07	1 135	302	0.68	69Z	L 01	v 21
92/02/07	1234	310	061	27 0	10 7	1 ● 6
92/02/07	1337	319	0 7 ●	25 6	10 i	9 5
92/02/07	1511	332	0.94	21 3	8 43	11 S
92/02/07	1524	334	0.98	20 4	8.09	11.0
92/02/07	9251	337	/ 18	17 0	6.72	61, 6
92/02/07	1556	338	11'1	18 1	7 17	9.79
92/02/08	925	127	1 LO	18 9	7.47	10 z
93/03/25	731	197	1 28	15 6	6 17	8.33
93/03/25	745	199	1 23	16 2	6 43	8 ?7
93/03/25	758	200	1 24	16 2	660	8.64
93/03/25	916	LOZ	1.21	16.5	6.55	8 84
93/03/25	902	209	1.23	16.2	6 42	8 67
93/03/25	1008	219	1 18	17 O	6 73	9 08
93/03/25	1021	221	91'1	17.3	616	9 26
93/03/25	1216	L a 7	1.10	18.3	CCL	9 76
93/03/25	0S21	6 a	1.10	18.3	7 24	U 6
93/03/25	1327	247	1.08	981	7 38	9.95
93/03/25	1340	6"Z	1.16	17 3	6.85	9 25
93/03/25	1421	255	1.13	17.9	7 09	9 57
93/03/26	6S6	35	1.41	iC 7	5.44	7 34
93/03/26	7IO	37	1 43	13.5	5 34	7.21
93/03/26	724	39	9S'1	1 0 4	5 7/	7 L
93/03/26	7C7	41	1 32	15 O	26s	108
93/03/26	OSL	43	1 30	15 O	6.04	8 15
93/03/26	833	49	1.23	16 O	6 45	8 70
93/03/26	866	51	1.23	16 O	6.44	8.69

Table 3. Photometry of Io (J1) at 8.7 μm (continued).

Date (UT)	Time (UT)	Orbital Phase Angle (deg.)	Observed			Spectral Emittance (10^{-2} Wm$^{-2}\mu$m^{-1})
			Magnitude	Flux Density		
				(Jy)	(10^{-17} Wcm$^{-2}\mu$m^{-1})	
93/03/26	934	75	1.21	991	6.59	1 89
93/03/26	1056	99	1.20	191	6.55	8 97
93/03/26	1143	76	1.13	17 9	7.08	9.55
93/03/26	1255	86	1 17	17.1	6.78	9 15
93/03/26	1308	88	1 16	17 C	689	926
93/03/26	1351	94	1 17	17 Z	6 81	616
93/03/26	1422	98	1 25	15 9	6.50	8.50
93/03/26	1435	100	1.20	16 8	6.64	8 95
93/03/27	6S7	237	1.17	17 z	6 83	026
93/03/27	659	239	1.18	691	6.70	9 04
93/03/27	715	652	1.17	17 z	6 82	6i 9
93/03/27	729	242	1 18	17 1	6 U	9 12
93/03/27	802	Z *	1 11	18 1	717	966
93/03/27	853	248	1.04	S 61	771	10.39
93/03/27	907	255	660	C0Z	8.06	10 86
93/03/27	941	257	0.97	20.7	8 18	11.03
93/03/27	1000	292	0 96	21 0	8 32	11 21
93/03/27	1046	270	090	22.1	1 96	11.81
93/03/27	1204	271	0 87	922	8 94	5021
93/03/27	1218	282	0.85	23.1	9 15	12 34
93/03/27	1307	291	0 89	ZZZ	8 79	11.85
93/03/27	1331	295	0 88	22 S	8 89	11.99
93/03/27	1345	297	010	22.2	8.81	11 87
93/03/27	1413	301	0 89	22 3	8 85	c6 11
93/03/27	1426	303	0.88	22.5	1 93	12 00
93/03/27	1440	C0C	0 87	22 7	9 00	1210
93/03/28	645	81	1 25	160	6 cc	8 55
93/03/28	702	83	1.17	17 z	6 81	9 18
93/03/28	715	85	1 18	17 1	6 76	9.11
93/03/28	746	90	1 11	18.1	7 18	196
93/03/28	759	91	1.10	18 3	727	676
93/03/28	827	96	1 W	18 9	700	1010
93/03/28	840	97	1 07	611	7 48	10 07
93/03/28	906	101	1 05	19 2	760	10 24
93/03/28	1006	109	1 01	18 0	7 26	9 71
93/03/28	1019	111	1 08	186	7 38	9 94
93/03/28	1209	127	1 09	18 S	7 33	9 88
93/03/28	1222	621	1 13	17.9	709	9 55
93/03/28	1010	135	1.15	17 6	6 %	9 37
93/03/28	1323	137	1 17	17 Z	6 82	9 18
93/03/28	1345	1 a	1.21	166	6 S9	8 88
93/03/29	644	: W	0 83	23.4	9 28	12 50
93/03/29	658	286	0 86	22 8	9.04	12.17
93/03/29	712	288	0 92	21 6	8 55	11 52
93/03/29	743	293	0. W	24 1	9S6	12 88
93/03/29	756	295	0.79	24 4	966	13 01

Table 3. Photometry of Io (J1) at 8.7 μm (continued).

Date (UT)	Time (UT)	Orbital Phase Angle (deg.)	Observed			Spectral Emittance (10^{-2} Wm$^{-2}\mu$m^{-1})
			Magnitude	Flux Density		
				(Jy)	(10^{-17} Wcm$^{-2}\mu$m^{-1})	
93/03/29	m	30Z	0.50	24.1	9.55	12.86
93/03/29	901	304	080	24.1	9 55	12 86
93/03/29	949	311	0.79	24.3	96S	1262
93/03/29	1002	312	0.81	24 0	9.51	12.80
93/03/29	1015	31C	0.80	24 2	9.55	0621
93/03/29	1120	323	0.80	24.1	9.54	12.84
93/03/29	1152	328	0 85	23.2	9.18	12 06
93/03/29	1204	330	0.84	23.3	9.22	12 41
93/03/29	1249	336	0.93	21 5	8.50	11.45
93/03/29	1301	338	090	022	8.72	11 75
93/03/29	1315	340	0.92	21.7	196	11.59
93/03/29	1330	342	0 90	21 5	8 51	4 1 6
93/03/29	1347	344	0.93	21.5	8.50	11.44
93/03/29	1402	346	ou	22.4	8.88	11.95

Table 4. N (10 μm) Photometry of Io (J1).

Date (UT)	Time (UT)	Orbital Phase Angle (deg.)	Observed			Spectral Emittance (10^{-1} $Wm^{-2}\mu m^{-1}$)
			Magnitude	Flux Density		
				(Jy)	(10^{-16} $Wcm^{-2}\mu m^{-1}$)	
80/04/12		35	0.25	30.6	0.870	1.32
83/02/18		326	0.07	36.1	1.03	2.08
83/02/18		328	0.08	35.8	1.02	2.06
83/02/18		332	0.12	34.5	0.981	1.99
83/02/18		336	0.14	33.9	0.963	1.95
83/02/18		339	0.14	33.9	0.963	1.95
83/02/18		340	0.15	33.6	0.954	1.93
83/03/06		339	-0.17	45.1	1.28	2.35
83/03/11	1504	101	-0.25	48.9	1.39	2.48
83/03/11	1506	102	-0.24	48.2	1.37	2.44
83/04/24		36	0.23	31.2	0.886	1.26
83/07/19	815	50	0.28	29.8	0.847	1.26
83/07/19	820	51	0.28	29.8	0.847	1.26
83/07/19	831	53	0.27	30.1	0.854	1.27
83/07/19	857	56	0.26	30.3	0.862	1.28
83/07/19	910	58	0.24	30.9	0.878	1.31
83/07/19	935	62	0.23	31.2	0.886	1.32
83/07/20	600	236	-0.08	41.5	1.18	1.77
83/07/20	608	237	-0.09	41.9	1.19	1.78
83/07/20	759	252	-0.16	44.7	1.27	1.90
83/07/20	812	254	-0.15	44.3	1.26	1.88
83/07/20	846	258	-0.20	46.3	1.32	1.97
83/07/20	857	260	-0.20	46.3	1.32	1.97
83/07/20	923	264	-0.25	48.5	1.38	2.06
83/07/20	934	265	-0.21	46.8	1.33	1.99
83/07/20	959	269	-0.25	48.5	1.38	2.06
83/07/20	1006	271	-0.30	50.8	1.44	2.16
83/07/21	529	74	0.16	33.3	0.946	1.42
83/07/21	552	78	0.15	33.6	0.954	1.44
83/07/21	614	81	0.16	33.3	0.946	1.42
83/07/21	703	87	0.12	34.5	0.981	1.48
83/07/21	733	92	0.11	34.8	0.990	1.49
83/07/21	754	95	0.11	34.8	0.990	1.49
83/07/21	932	107	0.09	35.5	1.01	1.52
83/07/21	940	109	0.08	35.8	1.02	1.53
83/08/07	809	316	-0.22	47.2	1.34	2.23
83/08/07	816	318	-0.21	46.8	1.33	2.20
83/08/07	825	319	-0.21	46.8	1.33	2.20
83/08/07	837	320	-0.21	46.8	1.33	2.20
83/08/07	849	323	-0.16	44.7	1.27	2.11
83/08/07	903	326	-0.21	46.8	1.33	2.20
83/08/07	916	328	-0.21	46.8	1.33	2.20
84/05/08	1241	115	0.06	36.5	1.04	1.49
84/05/08	1259	119	0.04	37.2	1.06	1.52
84/05/08	1331	121	0.03	37.5	1.07	1.53

Table 4. N (10 μm) of Io (J1)

Date (UT)	Time (UT)	Orbital Phase Angle (deg.)	Observed			Spectral Emittance (10^{-1} $Wm^{-2}\mu m^{-1}$)
			Magnitude	Flux Density		
				(Jy)	(10^{-16} $Wcm^{-2}\mu m^{-1}$)	
84/05/08	1344	122	0.02	37.8	1.08	1.54
84/05/08	1421	126	0.09	35.5	1.01	1.45
84/05/08	1434	128	0.06	36.5	1.04	1.49
84/06/27		194	-0.31	51.3	1.46	1.75
84/07/19	653	322	-0.62	68.7	1.95	2.40
84/07/19	702	323	-0.61	67.7	1.92	2.36
84/07/19	716	325	-0.61	68.1	1.93	2.37
84/07/19	731	328	-0.59	66.5	1.89	2.32
84/07/19	800	332	-0.61	67.8	1.93	2.36
84/07/19	833	336	-0.60	67.0	1.91	2.34
84/08/19	643	151	-0.07	41.1	1.17	1.63
84/08/19	721	157	-0.12	43.1	1.22	1.70
84/08/19	735	159	-0.12	43.1	1.22	1.70
84/08/19	808	163	-0.14	43.9	1.25	1.74
84/08/19	818	165	-0.12	43.1	1.22	1.70
84/08/19	827	166	-0.13	43.4	1.23	1.72
84/08/19	840	167	-0.16	44.7	1.27	1.77
84/08/19	842	168	-0.14	43.9	1.25	1.74
84/08/20	534	347	-0.39	55.2	1.57	2.20
84/08/20	1009	20	0.14	33.9	0.963	1.35
85/06/06	1145	325	-0.13	43.6	1.24	1.74
85/06/06	1155	326	-0.20	46.4	1.32	1.84
85/06/06	1236	332	-0.33	52.5	1.49	2.09
85/06/06	1244	333	-0.31	51.7	1.47	2.06
85/06/06	1251	334	-0.32	52.0	1.48	2.07
85/06/07	1057	162	-0.25	48.5	1.38	1.92
85/06/07	1112	164	-0.26	49.0	1.39	1.94
85/06/08	1240	20	0.00	38.8	1.10	1.52
85/06/08	1310	24	0.01	38.3	1.09	1.50
85/06/08	1352	30	0.03	37.8	1.07	1.48
85/06/08	1412	33	0.04	37.3	1.06	1.46
85/06/09	1121	212	-0.24	48.1	1.37	1.88
85/06/09	1136	214	-0.14	44.1	1.25	1.72
85/06/09	1203	218	-0.23	47.9	1.36	1.87
85/06/09	1217	220	-0.24	48.1	1.37	1.88
85/06/09	1224	221	-0.24	48.3	1.37	1.89
85/06/09	1241	223	-0.25	48.5	1.38	1.89
85/06/09	1250	225	-0.24	48.5	1.38	1.89
85/06/09	1259	226	-0.25	48.6	1.38	1.90
85/06/10	1149	60	0.01	38.2	1.09	1.48
85/06/10	1159	61	0.07	36.1	1.03	1.40
85/06/10	1209	62	0.02	37.8	1.08	1.47
85/06/10	1232	66	-0.07	41.1	1.17	1.60
85/06/10	1241	67	-0.07	41.1	1.17	1.60
85/06/10	1252	68	-0.03	39.6	1.13	1.54

Table 4. N (10 μm) Photometry of Io (J1) (continued).

Date (UT)	Time (UT)	Orbital Phase Angle (deg.)	Observed			Spectral Emittance (10^{-1} $Wm^{-2}\mu m^{-1}$)
			Magnitude	Flux Density		
				(Jy)	(10^{-16} $Wcm^{-2}\mu m^{-1}$)	
85/07/09	1111	198	-0.39	55.2	1.57	1.85
85/07/09	1112	198	-0.41	56.2	1.60	1.89
85/07/09	1152	200	-0.36	54.0	1.53	1.81
85/07/10	850	21	-0.10	42.0	1.20	1.42
85/07/10	904	23	-0.12	43.1	1.22	1.44
85/07/10	1014	33	-0.09	42.2	1.20	1.41
85/07/10	1137	45	-0.13	46.8	1.24	1.46
85/07/10	1354	W	-0.22	47.4	1.35	1.K
85/07/10	1409	W	-0.21	47.1	1.34	1.57
85/07/10	1421	W	-0.22	47.6	1.35	1.59
85/07/11	857	226	-0.37	65.6	1.55	1.82
85/07/11	942	232	-0.39	55.5	1.58	1.85
85/07/11	1101	236	-0.43	57.0	1.61	1.91
85/07/11	1021	238	-0.42	57.2	1.61	1.91
85/07/11	1042	241	-0.45	58.0	1.66	1.95
85/07/11	1202	252	-0.50	61.0	1.71	2.04
85/07/11	1222	255	-0.51	61.8	1.76	2.06
85/07/11	1245	258	-0.53	63.2	1.79	2.11
85/07/11	1301	261	-0.54	63.7	1.81	2.17
85/07/11	1346	267	-0.58	66.0	1.87	2.20
85/07/11	1429	275	-0.59	69.2	1.96	2.23
85/07/11	1452	278	-0.58	66.3	1.88	2.21
85/07/11	1526	281	-0.62	68.2	1.94	2.28
85/07/11	1536	282	-0.60	67.1	1.91	2.20
85/07/11	1546	284	-0.61	68.0	1.93	2.27
85/07/12	900	70	-0.11	43.0	1.22	1.43
85/07/12	949	77	-0.25	48.9	1.39	1.63
85/07/12	959	78	-0.25	48.8	1.39	1.62
85/07/12	1041	84	-0.35	53.0	1.52	1.77
85/07/12	1104	87	-0.37	54.2	1.54	1.80
85/09/12	703	77	-0.21	46.8	1.33	1.64
85/09/12	719	79	-0.21	46.8	1.33	1.W
85/09/12	808	86	-0.24	48.1	1.37	1.69
85/09/12	820	88	-0.22	47.3	1.34	1.66
86/06/25	1211	313	-0.45	58.5	1.66	1.92
86/06/25	1222	310	-0.44	57.8	1.W	1.97
86/06/25	1252	318	-0.40	55.8	1.59	2.38
86/06/25	1317	322	-0.38	55.1	1.57	2.35
86/07/02	1248	300	-0.41	59.5	1.61	1.J1
86/07/02	1257	303	-0.40	55.8	1.59	2.27
86/07/02	1321	307	-0.41	56.4	1.60	1.80
86/07/02	1334	309	-0.41	56.2	1.60	2.29
86/07/02	1422	315	-0.39	55.5	1.58	1.26
86/07/02	1444	317	-0.38	55.2	1.57	2.25
86/07/02	1334	318	-0.38	55.0	1.56	2.24

Table 4. N (10 μm) Photometry of Io (J1) (continued).

Date (UT)	Time (UT)	Orbital Phase Angle (deg.)	Observed			Spectral Emittance (10^{-1} $Wm^{-2}\mu m^{-1}$)
			Magnitude	Flux Density		
				(Jy)	(10^{-16} $Wcm^{-2}\mu m^{-1}$)	
86/08/03	1014	313	-0.62	68.6	1.561	2.31
86/08/03	1034	316	-0.61	67.6	1.92	2.29
86/08/03	1053	318	-0.60	67.3	1.91	2.26
86/08/03	1211	329	-0.38	27.2	0.775	0.917
86/08/03	1212	330	-0.54	65.7	1.81	2.1*
86/08/03	1233	333	-0.54	63.7	1.81	2.15
86/08/03	1311	338	-0.48	60.4	1.72	2.03
86/08/03	1326	340	-0.49	61.0	1.73	2.05
86/08/03	1353	344	0.55	23.2	0660	0.782
86/08/03	1406	346	0.62	21.9	0.621	0.736
86/08/04	920	149	-0.52	629	1.78	2.01
86/08/04	939	152	-0.51	61.8	1.76	2.08
86/08/04	953	154	-0.51	620	1.76	2.08
86/08/04	1009	156	-0.51	61.8	1.76	2.07
86/08/05	1207	91	-0.22	47.0	1.34	1.58
86/08/05	1213	17	-0.20	46.4	1.32	1.55
86/08/05	1229	19	-0.20	666	1.32	1.56
86/08/05	1243	21	-0.20	699	1.32	1.55
86/08/05	1259	24	-0.20	46.7	1.33	1.56
86/08/05	1320	27	-0.20	46.5	1.32	1.55
86/08/05	1336	29	-0.20	46.4	1.32	1.55
86/08/05	1351	31	-0.20	46.4	1.32	1.55
86/08/05	1406	33	-0.20	46.5	1.32	1.55
86/08/05	1426	36	-0.20	46.6	1.32	1.56
86/08/05	1441	38	-0.21	46.9	1.33	1.57
86/08/05	1456	40	-0.22	47.3	1.34	1.58
86/08/05	1508	42	-0.22	47.5	1.35	1.59
86/08/06	957	201	-0.42	57.0	1.62	1.89
86/08/06	1015	204	-0.44	57.9	1.W	1.92
86/08/06	1034	207	-0.43	57.3	1.69	1.90
86/08/06	1407	247	-0.47	65.1	1.70	1.99
86/08/06	1438	241	-0.50	61.0	1.74	2.04
86/08/07	956	48	-0.50	61.5	1.75	2.04
86/08/07	1029	53	-0.52	629	1.77	2.06
86/08/07	1042	55	-0.51	62.2	1.77	2.02
86/08/07	1206	67	-0.53	63.1	1.79	2.02
86/08/07	1325	78	-0.55	64.1	1.82	2.12
86/08/07	1328	78	-0.54	63.8	1.81	2.11
86/08/07	1345	81	-0.55	64.0	1.82	2.12
96/08/07	1418	86	-0.57	659	1.87	2.17
86/08/07	1431	87	-0.58	66.2	1.88	2.19
86/08/08	1055	252	-0.54	659	1.82	2.11
87/09/28	1155	281	-0.80	80.7	2.29	2.51
87/09/28	1158	283	-0.77	78.7	2.24	2.45
87/09/28	1209	286	-0.75	77.6	2.20	2.41

Table 4. N (10 μm) Photometry of Io (J1) (continued).

Date (UT)	Time (UT)	Orbital Phase Angle (deg.)	Observed			Spectral Emittance (10^{4} $Wm^{-2}\mu m^{-1}$)
			Magnitude	Flux Density		
				(Jy)	(10^{-16} $Wcm^{-2}\mu m^{-1}$)	
87/09/28	1230	292	^ 75	77.5	2.20	z 41
87/09/28	1309	300	-0.78	79.3	2.25	z 47
87/09/28	1409	301	-0.78	79.2	2.25	2.46
87/09/28	141 1	7OL	-0.80	80.6	62"2	2.51
87/09/28	1457	S09	-0.77	790	2 25	2 46
87/11/23	1507	116	-0.42	57 /	1 62	2.28
87/1 1/23	652	120	-0 42	57 2	1 63	2 31
87/1 1/23	740	1Z1	c78	57 5	T 63	z 34
87/11/23	816	/32	-0 43	57 7	/ M	z3O
87/ 1 1/23	830	10	-0.44	57 9	1.64	2.31
87/11/23	1049	T54	^ 47	59.8	1 70	6C:Z
87/11/23	1122	459	-0 52	62 S	1 78	2.49
87/ 1 1/25	504	152	-0.44	58 2	1.65	2 35
87/11/25	536	157	-0 46	58 9	1 68	2.38
87/1 1/25	610	162	^ 47	59 7	J.70	z 41
87/11/25	6Z ●	164	-0 48	60 2	1.71	2.43
87/11/25	M ^	166	-0 52	6Z z	1.77	z 52
87/1 1/25	1035	661	^ 43	57 6	I M	z 33
87/11/25	I0S0	[02	-0 42	57 1	1.62	z 31
87/1 1/2S	1120	S02	-0.43	57.3	1 63	z 32
87/11/26	751	19	-0 02	39 C	1.12	1 60
87/1 1/26	753	02	^ 02	39 C	1 12	/ W
87/11/26	808	22	-0 11	42 1	1.22	/ 74
87/ 1 1/26	823	24	^ 13	43 7	1 24	1 78
87/1 1/26	945	36	-0 14	44.1	1.25	1.80
87/1 1/26	1058	46	-0 23	930	1 36	i 95
88/11/16	802	S0	-0 31	51 S	1.46	1.62
88/11/16	804	S0	^ 31	51 C	1.46	1 61
88/11/16	839	55	-0 32	52 2	1 48	1 M
88/1 3/16	841	55	-0 32	51 9	1.48	1.63
88/11/16	952	W	^ 35	53 6	1.52	1.68
88/1 1/16	953	W	-0 34	52 3	T50	1.66
88/1 1/16	1007	68	^ CC	52 6	1.50	1.66
88/ 11/16	1009	68	^ 33	52 S	1 49	1 65
88/1 1/16	1022	70	-0 35	53 5	1 52	1.68
88/11/16	1023	70	-0 35	53 5	1 52	/ W
88/11/16	1129	79	^ 35	53 z	1.51	1.67
88/11/16	1130	79	-0 S6	90 S	1S ●	/ 70
89/01/18	7S9	286	-0 37	54 2	1 54	2.11
89/01/18	811	288	-0 CC	52 6	1.50	1.79
89/01/18	841	292	-0 33	52 2	1 48	1.77
89/01/18	9 1 9	298	^ 42	57 1	1 62	T 93
89/01/18	932	302	-0 40	SS 9	1 59	1 89
89/01/18	952	302\	-0 42	S6 9	1 62	1 92
89/01/18	1016	306	^ 47	S99	/ 70	z CC

Table 4. N (10 μm) Photometry of Io (J1) (continued).

Date (UT)	Time (UT)	Orbital Phase Angle (deg.)	Observed			Spectral Emittance (10^{4} $Wm^{-2}\mu m^{-1}$)
			Magnitude	Flux Density		
				(Jy)	(10^{-16} $Wcm^{-2}\mu m^{-1}$)	
89/01/18	1031	308	-0.48	60.0	/-7I	2 34
89/01/18	1044	310	-0.46	59.1	1.68	2 31
89/01/18	1046	3 I0	-0.50	61.4	1.75	2 39
89/12/12	845	S6	-0.03	39.9	1 13	T 35
89/12/12	3 S 7	38	-000	39 6	1.13	1.35
89/12/12	9 I 0	39	-0.04	40.1	1.14	1.36
89/12/12	9Z 7	42	-0.05	40 6	1.15	1 38
89/12/12	I0I0	48	-009	42.0	1.19	/ 43
89/12/12	1026	S0	-0.12	43.3	1.23	/ 47
89/12/12	1112	57	-0.15	44.3	1.26	/.S0
89/12/12	1 128	S9	-0.17	45.3	1.29	1 54
89/12/ 12	1239	69	-0.25	48.9	1 39	1.66
89/12/12	1253	71	^ 26	49.1	1 39	1 67
89/12/12	LOCI	n	^ 26	49 2	1 40	1 67
89/12/12	1336	n	-0 30	51 1	1 45	1 74
89/12/12	1350	79	^ 33	52 3	1 49	1 78
89/12/12	1421	83	0 ●	52 8	1 50	1 79
89/ 12/12	1435	85	-0 36	54 1	1 54	1 84
89/12/14	● 703	69	-0 22	45 3	1 29	1 53
89/12/14	● 0 1	72	0 21	45 2	1 28	/ 53
89/12/14	● 741	74	-0 20	44 6	1 27	1S 1
89/12/14	746	S1	-0 22	45 4	1 29	1 54
89/ 12/14	843	83	-0 24	46 3	1 32	1 57
89/12/14	900	85	0 12	41 3	1 17	T 40
89/12/14	921	88	^ 17	43 6	1 24	1.48
89/12/14	● 957	9O	-0.29	48.5	/ 38	i M
89/12/14	1017	96	-0.30	48.9	/ 39	991
89/12/14	1034	98	-0.33	50.5	/ M	/ 71
89/12/14	1108	103	^ CC	50.3	/.43	1 70
89/ 12/14	1128	106	-0 34	50.9	1 45	i 72
89/12/15	1235	319	-0.69	70 1	661	Z 37
89/12/15	1251	321	-0.67	68.6	/ 95	2 32
89/12/15	1400	CC1	-0.64	67.2	1 91	2 27
89/12/15	1416	333	-0 64	66.9	T.90	2 26
89/12/15	1443	337	-0.63	66.5	1.89	2 25
89/12/15	1500	340	-0.62	65.6	/.87	2 22
89/12/15	1517	342	-0.56	62.0	i 76	z 10
89/12/15	1530	344	0.05	35.6	1 0I	1 20
89/12/16	6 S 6	115	-0.40	53.5	1 52	1.80
89/12/16	718	118	-0.29	48.7	1 39	/ W
89/12/16	7C9	m	-0.26	47 3	/ 34	1 59
89/12/ 16	913	134	-0.31	49 4	1 41	1 67
89/12/16	9C0	137	-0 33	50.4	1 43	1 70
89/12/16	1028	145	-0 41	54.4	T 55	T 83
89/12/16	S601	1 "7	-070	53.7	1.53	i 81

Table 4. N (10 μm) Photometry of Io (J1) (continued).

Date (UT)	Time (UT)	Orbital Phase Angle (deg.)	Observed			Spectral Emittance (10^{-1} Wm$^{-2}\mu$m^{-1})
			Magnitude	Flux Density		
				(Jy)	(10^{-16} Wcm$^{-2}\mu$m^{-1})	
90/01/06	650	70	-0.20	46.6	1.32	1.57
90/01/06	704	71	-0.21	46.8	1.33	1.58
90/01/06	717	74	-0.22	47.6	1.35	1.61
90/01/06	738	77	-0.20	46.6	1.33	1.58
90/01/06	754	79	-0.21	46.8	1.33	1.59
90/01/06	819	83	-0.26	49.2	1.40	1.66
90/01/06	850	86	-0.26	49.0	1.39	1.65
90/01/06	1152	113	-0.24	48.2	1.37	1.63
90/01/06	1203	115	-0.22	47.0	1.34	1.60
90/01/06	1220	119	-0.29	50.1	1.44	1.71
90/01/06	1250	121	-0.29	50.6	1.44	1.71
90/01/07	558	266	-0.65	70.6	2.01	2.39
90/01/07	607	272	-0.66	70.8	2.01	2.39
90/01/07	622	274	-0.67	71.7	2.04	2.42
90/01/07	705	276	-0.71	74.0	2.11	2.51
90/01/07	718	278	-0.72	70.8	2.13	2.53
90/01/07	734	280	-0.73	75.7	2.15	2.56
90/01/07	804	284	-0.75	77.2	2.20	2.61
90/01/07	817	286	-0.75	77.5	2.20	2.62
90/01/07	831	288	-0.66	71.0	2.03	2.41
90/01/07	836	289	-0.77	78.3	2.23	2.65
90/01/07	906	293	-0.80	81.0	2.30	2.73
90/01/07	919	295	-0.80	81.2	2.31	2.75
90/01/07	932	297	-0.79	80.0	2.27	2.70
90/01/07	1050	308	-0.79	80.4	2.29	2.72
90/01/07	1101	309	-0.79	79.8	2.27	2.70
90/01/07	1117	311	-0.78	79.7	2.26	2.69
90/01/07	1136	315	-0.79	79.7	2.27	2.70
90/01/07	1159	317	-0.78	79.2	2.25	2.68
90/01/07	1237	323	-0.76	78.2	2.22	2.64
90/01/07	1250	325	-0.74	76.7	2.18	2.59
90/01/07	1313	328	-0.73	75.6	2.15	2.55
90/01/07	1326	330	-0.72	75.0	2.13	2.54
90/01/07	1340	332	-0.70	73.7	2.09	2.49
90/01/07	1353	333	-0.68	72.2	2.05	2.44
90/01/08	608	111	-0.26	49.3	1.40	1.67
90/01/08	621	113	-0.26	49.1	1.40	1.66
90/01/08	639	115	-0.26	49.1	1.39	1.66
90/01/08	736	124	-0.27	49.8	1.42	1.69
90/01/08	750	126	-0.27	49.8	1.42	1.68
90/01/08	804	128	-0.28	50.1	1.42	1.69
90/01/08	846	134	-0.30	50.9	1.45	1.72
90/01/08	859	136	-0.29	50.6	1.43	1.70
90/01/08	912	137	-0.29	50.6	1.44	1.71
90/01/08	939	141	-0.32	52.0	1.48	1.76

Table 4. N (10 μm) Photometry of Io (J1) (continued).

Date (UT)	Time (UT)	Orbital Phase Angle (deg.)	Observed			Spectral Emittance (10^{-1} Wm$^{-2}\mu$m^{-1})
			Magnitude	Flux Density		
				(Jy)	(10^{-16} Wcm$^{-2}\mu$m^{-1})	
90/01/08	952	143	-0.32	52.0	1.48	1.76
90/01/08	1015	146	-0.33	52.5	1.49	1.77
90/01/08	1028	148	-0.32	52.1	1.48	1.76
90/01/08	1050	151	-0.32	52.0	1.48	1.76
90/01/08	1102	153	-0.32	52.1	1.48	1.76
90/01/08	1124	156	-0.33	52.5	1.49	1.77
90/01/08	1136	157	-0.33	52.6	1.49	1.78
90/01/08	1147	159	-0.34	53.1	1.51	1.79
90/01/08	1210	162	-0.33	52.2	1.48	1.77
90/01/08	1226	162	-0.34	53.0	1.51	1.79
90/01/08	1241	167	-0.38	54.7	1.56	1.85
90/01/09	711	324	-0.77	78.9	2.24	2.68
90/01/09	725	326	-0.77	78.6	2.24	2.67
90/01/09	738	328	-0.76	77.7	2.21	2.64
90/01/09	811	331	-0.75	77.1	2.19	2.62
90/01/09	815	333	-0.74	76.4	2.17	2.59
90/01/09	856	338	-0.70	74.0	2.10	2.51
90/01/09	911	341	-0.68	72.5	2.06	2.46
90/01/09	927	343	-0.67	71.9	2.04	2.44
90/01/09	943	345	-0.66	71.3	2.03	2.42
90/01/09	958	347	-0.66	71.2	2.03	2.42
90/01/09	1006	349	-0.57	65.6	1.86	2.22
90/01/10	648	164	-0.32	52.0	1.48	1.77
90/01/10	657	167	-0.33	52.3	1.49	1.78
90/01/10	701	167	-0.34	52.7	1.50	1.79
90/01/10	1029	195	-0.28	50.1	1.42	1.70
90/01/10	1041	197	-0.24	48.2	1.37	1.64
90/01/10	1101	200	-0.29	50.6	1.44	1.72
90/01/10	1131	204	-0.31	51.5	1.46	1.75
90/01/10	1145	206	-0.28	50.3	1.43	1.71
90/01/10	1201	208	-0.29	50.4	1.43	1.71
90/01/10	1227	212	-0.32	51.8	1.47	1.76
90/01/10	1242	214	-0.31	51.6	1.47	1.76
90/01/10	1257	216	-0.33	52.2	1.48	1.78
90/01/10	1320	220	-0.35	53.4	1.52	1.82
92/02/04	1237	59	-0.10	34.2	0.970	1.34
92/02/04	1300	63	-0.12	34.5	0.981	1.35
92/02/04	1311	64	-0.10	34.2	0.972	1.34
92/02/04	1338	68	-0.11	34.8	0.990	1.37
92/02/04	1356	71	-0.10	35.2	0.999	1.38
92/02/05	1000	246	-0.03	39.6	1.13	1.55
92/02/05	1046	247	-0.04	40.0	1.14	1.56
92/02/05	1100	248	-0.13	43.4	1.23	1.70
92/02/05	1323	270	-0.13	43.4	1.23	1.70
92/02/05	1349	272	-0.10	43.9	1.25	1.71

Table 4. N (10 μm) Photometry of Io (J1) (continued).

Date (UT)	Time (UT)	Orbital Phase Angle (deg.)	Observed			Spectral Emittance (10^{-1} $Wm^{-2}\mu m^{-1}$)
			Magnitude	Flux Density		
				(Jy)	(10^{-16} $Wcm^{-2}\mu m^{-1}$)	
92/02/05	1401	275	-0.14	43.9	1.25	1.71
92/02/07	906	270	-0.21	46.9	1.33	1.82
92/02/07	918	282	-0.18	45.9	1.30	1.78
92/02/07	951	287	-0.21	46.9	1.33	1.82
92/02/07	1007	289	-0.21	46.9	1.33	1.82
92/02/07	1124	300	-0.23	47.9	1.36	1.86
92/02/07	1155	302	-0.23	47.7	1.35	1.85
92/02/07	1223	308	-0.21	47.1	1.33	1.83
92/02/07	1236	310	-0.20	46.6	1.32	1.81
92/02/07	1318	316	-0.18	45.7	1.30	1.77
92/02/07	1344	320	-0.17	45.4	1.29	1.76
92/02/07	1501	331	-0.10	42.5	1.21	1.65
92/02/07	1514	332	-0.07	41.3	1.17	1.61
92/02/07	1527	333	-0.05	40.5	1.15	1.57
92/02/07	1530	333	-0.05	40.6	1.15	1.58
92/02/07	1539	336	-0.06	40.7	1.16	1.58
92/02/07	1554	338	-0.07	41.2	1.17	1.60
92/02/07	1559	339	-0.06	40.9	1.16	1.59
92/02/08	914	125	-0.00	39.8	1.13	1.55
92/02/08	928	127	0.07	41.2	1.17	1.61
92/02/08	1140	146	-0.08	41.8	1.19	1.62
92/02/08	1155	148	-0.04	40.0	1.14	1.55
93/03/25	735	197	0.00	38.8	1.10	1.49
93/03/25	749	199	0.01	39.1	1.11	1.51
93/03/25	834	206	0.00	38.6	1.10	1.48
93/03/25	852	208	-0.01	39.1	1.11	1.50
93/03/25	958	217	0.00	38.8	1.10	1.49
93/03/25	1011	219	-0.01	39.1	1.11	1.50
93/03/25	1025	221	0.01	38.9	1.11	1.49
93/03/25	1206	236	0.03	39.6	1.13	1.52
93/03/25	1220	237	-0.00	39.9	1.13	1.53
93/03/25	1316	245	-0.04	40.3	1.15	1.55
93/03/25	1331	248	0.01	38.9	1.11	1.49
93/03/25	1412	253	-0.05	40.5	1.15	1.55
93/03/25	K* I	255	-0.02	39.5	1.12	1.52
93/03/26	642	66	0.17	33.0	0.938	1.27
93/03/26	700	95	0.17	33.2	0.944	1.27
93/03/26	714	38	0.18	32.9	0.935	1.26
93/03/26	727	40	0.15	33.6	0.956	1.29
93/03/26	740	42	0.14	34.0	0.967	1.30
93/03/26	823	W	0.10	34.9	0.993	1.34
93/03/26	836	69	0.12	34.6	0.982	1.32
93/03/26	924	56	0.09	35.6	1.01	1.37
93/03/26	1026	65	0.09	35.5	1.01	1.36
93/03/26	1133	74	0.05	36.9	1.05	1.42

Table 4. N (10 μm) Photometry of Io (J1) (continued).

Date (UT)	Time (UT)	Orbital Phase Angle (deg.)	Observed			Spectral Emittance (10^{-1} $Wm^{-2}\mu m^{-1}$)
			Magnitude	Flux Density		
				(Jy)	(10^{-16} $Wcm^{-2}\mu m^{-1}$)	
93/03/26	1245	15	0.04	37.2	1.06	1.43
93/03/26	1258	86	0.07	37.0	1.05	1.42
93/03/26	1340	92	0.02	37.9	1.08	1.45
93/03/26	1410	76	0.00	38.1	1.08	1.46
93/03/26	1425	99	0.00	37.6	1.07	1.44
93/03/26	1439	101	0.00	38.6	1.10	1.48
93/03/27	634	236	-0.08	41.7	1.19	1.60
93/03/27	647	238	-0.06	41.0	1.17	1.57
93/03/27	705	240	0.08	41.1	1.17	1.58
93/03/27	720	242	-0.08	41.5	1.18	1.59
93/03/27	753	247	-0.11	42.9	1.22	1.64
93/03/27	844	254	-0.13	43.7	1.24	1.67
93/03/27	856	256	-0.13	43.5	1.24	1.67
93/03/27	931	261	-0.17	45.2	1.29	1.73
93/03/27	1021	268	-0.17	45.0	1.29	1.74
93/03/27	1035	270	-0.15	44.6	1.27	1.71
93/03/27		272	-0.19	46.2	1.31	1.77
93/03/27	1154	281	-0.20	46.7	1.33	1.79
93/03/27	1208	283	-0.19	46.1	1.31	1.77
93/03/27	1256	290	-0.10	46.6	1.33	1.79
93/03/27	1321	295	-0.20	46.9	1.32	1.78
93/03/27	1335	295	-0.20	46.3	1.32	1.78
93/03/27	1403	299	-0.19	46.0	1.31	1.76
93/03/27	1416	301	-0.17	45.4	1.29	1.74
93/03/27	1430	303	-0.20	46.7	1.33	1.79
93/03/28	634	64	0.00	38.0	1.08	1.45
93/03/28	647	81	0.16	33.5	0.951	1.28
93/03/28	657	83	0.00	37.8	1.07	1.45
93/03/28	705	84	0.01	37.0	1.05	1.42
93/03/28	737	88	0.03	37.8	1.07	1.45
93/03/28	749	90	0.04	37.3	1.06	1.43
93/03/28	818	94	0.00	38.6	1.10	1.48
93/03/28	830	96	0.00	38.6	1.10	1.48
93/03/28	858	100	0.00	38.9	1.10	1.49
93/03/28	957	108	0.02	38.1	1.08	1.46
93/03/28	1009	110	0.00	38.3	1.08	1.47
93/03/28	1125	125	-0.02	39.2	1.12	1.51
93/03/28	1212	127	0.00	38.5	1.09	1.46
93/03/28	1301	134	0.00	38.5	1.09	1.47
93/03/28	1314	136	0.02	38.1	1.08	1.46
93/03/28	1335	139	-0.01	38.9	1.11	1.49
93/03/29	600	283	-0.09	42.2	1.20	1.61
93/03/29	647	285	-0.14	44.2	1.26	1.69
93/03/29	702	287	-0.15	44.5	1.27	1.70
93/03/29	734	291	-0.20	46.6	1.33	1.78

Table 4. N (10 μm) Photometry of Io (J1) (continued).

Date (UT)	Time (UT)	Orbital Phase Angle (deg.)	Observed			Spectral Emittance (10^{-1} $Wm^{-2}\mu m^{-1}$)
			Magnitude	Flux Density		
				(Jy)	(10^{-26} $Wcm^{-2}\mu m^{-1}$)	
93/03/29	747	293	-0.22	47.0	1.34	1.81
93/03/29	839	301	-0.25	48.5	1.38	1.86
93/03/29	851	302	-0.24	48.0	1.37	1.85
93/03/29	939	309	-0.24	48.3	1.37	1.85
93/03/29	952	311	-0.24	48.4	1.38	1.85
93/03/29	1050	319	-0.27	49.5	1.41	1.89
93/03/29	1108	322	-0.25	48.6	1.38	1.86
93/03/29	1141	326	-0.22	47.5	1.35	1.82
93/03/29	1155	328	-0.21	46.8	1.33	1.79
93/03/29	1240	335	-0.17	45.1	1.28	1.70
93/03/29	1252	336	-0.15	44.6	1.27	1.71
93/03/29	1305	338	-0.13	43.7	1.24	1.67
93/03/29	1319	340	-0.13	44.4	1.23	1.66
93/03/29	1333	342	-0.11	42.9	1.22	1.64
93/03/29	1352	345	-0.10	42.0	1.21	1.62
93/03/29	1405	347	-0.13	43.6	1.24	1.67

Table 5. Q (20 μm) Photometry of Io (J1).

Date (UT)	Time (UT)	Orbital Phase Angle (deg.)	Observed			Spectral Emittance (10^{-1} $Wm^{-2}\mu m^{-1}$)
			Magnitude	Flux Density		
				(Jy)	(10^{-26} $Wcm^{-2}\mu m^{-1}$)	
80/04/12		35	-3.63	278	2.09	3.16
82/03/19		342	-3.96	377	2.83	4.26
82/03/19		343	-3.94	370	2.78	4.20
83/02/11		326	-3.51	249	1.87	2.79
83/02/18		333	-3.53	254	1.90	2.86
83/02/18		337	-3.52	252	1.89	2.82
83/02/18		340	-2.77	126	0.946	1.91
83/02/18		340	-2.78	123	0.920	1.86
83/03/06		339	-3.90	357	2.68	4.02
83/03/11	0851	102	-3.93	366	2.74	4.08
83/03/11	1510	102	-3.92	362	2.72	4.03
83/04/24		56	-3.90	357	2.68	3.79
83/07/19	828	51	-3.62	276	2.07	3.08
83/07/19	837	53	-3.61	273	2.05	3.05
83/07/19	904	57	-3.60	271	2.03	3.02
83/07/19	907	59	-3.58	266	1.99	2.97
83/07/19	942	63	-3.61	273	2.05	3.05
83/07/19	945	64	-3.61	273	2.05	3.05
83/07/20	602	236	-3.79	323	2.42	3.62
83/07/20	606	237	-3.80	326	2.44	3.65
83/07/20	801	253	-3.81	329	2.46	3.69
83/07/20	810	254	-3.79	323	2.42	3.62
83/07/20	847	259	-3.82	338	2.53	3.79
83/07/20	855	260	-3.82	332	2.49	3.72
83/07/20	924	265	-3.72	298	2.27	3.40
83/07/20	933	266	-3.79	323	2.42	3.62
83/07/20	958		-3.81	326	2.44	3.65
83/07/20	1007	270	-3.73	305	2.29	3.43
83/07/21	524	74	-3.66	286	2.15	3.23
83/07/21	533	75	-3.59	268	2.01	3.00
83/07/21	556	78	-3.59	268	2.01	3.03
83/07/21	617	82	-3.57	263	1.98	2.97
83/07/21	706	91	-3.65	284	2.13	3.20
83/07/21	706	92	-3.62	276	2.07	3.11
83/07/21	757	95	-3.77	281	2.11	3.17
83/07/21	935	109	-3.66	286	2.15	3.23
83/07/21	943	110	-3.77	286	2.15	3.23
83/08/07	811	317	-3.75	311	2.33	3.87
83/08/07	827	319	-3.78	320	2.40	3.98
83/08/07	839	321	-3.76	314	2.35	3.90
83/08/07	851	324	-3.76	314	2.35	3.90
83/08/07	905	326	-3.80	326	2.44	4.05
84/05/08	1252	114	-3.92	364	2.73	3.92
84/05/08	1308	116	-3.91	360	2.70	3.88
84/05/08	1341	121	-3.89	354	2.65	3.81
84/05/08	1354	123	-3.87	347	2.60	3.74

Table 5. Q (20 μm) Photometry of Io (J1) (continued).

Date (UT)	Time (UT)	Orbital Phase Angle (deg.)	Observed			Spectral Emittance (10^{-4} Wm$^{-2}\mu$m^{-1})
			Magnitude	Flux Density (Jy)	Flux Density (10^{-16} Wcm$^{-2}\mu$m^{-1})	
84/05/08	1431	128	-3.82	332	2.49	3.57
84/05/08	1443	130	-3.83	335	2.51	3.60
84/07/19	656	323	-4.17	456	3.42	4.20
84/07/19	718	326	-4.21	462	3.55	4.35
84/07/19	729	327	-4.16	454	3.40	4.18
84/07/19	802	332	-4.13	442	3.31	4.07
84/07/19	820	334	-4.12	436	3.27	4.01
84/08/19	657	153	-3.96	377	2.83	3.94
84/08/19	732	158	-4.03	402	3.02	4.20
84/08/19	816	165	-3.98	384	2.88	4.01
84/08/19	825	166	-3.98	384	2.88	4.01
84/08/19	835	167	-3.99	388	2.91	4.05
84/08/20	545	347	-4.08	423	3.16	4.29
84/08/20	1019	20	-3.78	320	2.40	3.36
85/06/06	1146	325	-3.59	292	2.01	2.82
85/06/06	1157	327	-3.66	286	2.15	3.00
85/06/06	1237	332	-3.93	367	2.75	3.85
85/06/06	1245	333	-3.89	354	2.65	3.71
85/06/07	1058	162	-4.15	449	3.37	4.69
85/06/07	1111	163	-4.02	399	2.99	4.16
85/06/08	1243	20	-3.60	271	2.03	2.81
85/06/08	1313	24	-3.71	305	2.29	3.16
85/06/08	1355	30	-3.90	357	2.68	3.70
85/06/08	1420	30	-3.80	326	2.44	3.38
85/06/09	1123	212	-3.97	381	2.86	3.92
85/06/09	1134	214	-3.91	360	2.70	3.71
85/06/09	1202	218	-3.87	347	2.60	3.58
85/06/09	1226	222	-3.90	357	2.68	3.68
85/06/09	1243	225	-3.89	354	2.65	3.64
85/06/09	1252	225	-3.94	370	2.78	3.82
85/06/10	1152	60	-3.62	276	2.07	2.83
85/06/10	1201	59	-3.70	297	2.23	3.04
85/06/10	1211	63	-3.70	297	2.23	3.04
85/06/10	1234	66	-3.71	300	2.25	3.07
85/06/10	1244	67	-3.70	297	2.23	3.04
85/06/10	1256	69	-3.71	300	2.25	3.07
85/07/09	1114	191	-4.15	449	3.37	3.98
85/07/10	852	22	-3.85	301	2.26	3.10
85/07/10	1017	30	-3.85	341	2.56	3.10
85/07/10	1219	45	-3.96	377	2.83	3.88
85/07/10	1356	65	-4.01	395	2.96	3.49
85/07/10	1411	69	-4.01	395	2.96	3.49
85/07/11	859	226	-4.08	421	3.16	3.71
85/07/11	945	233	-4.11	433	3.25	3.81
85/07/11	1013	237	-4.18	462	3.47	4.06
85/07/11	1033	239	-4.18	462	3.47	4.06

Table 5. Q (20 μm) Photometry of Io (J1) (continued).

Date (UT)	Time (UT)	Orbital Phase Angle (deg.)	Observed			Spectral Emittance (10^{-4} Wm$^{-2}\mu$m^{-1})
			Magnitude	Flux Density (Jy)	Flux Density (10^{-16} Wcm$^{-2}\mu$m^{-1})	
85/07/11	1044	241	-4.23	484	3.63	4.26
85/07/11	1205	252	-4.23	484	3.63	4.26
85/07/11	1223	255	-4.25	493	3.70	4.34
85/07/11	1247	258	-4.36	545	4.09	4.80
85/07/11	1310	262	-4.29	515	3.86	4.50
85/07/11	1348	267	-4.30	516	3.87	4.54
85/07/11	1431	273	-4.17	458	3.43	4.03
85/07/11	1454	276	-4.20	471	3.53	4.14
85/07/11	1528	281	-4.12	437	3.28	3.85
85/07/11	1539	283	-4.14	445	3.34	3.92
85/07/12	902	70	-3.93	367	2.75	3.22
85/07/12	1158	87	-4.14	445	3.34	3.90
85/07/12	1001	87	-4.17	458	3.43	4.03
85/07/12	1043	84	-4.17	458	3.43	4.02
85/07/12	1111	88	-4.22	479	3.60	4.20
85/09/12	716	79	-4.08	422	3.16	3.91
85/09/12	817	87	-4.15	448	3.36	4.16
86/06/25	1213	313	-4.08	419	3.14	4.11
86/06/25	1220	310	-4.00	391	2.93	4.39
86/06/25	1254	310	-3.89	352	2.64	3.96
86/06/25	1320	322	-3.89	351	2.64	3.95
86/07/02	1253	303	-4.05	407	3.05	4.37
86/07/02	1302	304	-4.06	411	3.08	4.41
86/07/02	1326	307	-4.07	415	3.11	4.46
86/07/02	1339	309	-4.08	421	3.15	4.52
86/07/02	1426	316	-4.00	389	2.92	4.18
86/07/02	1437	317	-4.03	401	3.01	4.31
86/07/02	1449	319	-4.03	401	3.01	4.31
86/08/03	1018	313	-4.01	392	2.96	4.18
86/08/03	1039	316	-4.00	391	2.94	4.18
86/08/03	1056	319	-4.05	410	3.07	4.64
86/08/03	1219	331	-4.05	409	3.07	4.63
86/08/03	1236	333	-4.10	429	3.22	4.81
86/08/03	1315	338	-4.07	416	3.12	4.70
86/08/03	1356	344	-3.25	196	1.47	1.70
86/08/04	923	149	-4.29	512	3.84	4.53
86/08/04	942	152	-4.25	491	3.69	4.35
86/08/04	956	154	-4.22	476	3.57	4.22
86/08/04	1011	156	-4.20	470	3.53	4.16
86/08/05	1215	17	-4.02	397	2.98	3.50
86/08/05	1232	20	-3.98	382	2.86	3.38
86/08/05	1246	22	-3.99	386	2.89	3.40
86/08/05	1323	27	-3.97	379	2.85	3.34
86/08/05	1338	29	-3.94	370	2.78	3.27
86/08/05	1354	31	-3.99	388	2.91	3.42
86/08/05	1429	36	-4.03	399	2.99	3.52

Table 5. Q (20 μm) Photometry of Io (J1) (continued).

Date (UT)	Time (UT)	Orbital Phase Angle (deg.)	Observed			Spectral Emittance (10^{-1} $Wm^{-2}\mu m^{-1}$)
			Magnitude	Flux Density		
				(Jy)	(10^{-16} $Wcm^{-2}\mu m^{-1}$)	
86/08/06	1443	38	-4.05	409	3.07	3.61
86/08/06	1001	202	-4.06	411	3.08	3.60
86/08/06	1018	204	-4.12	436	3.27	3.82
86/08/06	1036	207	-4.13	442	3.32	3.85
86/08/06	1410	237	-4.23	483	3.63	4.24
86/08/06	1440	241	-4.28	505	3.78	4.43
86/08/07	0956	49	-4.08	421	3.16	3.68
86/08/07	1001	53	-4.06	412	3.09	3.60
86/08/07	1044	55	-4.09	423	3.17	3.70
86/08/07	1221	69	-4.16	454	3.41	3.97
86/08/07	1331	79	-4.19	463	3.47	4.04
86/08/07	1348	81	-4.18	459	3.44	4.00
86/08/07	1422	86	-4.16	452	3.39	3.95
86/08/07	1434	88	-4.17	455	3.42	3.98
86/08/08	1048	252	-4.24	485	3.64	4.22
87/09/28	1232	282	-4.38	552	4.14	4.53
87/09/28	1312	292	-4.28	506	3.79	4.15
87/09/28	1413	301	-4.35	539	4.04	4.42
87/09/28	1521	310	-4.27	498	3.74	4.09
87/09/28	1509	309	-4.25		3.59	4.02
87/11/23	1159	121	-4.31	520	3.90	5.47
87/11/23	1216	124	-4.26	497	3.73	5.23
87/11/23	820	131	-4.30	513	3.85	5.40
87/11/23	835	135	-4.29	511	3.83	5.38
87/11/23	944	145	-4.26	497	3.72	5.23
87/11/23	1053	154	-4.31	519	3.89	5.47
87/11/23	1127	159	-4.38	553	4.15	5.82
87/11/25	508	153	-4.23	480	3.60	5.12
87/11/25	540	157	-4.26	498	3.73	5.31
87/11/25	619	162	-4.29	510	3.83	5.44
87/11/25	630	163	-4.33	535	3.98	5.66
87/11/25	644	163	-4.41	568	4.26	6.06
87/11/25	1040	200	-4.24	486	3.64	5.18
87/11/25	1050	202	-4.22	477	3.57	5.08
87/11/25	1111	206	-4.20	471	3.53	5.02
87/11/26	758	20	-3.94	369	2.77	3.97
87/11/26	813	23	-3.96	376	2.82	4.04
87/11/26	933	34	-3.94	371	2.78	3.98
87/11/26	956	36	-3.92	365	2.74	3.88
87/11/26	1102	49	-3.90	355	2.66	3.81
88/11/16	756	50	-4.06	414	3.10	3.44
88/11/16	800	50	-4.06	414	3.10	3.44
88/11/16	848	56	-4.04	406	3.05	3.37
88/11/16	849	57	-4.05	410	3.08	3.40
88/11/16	949	65	-4.19	464	3.48	3.85
88/11/16	1004	67	-4.12	438	3.28	3.63

Table 5. Q (20 μm) Photometry of Io (J1) (continued).

Date (UT)	Time (UT)	Orbital Phase Angle (deg.)	Observed			Spectral Emittance (10^{-1} $Wm^{-2}\mu m^{-1}$)
			Magnitude	Flux Density		
				(Jy)	(10^{-16} $Wcm^{-2}\mu m^{-1}$)	
88/11/16	1001	67	-4.13	441	3.31	3.66
88/11/16	1018	69	-4.23	483	3.62	4.01
88/11/16	1020	69	-4.20	469	3.52	3.90
88/11/16	1114	77	-4.16	450	3.38	3.74
88/11/16	1200	80	-4.20	467	3.50	3.88
89/01/18	1001	287	-4.12	437	3.28	4.50
89/01/18	1036	292	-4.16	452	3.39	4.04
89/01/18	1124	298	-4.13	440	3.30	3.93
89/01/18	1137	300	-4.11	431	3.23	3.85
89/01/18	1147	302	-4.05	408	3.06	3.64
89/01/18	1221	307	-4.28	504	3.78	5.18
89/01/18	1223	307	-4.30	514	3.85	5.28
89/01/18	1237	309	-4.30	516	3.87	5.31
89/12/12	1251	37	-3.79	322	2.41	3.89
89/12/12	1326	41	-3.83	334	2.50	3.00
89/12/12		47	-3.94	368	2.76	3.30
89/12/12	1101	49	-3.95	372	2.79	3.35
89/12/12	1117	57	-4.02	396	2.97	3.56
89/12/12	1244	70	-4.11	431	3.24	3.87
89/12/12	1259	72	-4.06	412	3.09	3.69
89/12/12	1341	78	-4.08	418	3.14	3.75
89/12/12	1428	78	-4.10	427	3.20	3.83
89/12/14	708	69	-4.13	438	3.29	3.91
89/12/14	809	77	-4.13	438	3.29	3.91
89/12/14	849	84	-4.14	442	3.32	3.96
89/12/14	1058	98	-4.28	504	3.78	4.50
89/12/14	1023	96	-4.34	536	4.02	4.79
89/12/14	1115	104	-4.35	539	4.04	4.81
89/12/15	1240	320	-4.38	554	4.16	4.95
89/12/15	1405	332	-4.27	501	3.76	4.47
89/12/15	1448	338	-4.17	457	3.43	4.07
89/12/16	702	341	-4.14	443	3.33	3.95
89/12/16	723	349	-4.13	441	3.31	3.93
89/12/16	918	135	-4.07	417	3.13	3.71
89/12/16	1000	146	-3.90	357	2.67	3.17
90/01/06	1139	11	-4.13	439	3.29	3.91
90/01/06	1201	11	-4.12	434	3.25	3.86
90/01/06	742	35	-4.09	424	3.18	3.77
90/01/06	1141	83	-4.08	418	3.14	3.73
90/01/06		113	-4.09	426	3.19	3.79
90/01/06	1236	113	-4.17	454	3.41	4.05
90/01/07	956	266	-4.11	433	3.25	3.85
90/01/07	1139	268	-4.19	466	3.49	4.15
90/01/07	1201	276	-4.30	517	3.87	4.61
90/01/07	1241	276	-4.33	529	3.96	4.73

Table 5. Q (20 μm) Photometry of Io (J 1) (continued).

Date (UT)	Time (UT)	Orbital Phase Angle (deg.)	Observed			Spectral Emittance (10^{-1} $Wm^{-2}\mu m^{-1}$)
			Magnitude	Flux Density (Jy)	Flux Density (10^{-16} $Wcm^{-2}\mu m^{-1}$)	
90/01/07	CZL	278	-4.33	6ZS	3.97	4.75
90/01/07	LO/10/06	284	-4.32	525	3.94	4.68
90/01/07	820	286	-4.29	508	3.81	4.53
90/01/07	100	293	-4.36	C*S	4.08	4.85
90/01/07	922	295	-4.38	9SS	4.17	4.96
90/01/07	1053	WC	-4.30	514	3.86	4.59
90/01/07	9011	310	-4.28	S06	3.79	4.51
90/01/07	LO/10/06	315	-4.28	C0S	3.77	4.49
90/01/07	LO/10/6CZ	323	-4.25	493	3.70	4.40
90/01/07	1315	328	-4.27	S00	3.75	4.46
90/01/07	1329	330	-4.26	495	3.71	4.42
90/01/07	1342	332	-4.27	501	3.76	4.47
90/01/08	019	112	-4.10	428	3.21	3.82
90/01/08	624	114	-4.11	430	3.23	3.84
90/01/08	mii	124	-4.13	439	3.29	3.91
90/01/08	754	921	-4.16	454	3.40	4.05
90/01/08	CW10K16	134	-4.18	460	3.45	4.11
90/01/08	106	136	-4.19	464	3.48	4.14
90/01/08	941	141	-4.22	476	3.57	4.24
90/01/08	L10I	147	-4.23	483	3.62	4.31
90/01/08	1052	152	-4.28	504	3.78	4.50
90/01/08	1126	156	-4.18	462	3.46	4.12
90/01/08	1136	158	-4.28	504	3.78	4.49
90/01/08	1212	163	-4.32	525	3.94	4.68
90/01/08	1228	165	-4.34	532	3.99	4.75
90/01/08	1244	167	-4.42	574	052	5.12
90/01/09	714	324	-4.38	551	4.14	4.94
90/01/09	727	326	-4.36	ch-	L0P	4.86
90/01/09	805	332	-4.32	526	3.94	4.71
90/01/09	858	339	-4.29	01S	3.83	4.57
90/01/09	914	301	-4.28	503	3.77	4.50
90/01/09	926	343	-4.27	S00	3.75	4.47
90/01/09	945	346	-4.25	493	3.70	4.41
90/01/10	10L	166	-4.08	420	3.15	3.77
01/10/06	1033	196	-4.18	462	3.46	4.14
90/01/10	1049	198	-4.23	484	3.63	4.34
90/01/10	1133	208	-4.26	497	3.72	4.46
90/01/10	1149	207	-4.29	510	3.83	4.58
90/01/10	1230	213	-4.28	S07	3.80	4.55
90/01/10	1246	215	-4.25	492	3.69	4.42
01/10/06	1322	220	-4.29	01S		4.58
90/01/10	1337	222	-4.14	444	3.33	3.99
92/02/04	1228	58	-3.70	Z97	2.23	3.07
92/02/04	1304	63	-3.78	320	2.40	3.31
92/02/04	1343	69	-3.75	311	2.33	3.22

Table 5. Q (20 μm) Photometry of Io (J1) (continued)

Date (UT)	Time (UT)	Orbital Phase Angle (deg.)	Observed			Spectral Emittance (10^{-1} $Wm^{-2}\mu m^{-1}$)
			Magnitude	Flux Density (Jy)	Flux Density (10^{-16} $Wcm^{-2}\mu m^{-1}$)	
92/02/05		246	-3.92	3M	2.73	3.75
92/02/05	1315	268	-3.96	377	2.83	3.89
92/02/05	1353	274	-3.97	384	2.88	3.96
92/02/07	908	281	-3.99	385	2.89	3.98
92/02/07	956	288	-3.91	S60	2.70	3.69
92/02/07	1129	305	-4.00	391	2.93	4.01
92/02/07	1228	309	-3.96	375	2.82	3.85
92/02/07	1324	317	-3.85	338	2.54	3.47
92/02/07	1506	331	-3.83	332	2.49	3.41
92/02/08	916	126	-3.95	373	2.80	3.82
92/02/08	1146	147	-4.01	396	2.96	4.04
93/03/25	741	198	-3.97	370	2.77	3.74
93/03/25	754	200	-3.95	374	2.80	3.78
93/03/25	840	206	-3.98	384	2.88	3.89
93/03/25	857	602	-3.98	3*C	2.88	3.89
93/03/25	1004	218	-4.04	406	3.05	4.11
93/03/25	1016	220	-4.05	407	3.05	4.12
93/03/25	1021	9CZ	LOW	418	3.13	4.23
93/03/25	1226	238	-4.06	414	3.10	4.19
93/03/25	1322	246	-3.99	387	2.90	3.91
93/03/25	1336	248	-3.97	378	2.83	3.83
93/03/25	1417	254	-3.96	363	2.72	3.68
93/03/25	1430	256	-4.09	S69	2.76	3.73
93/03/26	652	35	-3.72	3M	2.27	3.06
93/03/26	706	37	-3.75	311	2.33	3.14
93/03/26	719	S9	-3.83	335	2.51	3.38
93/03/26	732	40	-3.79	321	2.41	3.25
93/03/26	746	42	-3.81	323	2.42	3.27
93/03/26	828	48	-3.90	357	2.68	3.61
93/03/26	841	S0	-3.91	S60	2.70	3.64
93/03/26	926	57	-3.89	353	2.65	3.57
93/03/26	1032	W	-3.86	344	2.58	3.48
93/03/26	1138	75	-3.87	345	2.59	3.49
93/03/26	1250	85	-3.97	378	2.84	3.82
93/03/26	1304	87	-3.96	370	2.77	3.74
93/03/26	1346	93	-3.94	S69	2.77	3.73
93/03/26	1416	97	-3.95	373	2.80	3.78
93/03/26	1431	100	-3.93	367	2.75	3.71
93/03/27	609	236	-4.26	495	3.72	5.01
93/03/27	653	238	-4.19	465	3.49	4.70
93/03/27	710	241	-4.12	437	3.28	4.42
93/03/27	725	243	-4.11	430	3.23	4.35
93/03/27	758	248	-4.11	432	3.24	4.37
93/03/27	849	255	-4.04	406	3.04	4.10
93/03/27	902	257	-4.02	397	2.98	4.01
93/03/27	936	262	-3.98	382	2.87	3.86

Table 5. Q (20 μm) Photometry of Io (J1) (continued).

Date (UT)	Time (UT)	Orbital Phase Angle (deg)	Observed			Spectral Emittance (10^{-} $Wm^{-2}\mu m^{-1}$)
			Magnitude	Flux Density		
				(Jy)	(10^{-20} $Wcm^{-2}\mu m^{-1}$)	
93/03/27	TOZ7	269	-4 00	390	2.92	3.94
93/03/27	1041	271	*0 I	395	Z96	3.99
93/03/27	1200	282	-3 9S	372	2 79	ↄ76
93/03/27	1213	Z8*	-ↄ 96	375	2.82	3.79
93/03/27	1302	291	-3 93	365	2.74	3.69
93/03/27	1327	294	-3 96	377	Z 82	ↄ 81
93/03/27	1340	296	-3 97	380	2.85	3.84
93/03/27	1408	soo	-ↄ 98	381	2.86	3.86
93/03/27	1421	302	-3 98	382	2.86	3.86
93/03/27	1436	ↄM	*ↄ ↄ	402	ↄ 02	4 06
93/03/28	640	80	-3 83	335	2 SI	ↄ SC
93/03/28	652	82	-3 87	345	Z 58	3.48
93/03/28	7IO	8●	-3 85	340	2.55	ↄ 43
93/03/28	742	89	-3 86	343	Z 57	ↄ 47
93/03/28	755	9I	-ↄ 84	ↄ K	2 54	ↄ ¿Z
93/03/28	823	95	-3 88	349	Z 62	ↄ 53
93/03/28	SS6	97	-3 87	348	2 6I	ↄ 51
93/03/28	902	100	-3 89	354	Z 65	ↄ 57
93/03/28	1002	i99	-3 87	345	2.59	ↄ 49
93/03/28	1014	III	-ↄ 89	352	2 64	3 56
93/03/28	1204	I26	-3 91	360	ZTO	3.64
93/03/28	1217	i28	-3 89	354	2 ↄS	3 5S
93/03/28	1306	135	ↄ 9ↄ	ↄM	2.7ↄ	3.68
93/03/28	1319	137	-3 91	360	Z 70	ↄ 63
93/03/28	1341	140	-3 9I	S60	ZTO	3.64
93/03/29	638	284	*ↄ S	409	ↄ 07	4 13
93/03/29	652	286	-4 08	419	3.14	4 23
93/03/29	708	288	-4 05	410	ↄ 07	*I●
93/03/29	739	292	-4 09	424	ↄ 18	●28
93/03/29	752	294	-4 08	419	3.14	4 23
93/03/29	844	301	-4 09	425	ↄ19	4.29
93/03/29	857	303	-4 09	424	3 18	¿ 28
93/03/29	945	310	-4 I0	426	ↄ19	4 30
93/03/29	957	312	-4 10	427	ↄ ZO	4 31
93/03/29	i0S6	320	+O7	417	3. Iↄ	¿ 21
93/03/29	1115	323	-ↄ06	412	3 09	4 16
93/03/29	1147	ↄZ7	4 06	410	3 08	●15
93/03/29	1200	ↄZ9	*96	412	3 09	4 T6
93/03/29	IZ●	335	-3 99	387	2 90	ↄ 9I
93/03/29	1257	337	-3 98	385	Z 88	3 88
93/03/29	1310	339	-3 91	359	Z69	ↄ 62
93/03/29	1323	34i	-ↄ S9	353	2.65	ↄ 57
93/03/29	T342	344	-3 93	ↄ67	Z 76	ↄ 7I
93/03/ 29	1356	346	-3 93	S66	2.75	3 T0
93/03/29	1 410	347	-4 10	429	3 21	4 33

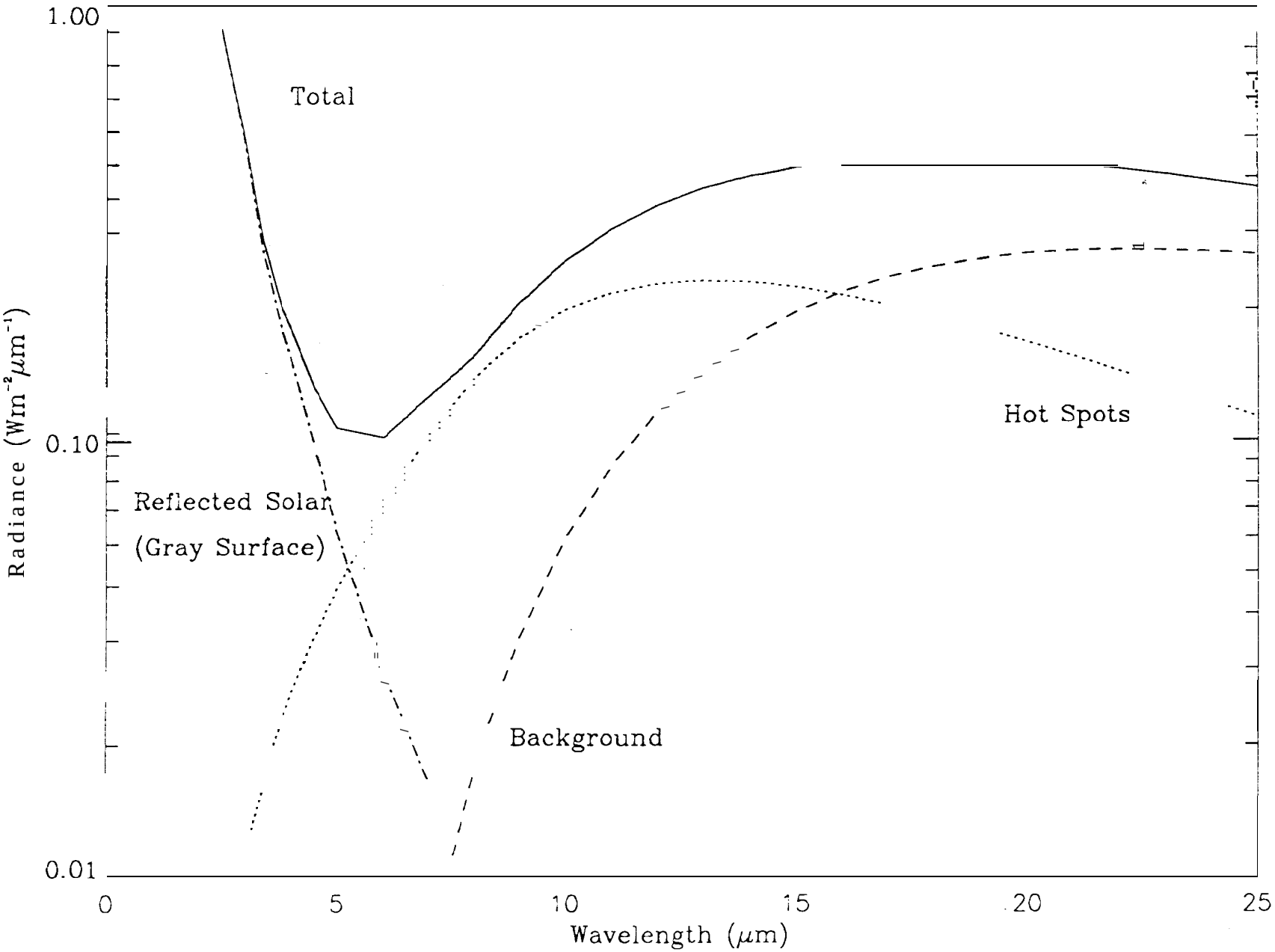
1.00
0.10
0.01
Radiance ($Wm^{-2}\mu m^{-1}$)
Total
Reflected Solar
(Gray Surface)
Background
Hot Spots
0
5
10
15
20
25
Wavelength (μm)

Fig. 1

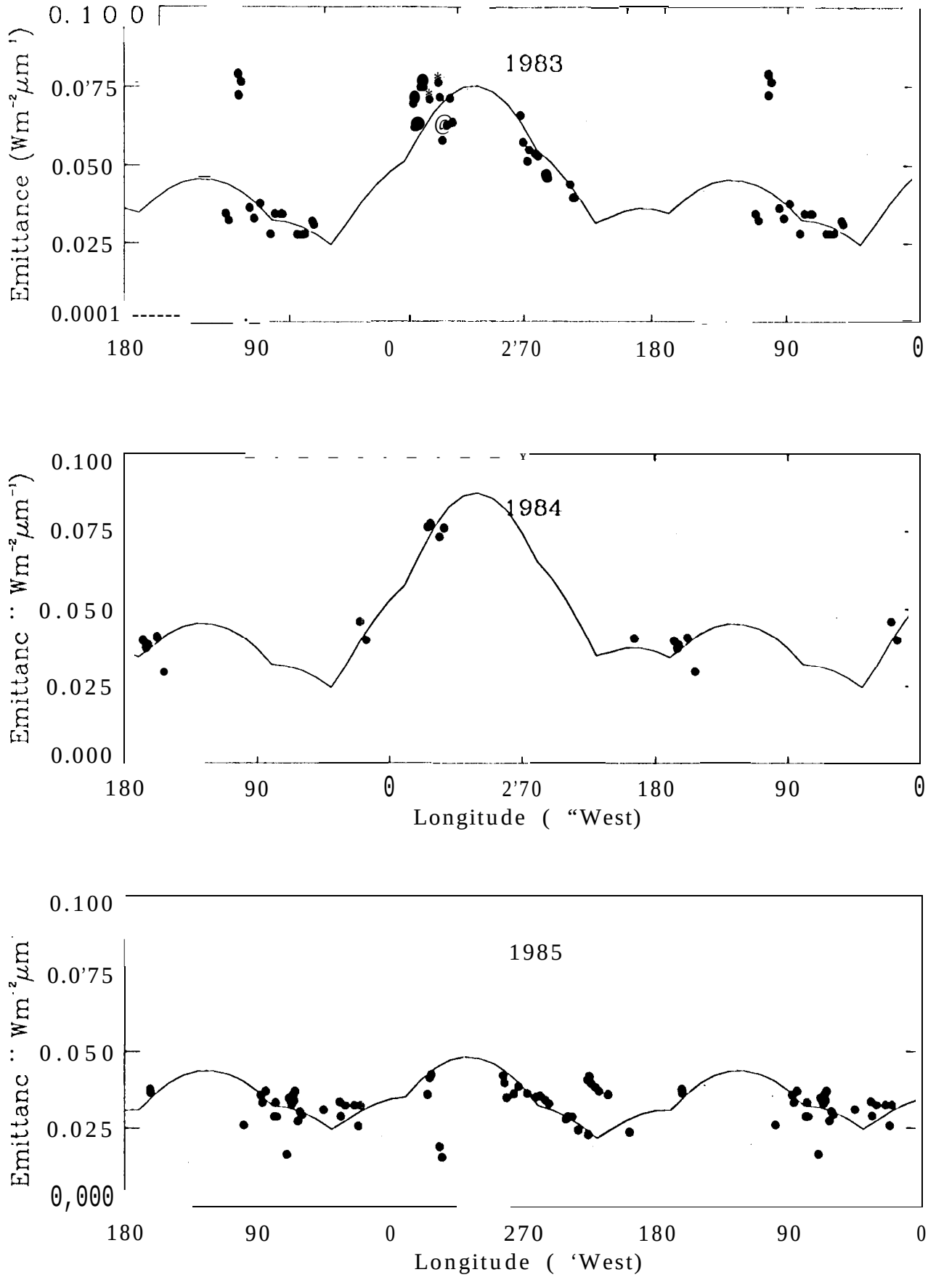
0.100
0.075
0.050
0.025
0.0001
Emittance (Wm$^{-2}\mu$m^{-1})
1983
180
90
0
270
180
90
0
1984
0.100
0.075
0.050
0.025
0.000
Emittanc : Wm$^{-2}\mu$m^{-1})
180
90
0
270
180
90
0
Longitude ("West)
1985
0.100
0.075
0.050
0.025
0,000
Emittanc : Wm$^{-2}\mu$m
180
90
0
270
180
90
0
Longitude ('West)

Fig. 2a

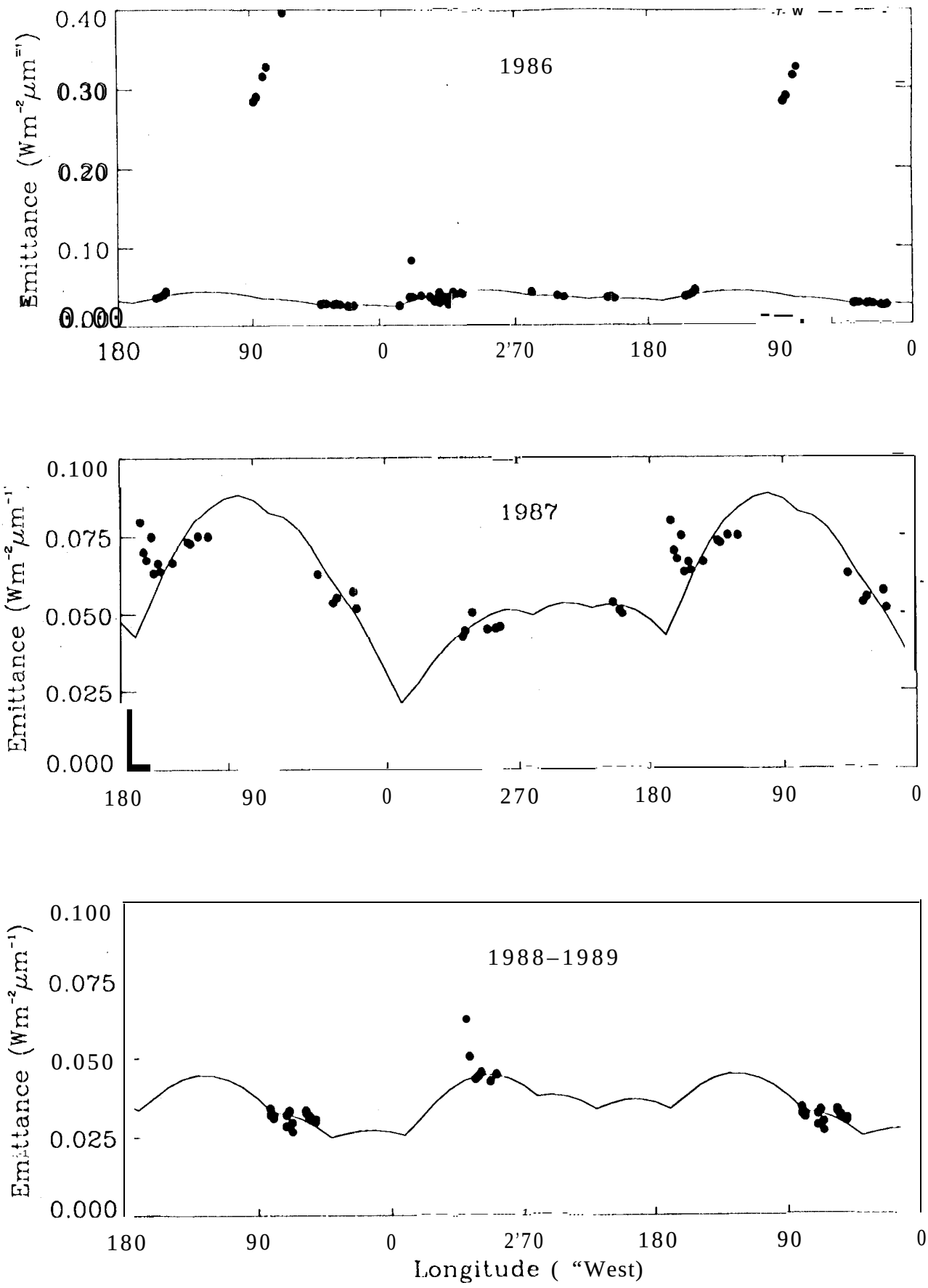
1986
1987
1988–1989
Emittance (Wm$^{-2}\mu$m^{-1})
0.40
0.30
0.20
0.10
0.000
0.100
0.075
0.050
0.025
180
90
0
270
2'70
Longitude ("West)

Fig 2b

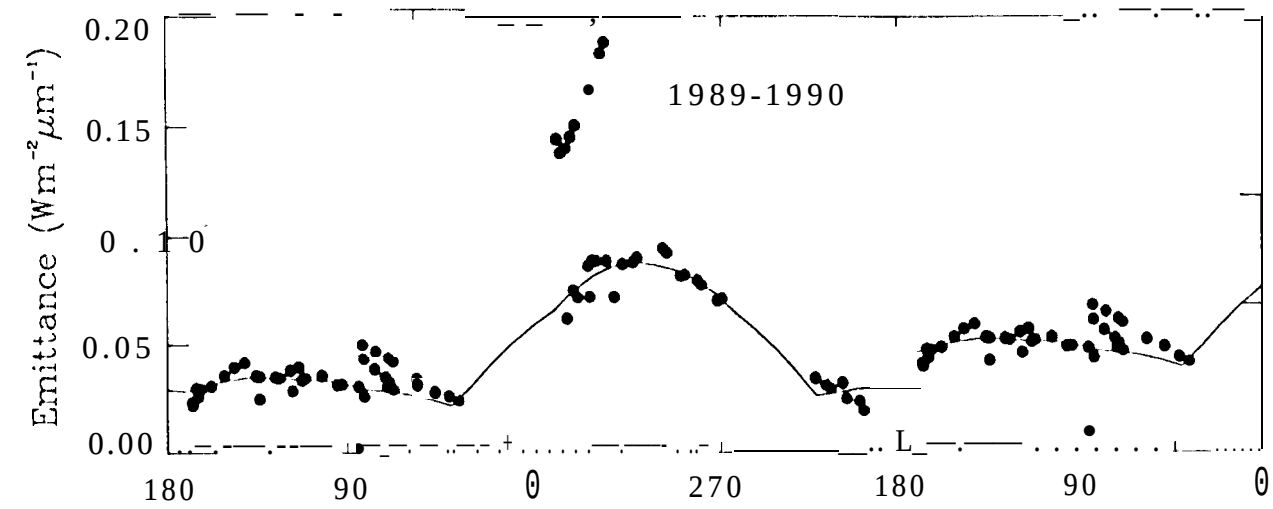
1989-1990
Emittance (Wm$^{-2}\mu m^{-1}$)
0.20
0.15
0.10
0.05
0.00
180
90
0
270
180
90
0

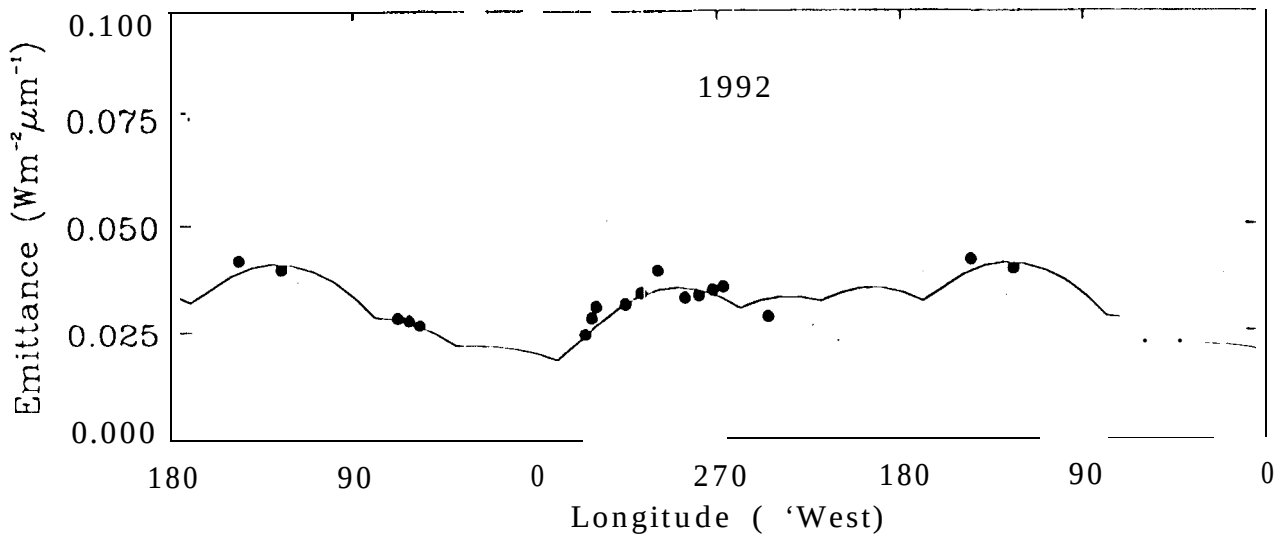
1992
Emittance (Wm$^{-2}\mu m^{-1}$)
0.100
0.075
0.050
0.025
0.000
180
90
0
270
180
90
0
Longitude ('West)

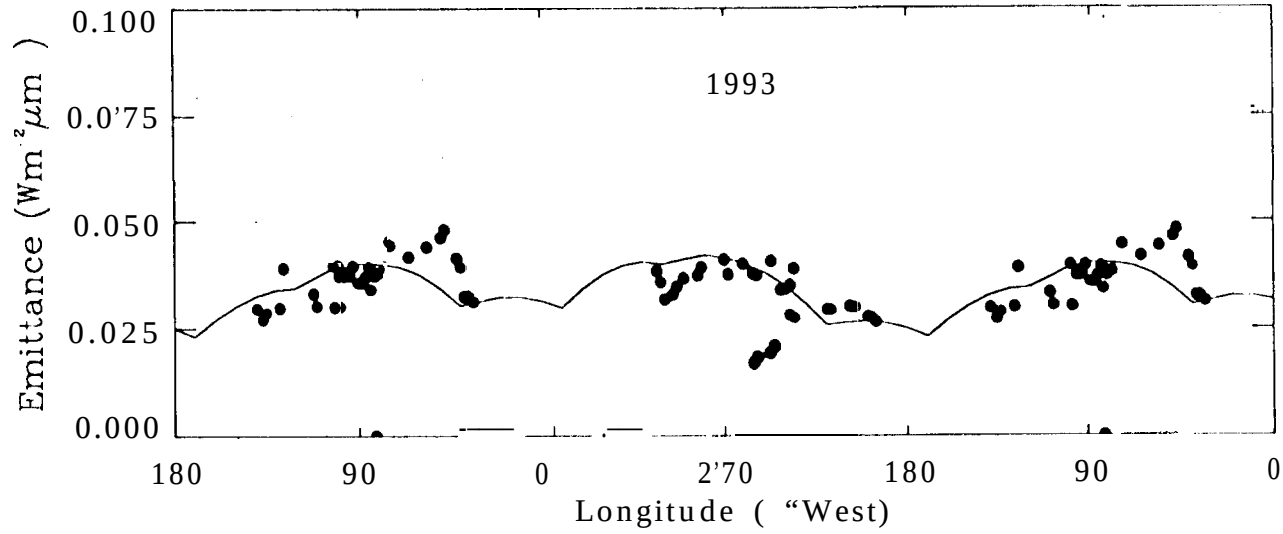
1993
Emittance (Wm$^{-2}\mu m$)
0.100
0.075
0.050
0.025
0.000
180
90
0
270
180
90
0
Longitude ("West)

Fig 2c

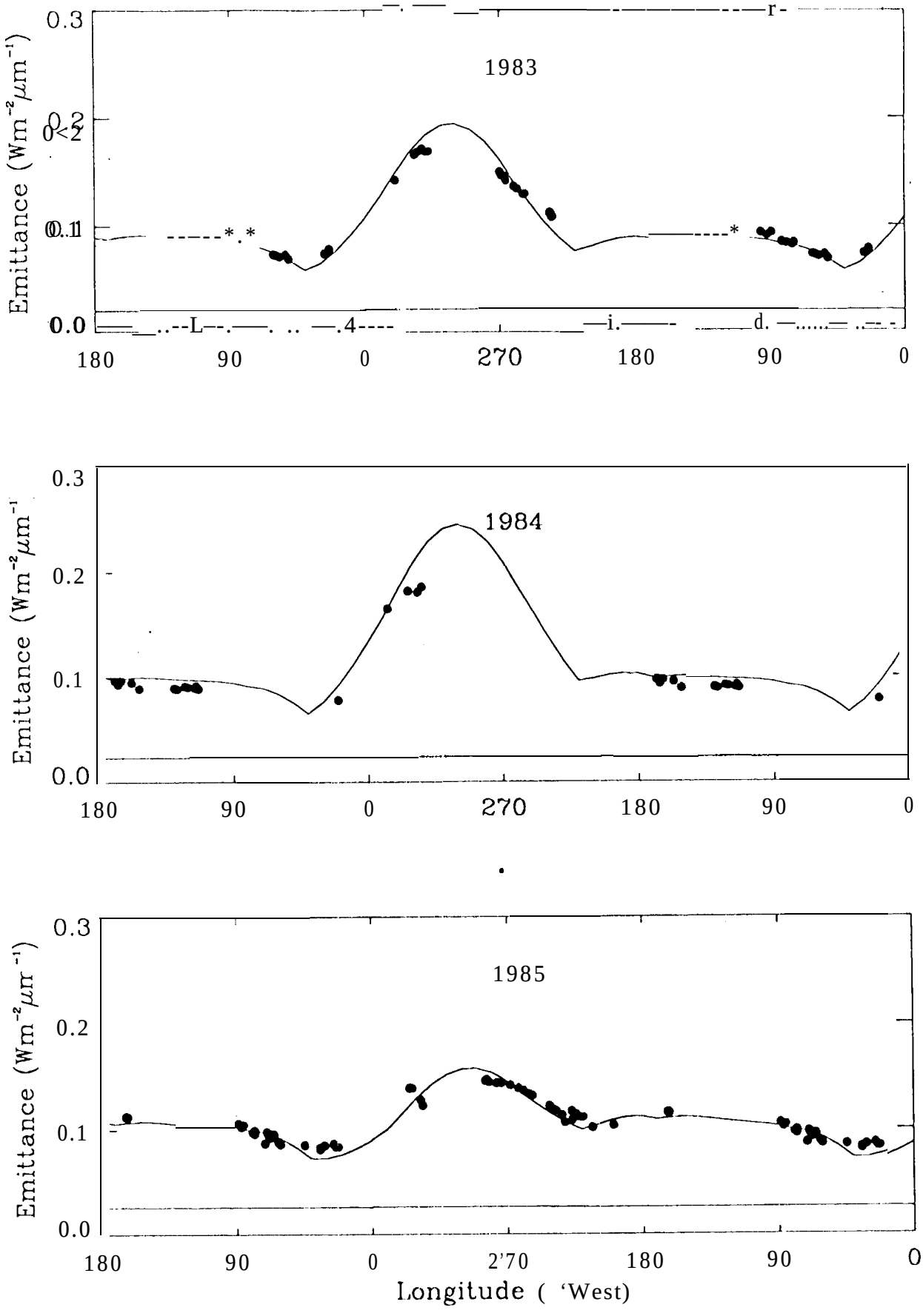
1983
1984
1985
Emittance (Wm$^{-2}\mu$m^{-1})
0.3
0.2
0.1
0.0
180
90
0
270
Longitude ('West)

Fig. 3a

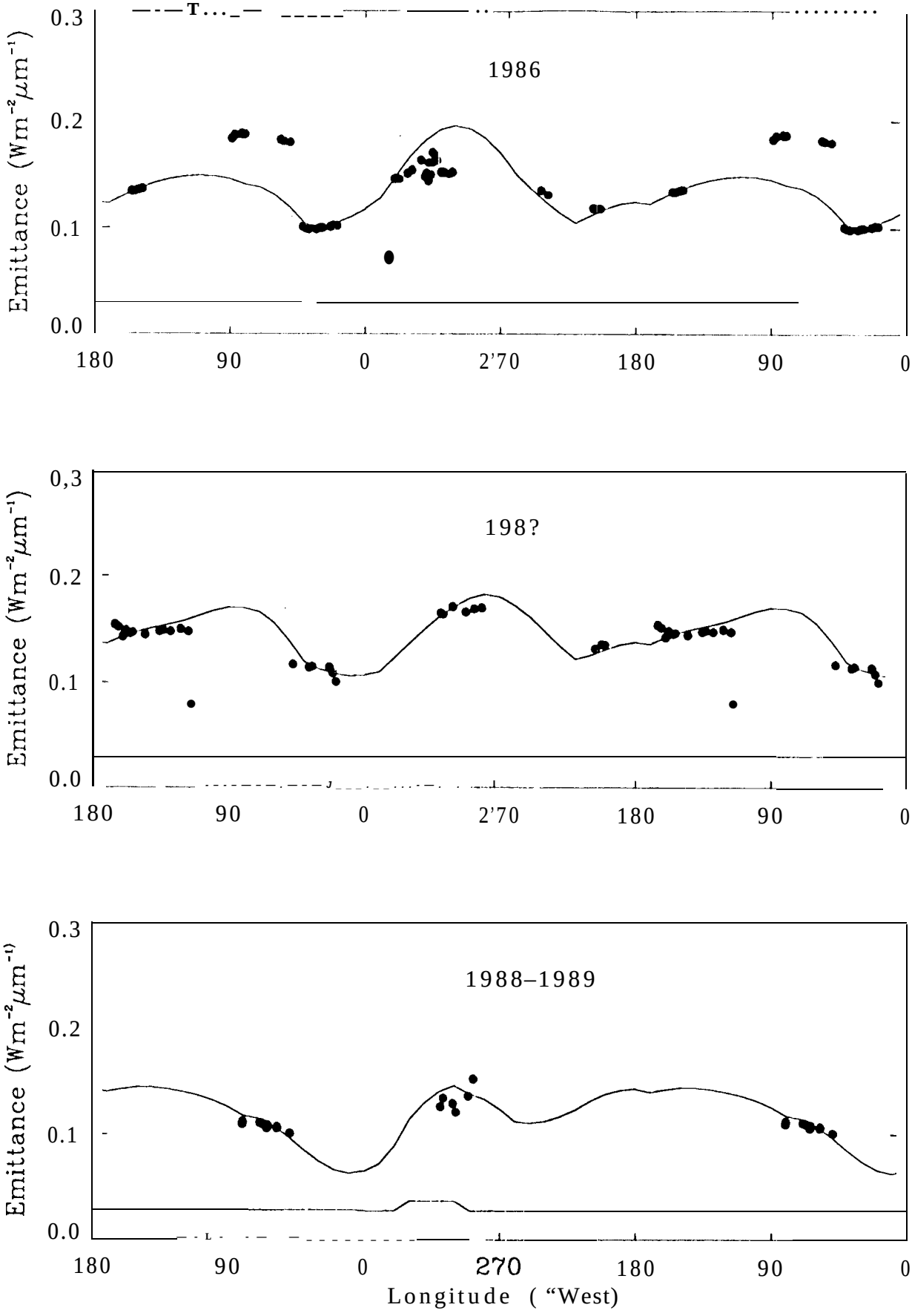
1986
198?
1988–1989
Emittance (Wm$^{-2}\mu$m^{-1})
0.3
0.2
0.1
0.0
180
90
0
270
Longitude ("West)

Fig. 3b

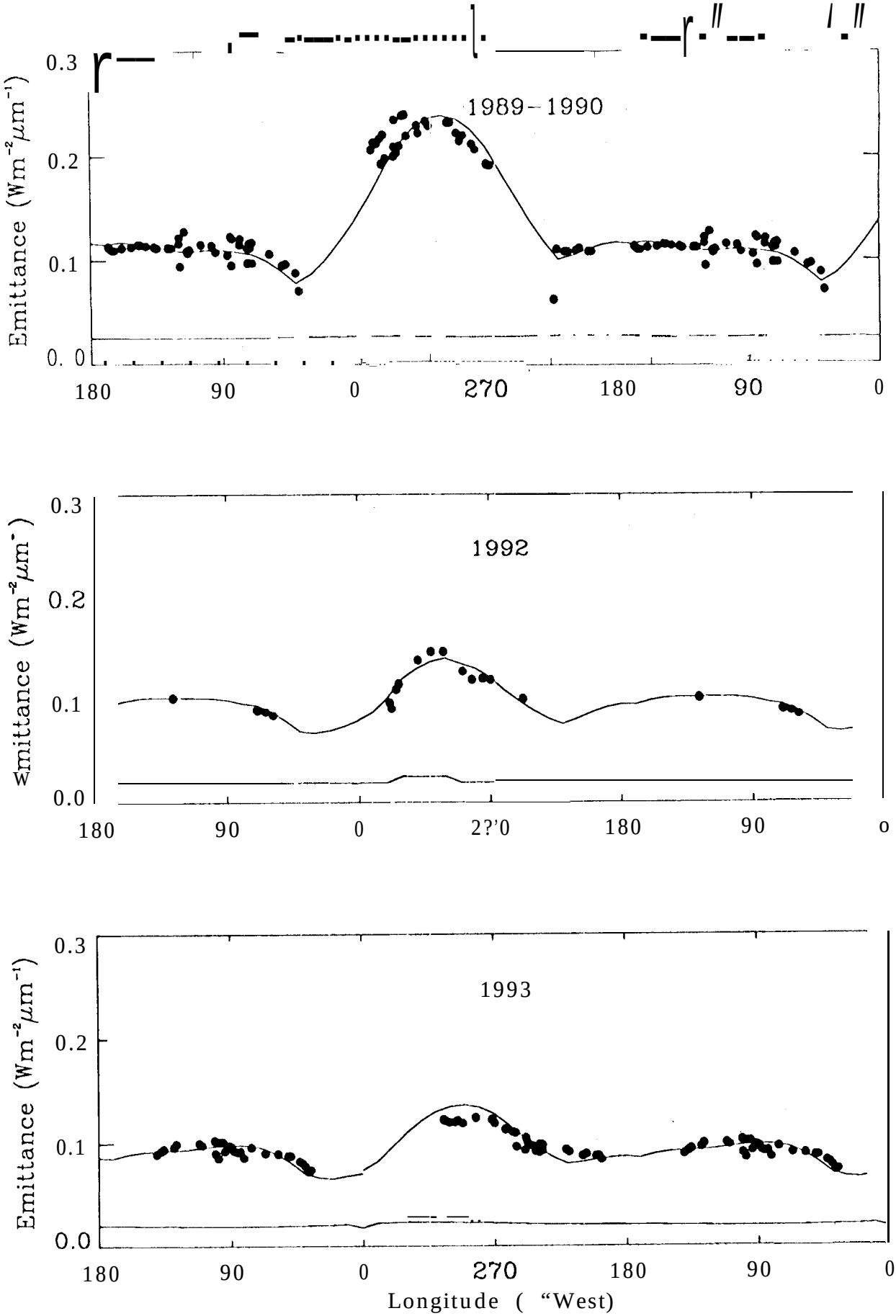
1989-1990
1992
1993
Emittance (Wm$^{-2}\mu$m^{-1})
0.3
0.2
0.1
0.0
180
90
0
270
180
90
0
Longitude ("West)

Fig B

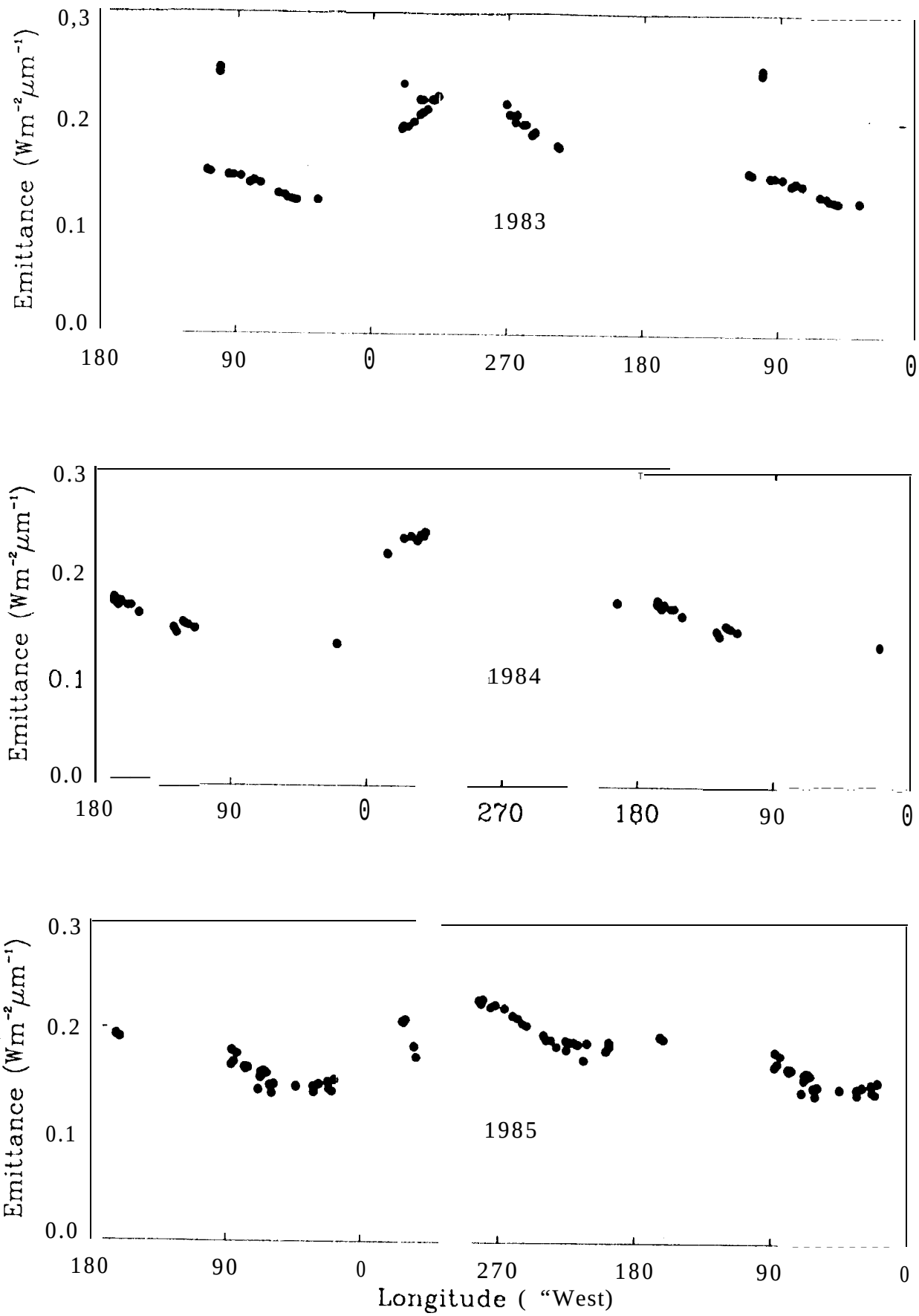
0,3
0.2
0.1
0.0
Emittance ($Wm^{-2}\mu m^{-1}$)
1983
180
90
0
270
180
90
0
0.3
0.2
0.1
0.0
Emittance ($Wm^{-2}\mu m^{-1}$)
1984
180
90
0
270
180
90
0
0.3
0.2
0.1
0.0
Emittance ($Wm^{-2}\mu m^{-1}$)
1985
180
90
0
270
180
90
0
Longitude ("West)

Fig. 4a

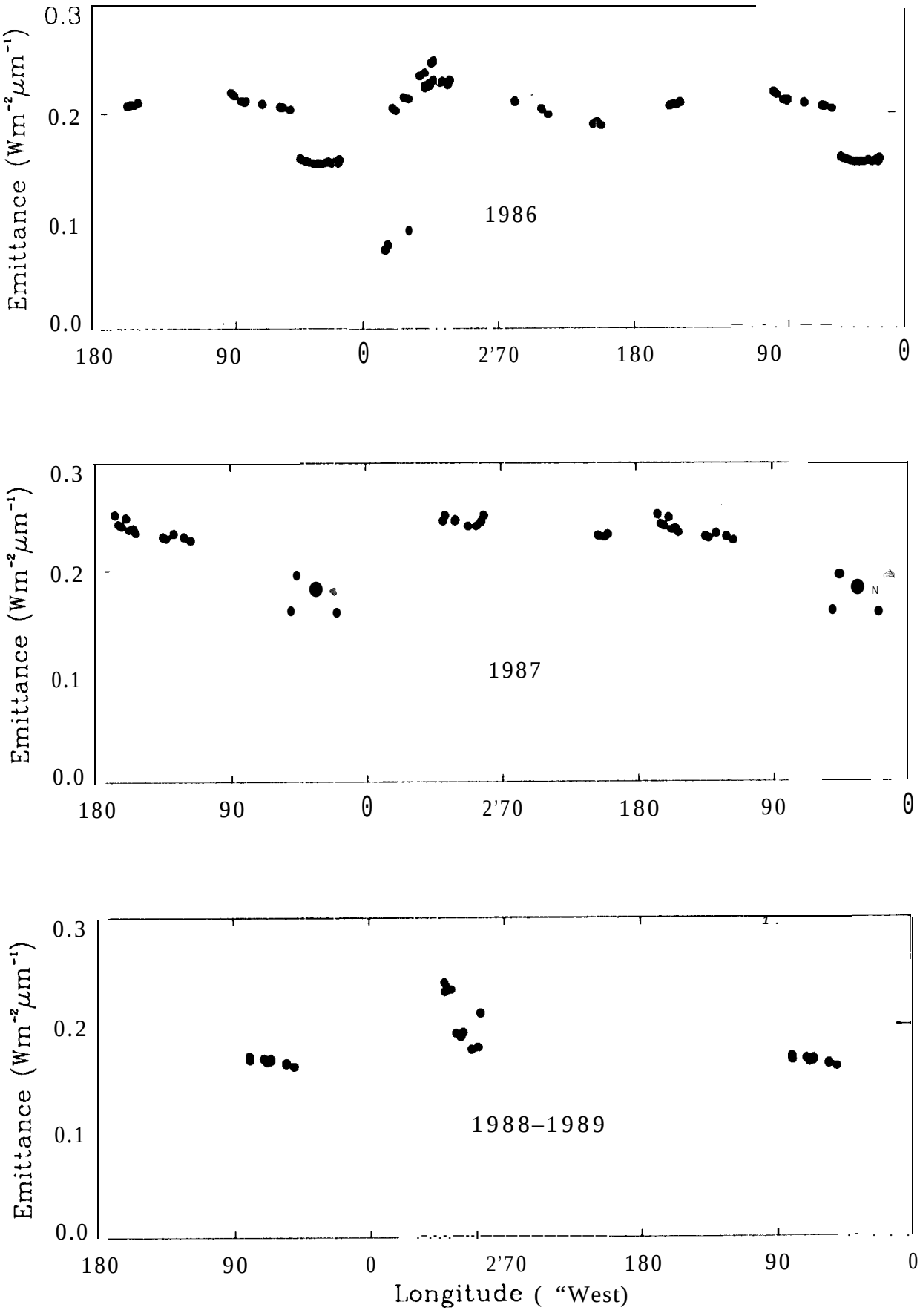
0.3
0.2
0.1
0.0
Emittance (Wm$^{-2}\mu$m^{-1})
1986
180
90
0
270
180
90
0
1987
1988–1989
Longitude ("West)

Fig 4b

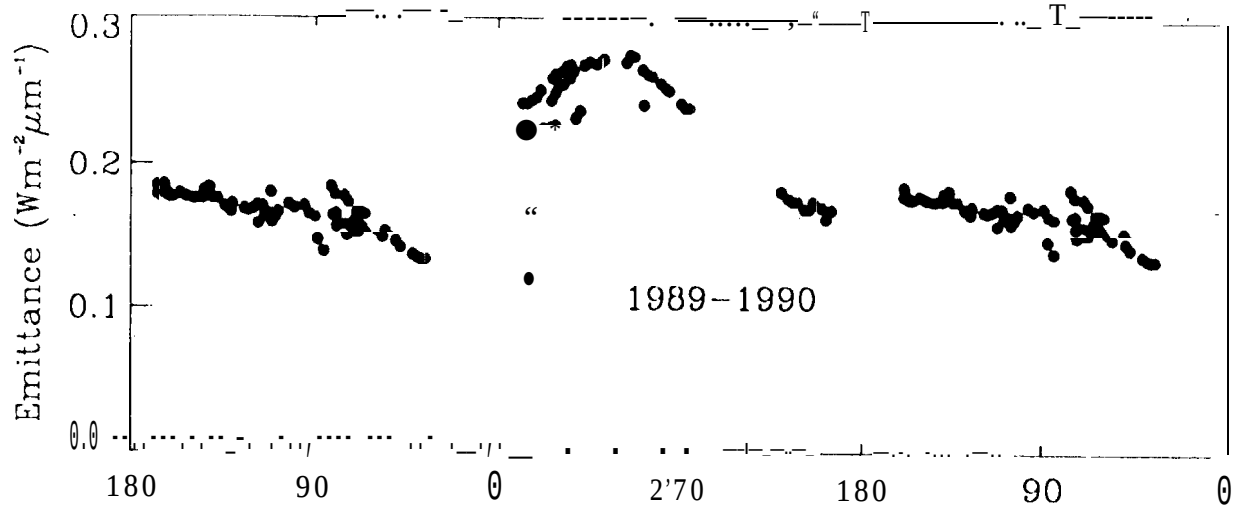
0.3
0.2
0.1
0.0
Emittance (Wm$^{-2}\mu$m^{-1})
1989–1990
180
90
0
270
180
90
0

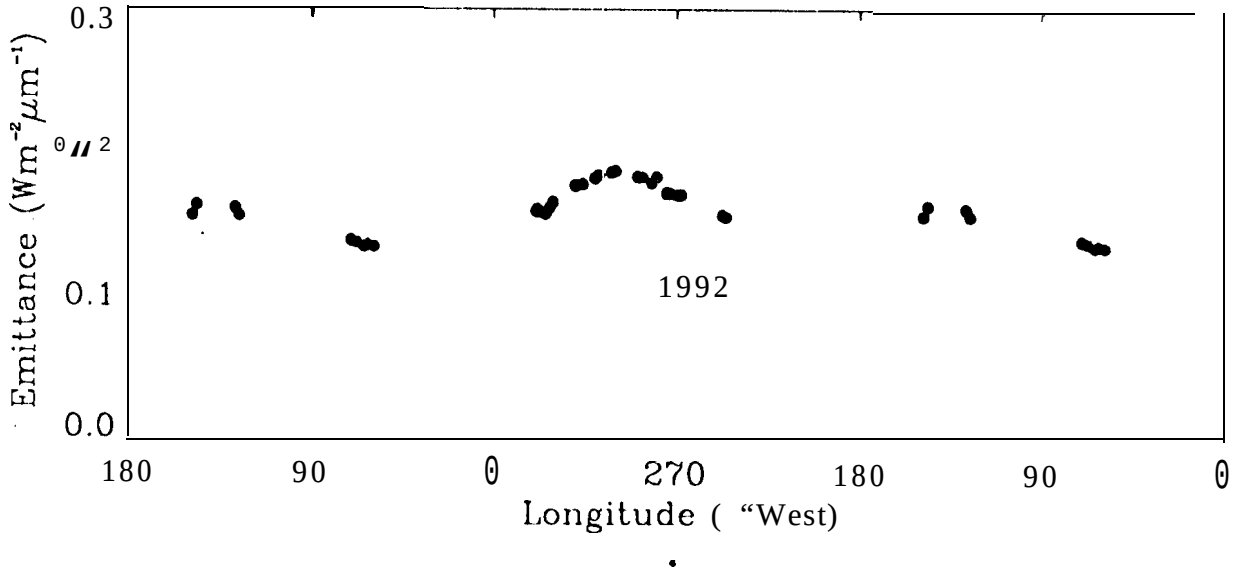
0.3
0.1
0.0
Emittance (Wm$^{-2}\mu$m^{-1})
1992
180
90
0
270
180
90
0
Longitude ("West)

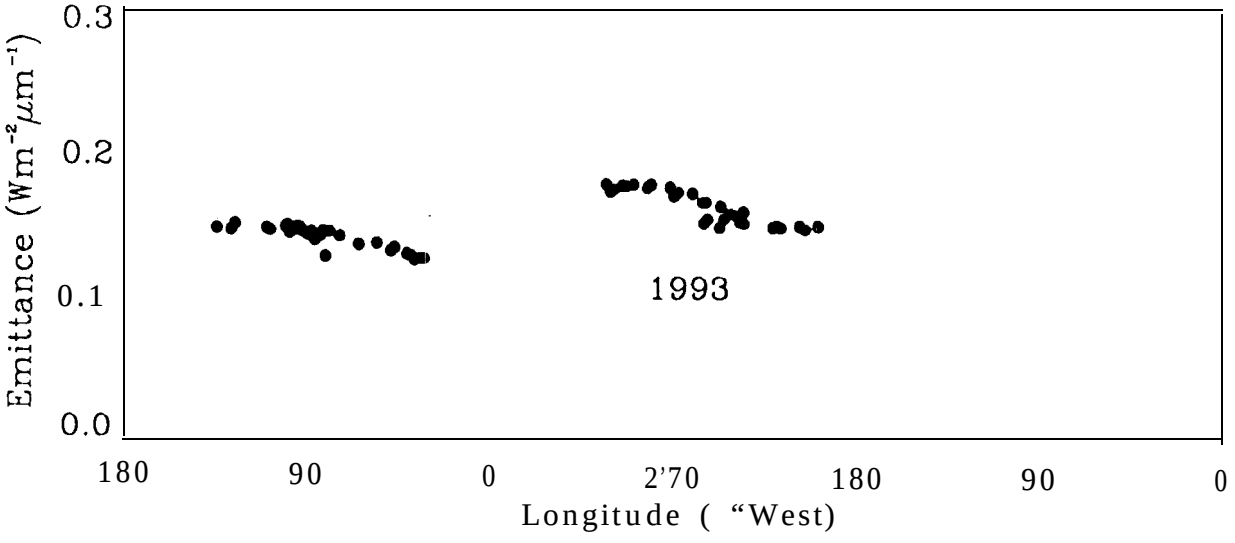
0.3
0.2
0.1
0.0
Emittance (Wm$^{-2}\mu$m^{-1})
1993
180
90
0
270
180
90
0
Longitude ("West)

Fig. 4C

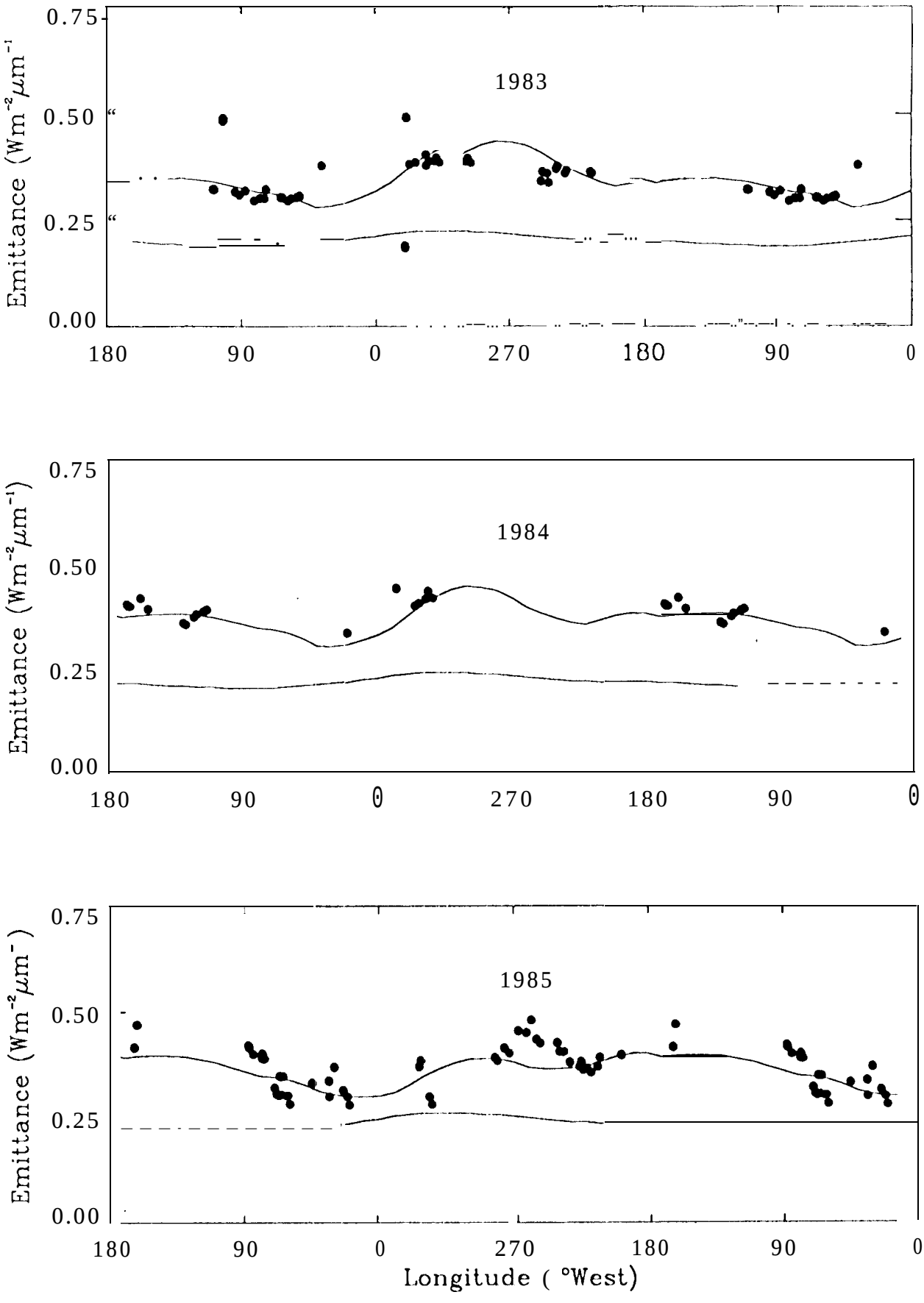
1983
1984
1985
Emittance (Wm$^{-2}\mu$m^{-1})
0.75
0.50
0.25
0.00
180
90
0
270
Longitude (°West)

Fig. 5

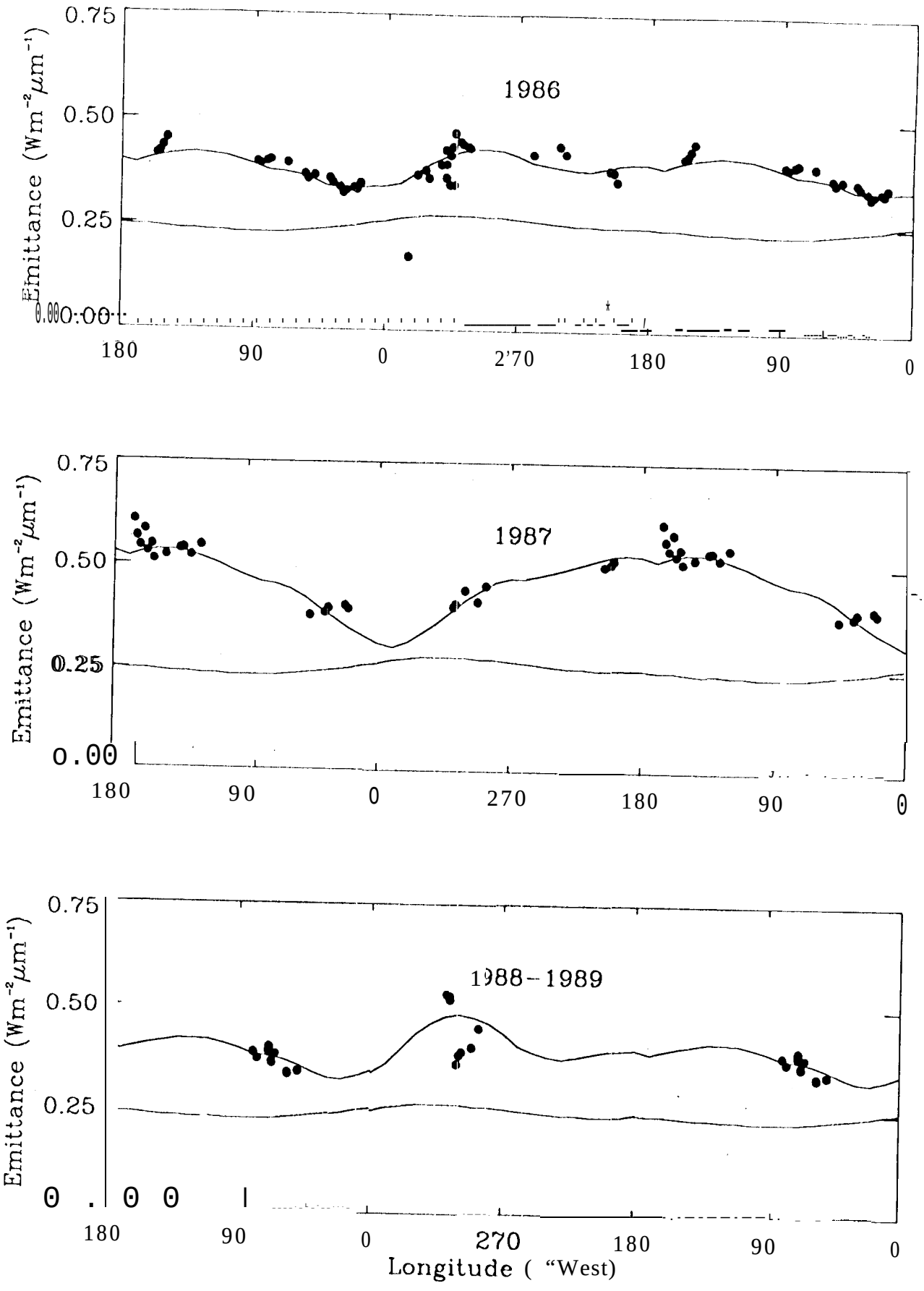
0.75
0.50
0.25
0.00
Emittance (Wm$^{-2}\mu$m^{-1})
1986
180
90
0
270
180
90
0
1987
1988--1989
Longitude ("West)

Fig. 5b

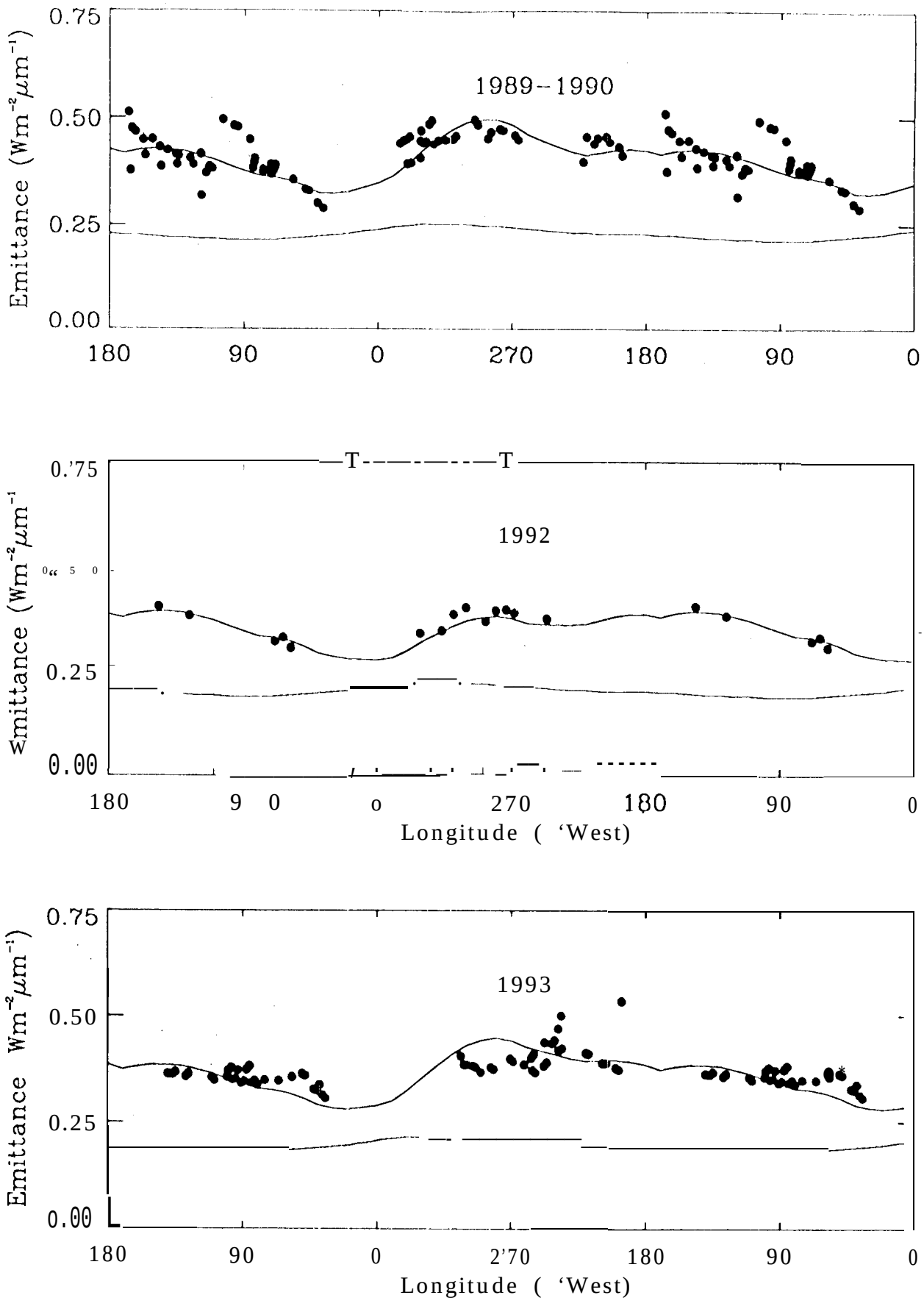
0.75
0.50
0.25
0.00
Emittance (Wm$^{-2}\mu$m^{-1})
1989--1990
180
90
0
270
180
90
0
1992
1993
Longitude ('West)

Fig 5c

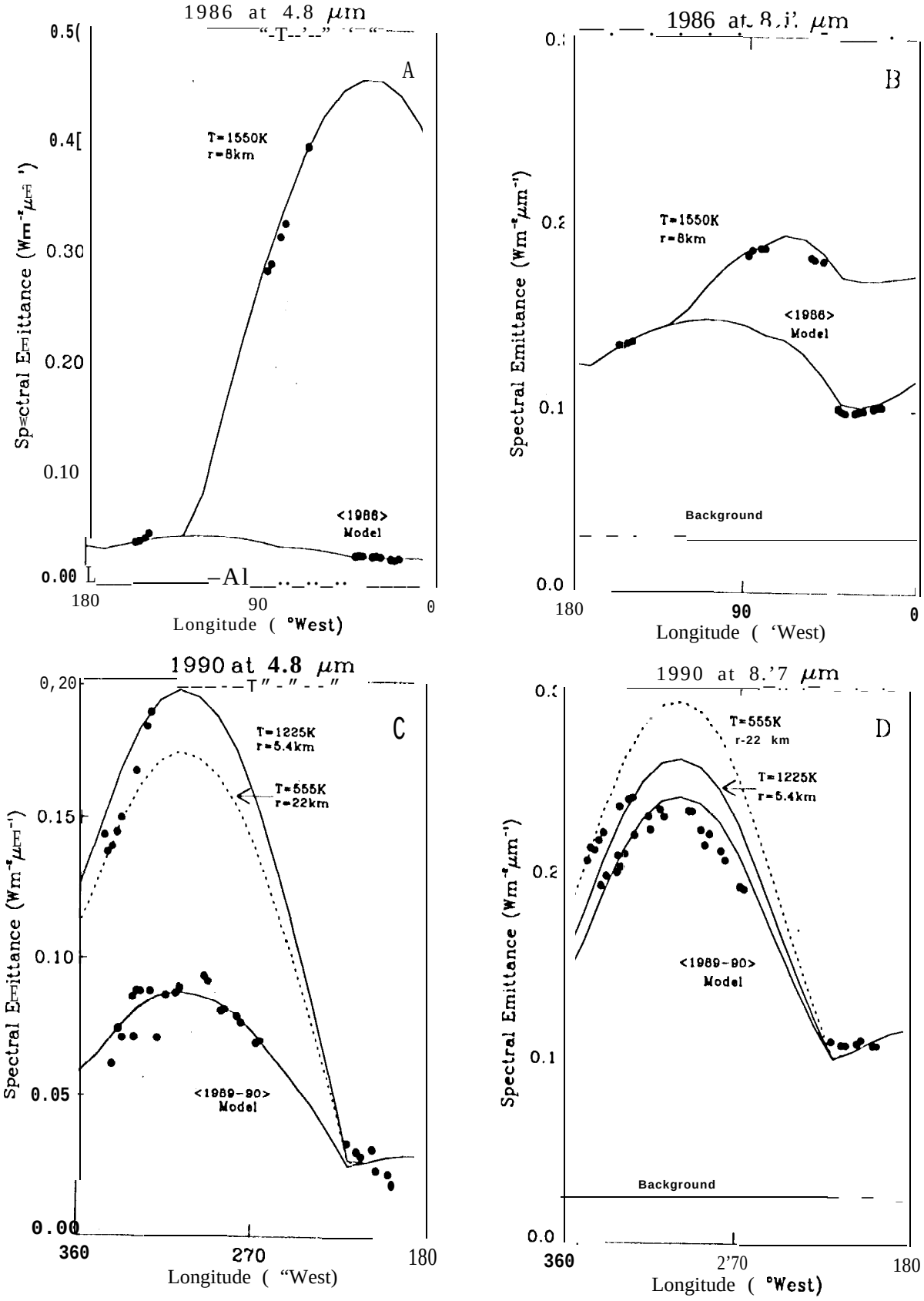
1986 at 4.8 μm
A
T=1550K
r=8km
<1986>
Model
Spectral Emittance (Wm⁻²μm⁻¹)
0.5(
0.4[
0.30
0.20
0.10
0.00
180
90
0
Longitude (°West)
1986 at 8.7 μm
B
T=1550K
r=8km
<1986>
Model
Background
Spectral Emittance (Wm⁻²μm⁻¹)
0.2
0.1
0.0
180
90
0
Longitude ('West)
1990 at 4.8 μm
C
T=1225K
r=5.4km
T=555K
r=22km
<1989-90>
Model
Spectral Emittance (Wm⁻²μm⁻¹)
0,20
0.15
0.10
0.05
0.00
360
270
180
Longitude ("West)
1990 at 8.7 μm
D
T=555K
r-22 km
T=1225K
r=5.4km
<1989-90>
Model
Background
Spectral Emittance (Wm⁻²μm⁻¹)
0.2
0.1
0.0
360
2'70
180
Longitude (°West)

Fig. 9

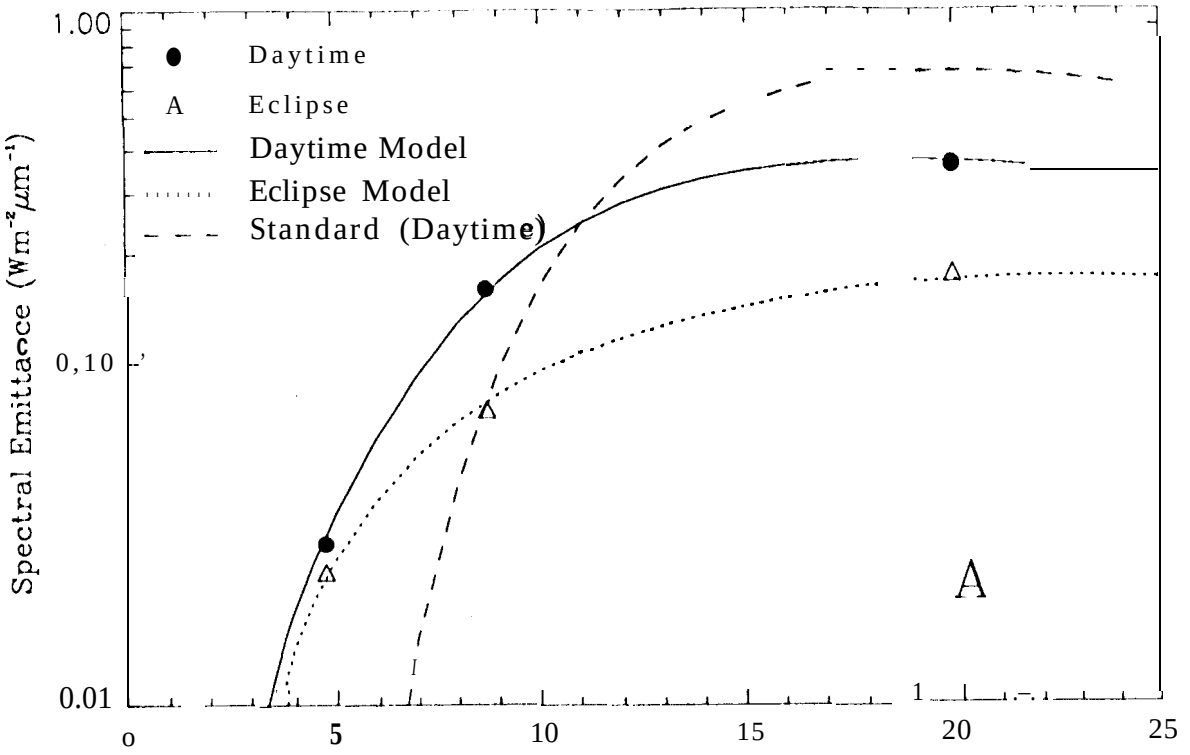
1.00
0.10
0.01
Spectral Emittance ($Wm^{-2}\mu m^{-1}$)
Daytime
Eclipse
Daytime Model
Eclipse Model
Standard (Daytime)
A
0
5
10
15
20
25

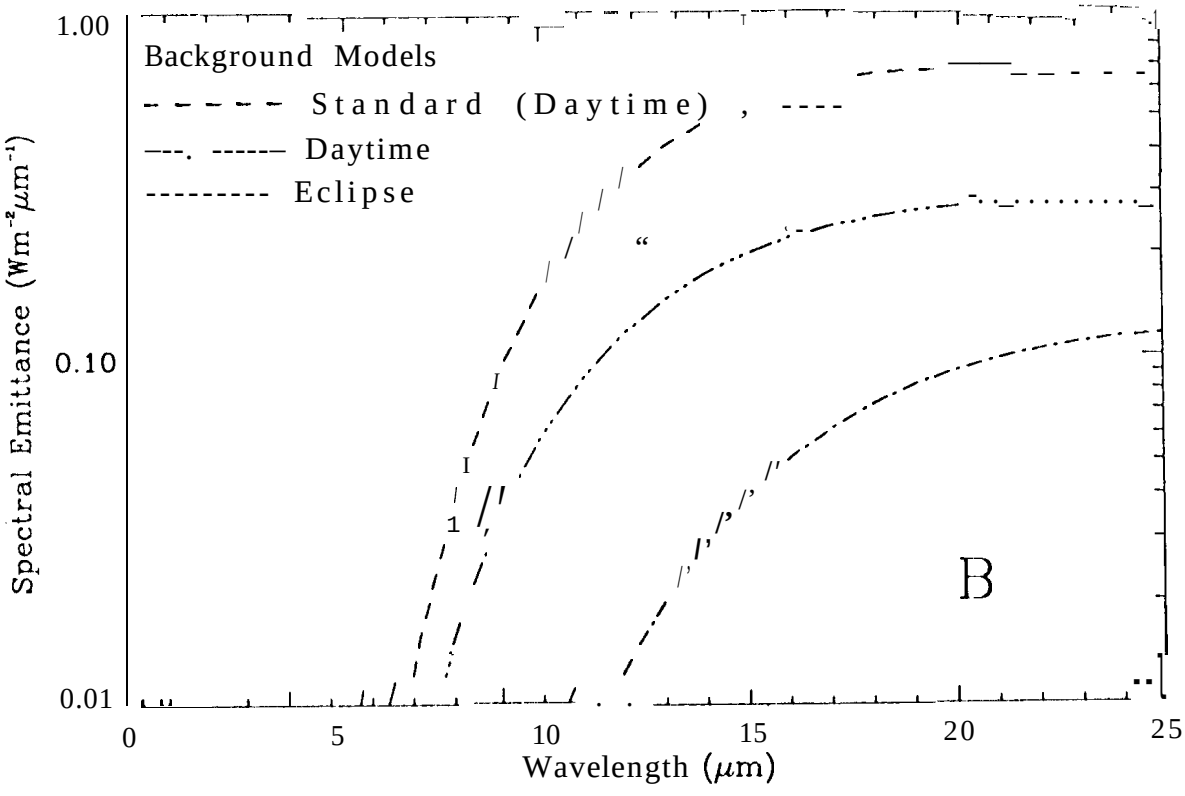
1.00
0.10
0.01
Spectral Emittance ($Wm^{-2}\mu m^{-1}$)
Background Models
Standard (Daytime)
Daytime
Eclipse
B
0
5
10
15
20
25
Wavelength (μm)

Fig. 6

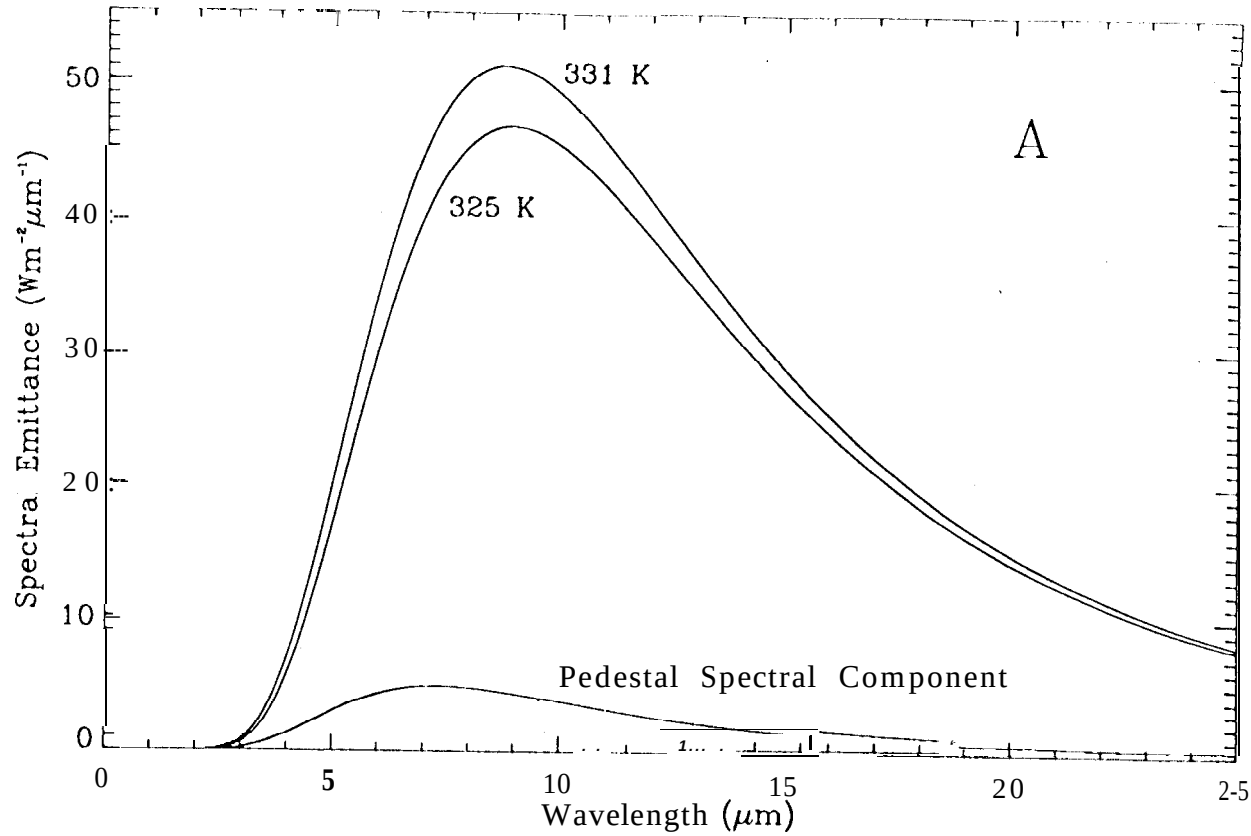
331 K
325 K
A
Pedestal Spectral Component
Spectra Emittance ($Wm^{-2}\mu m^{-1}$)
Wavelength (μm)
0
10
20
30
40
50
5
15
20
25

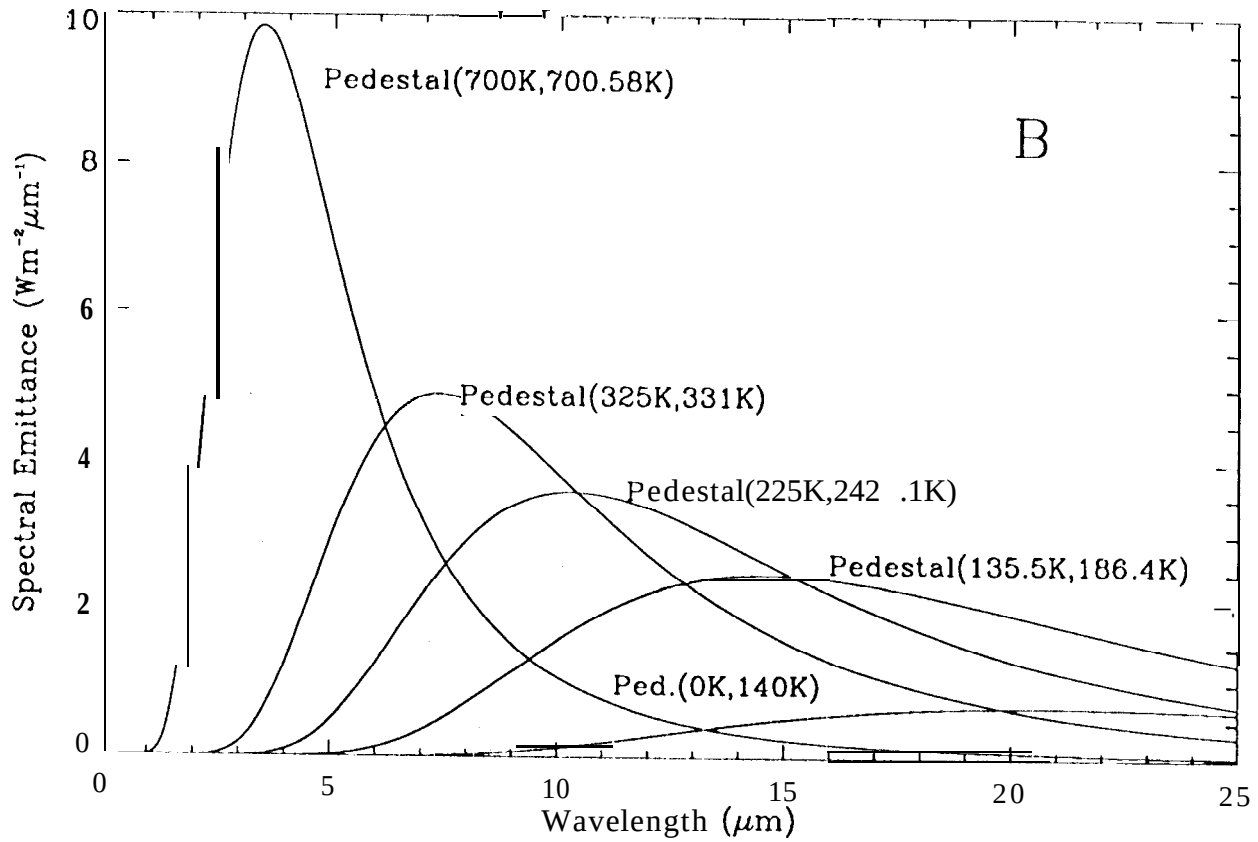
Pedestal(700K,700.58K)
B
Pedestal(325K,331K)
Pedestal(225K,242 .1K)
Pedestal(135.5K,186.4K)
Ped.(0K,140K)
Spectral Emittance ($Wm^{-2}\mu m^{-1}$)
Wavelength (μm)
0
2
4
6
8
10
5
15
20
25

Fig. 7

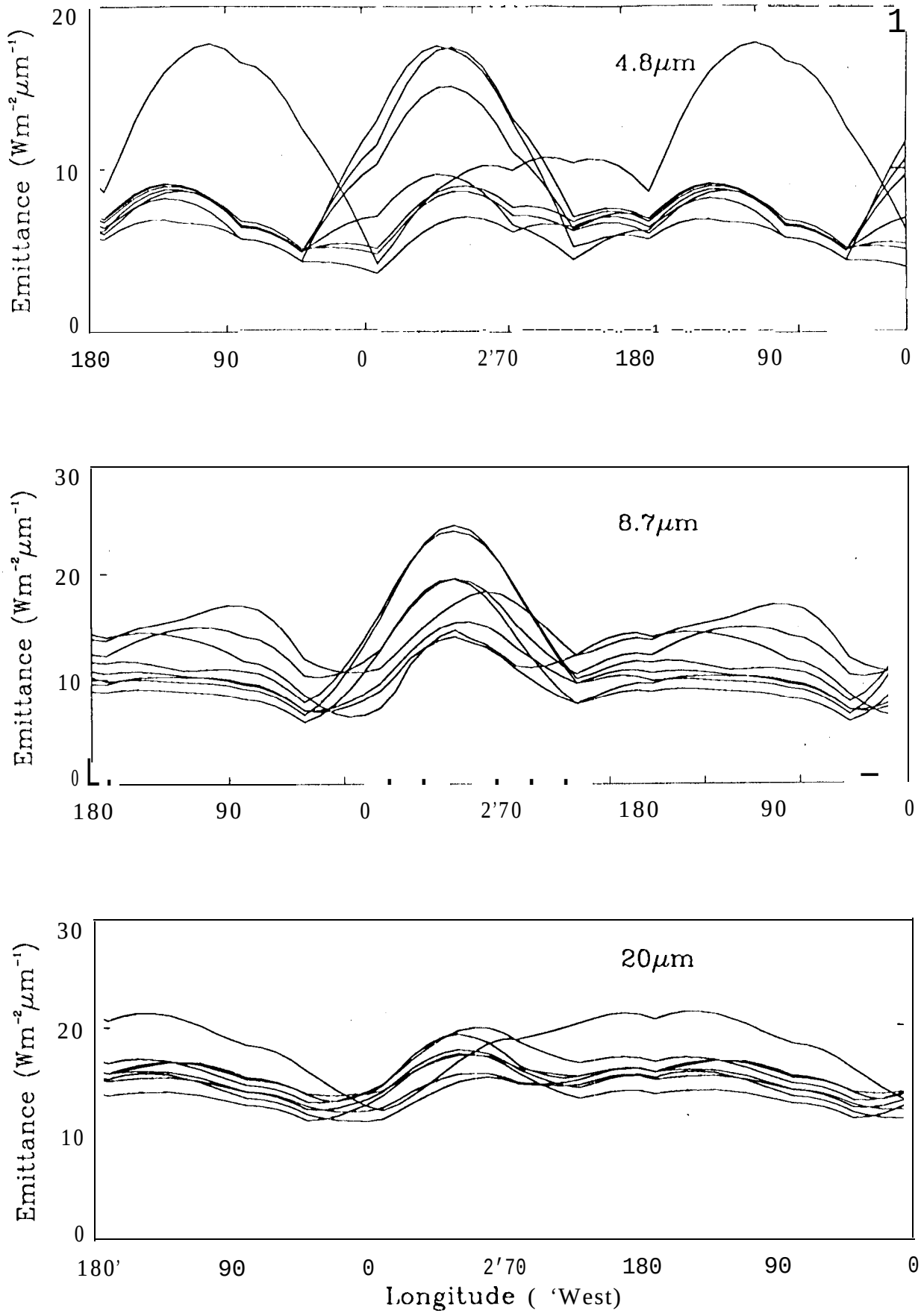
4.8μm
8.7μm
20μm
Emittance (Wm⁻²μm⁻¹)
20
10
0
30
180
90
0
270
Longitude ('West)

Fig. 8

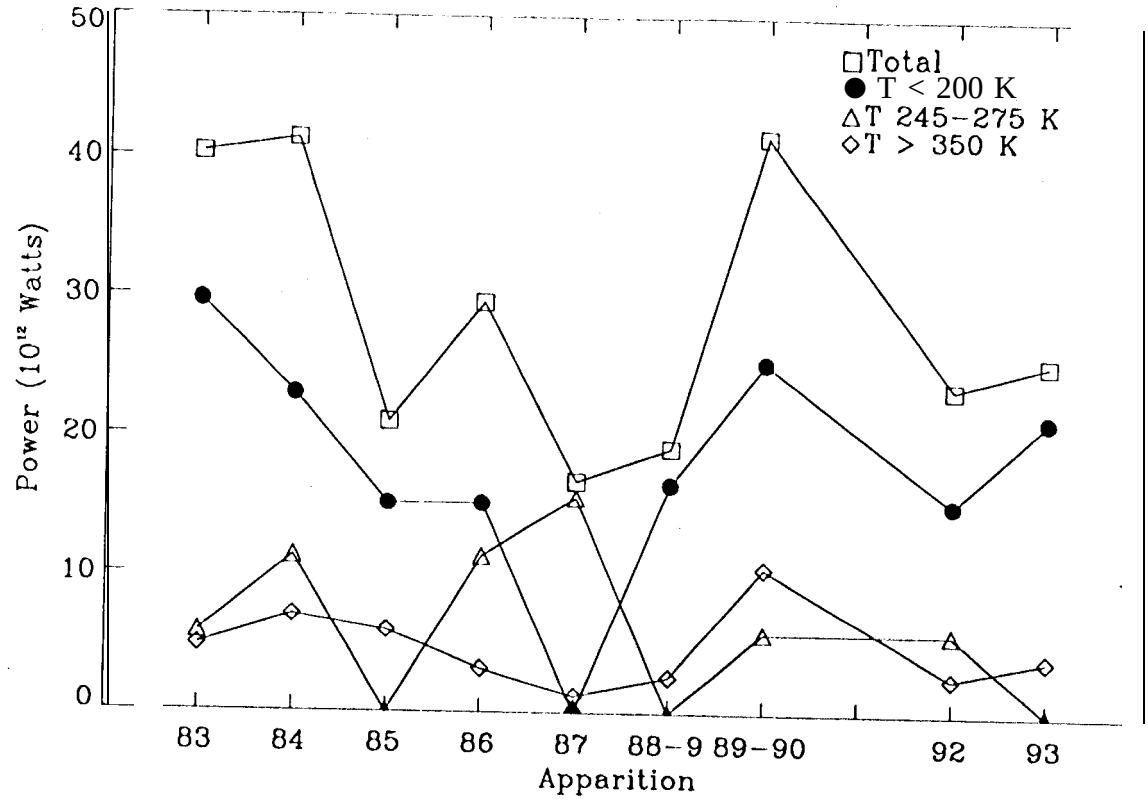
Total
T < 200 K
T 245–275 K
T > 350 K
Power (10¹² Watts)
50
40
30
20
10
0
83
84
85
86
87
88–9
89–90
92
93
Apparition

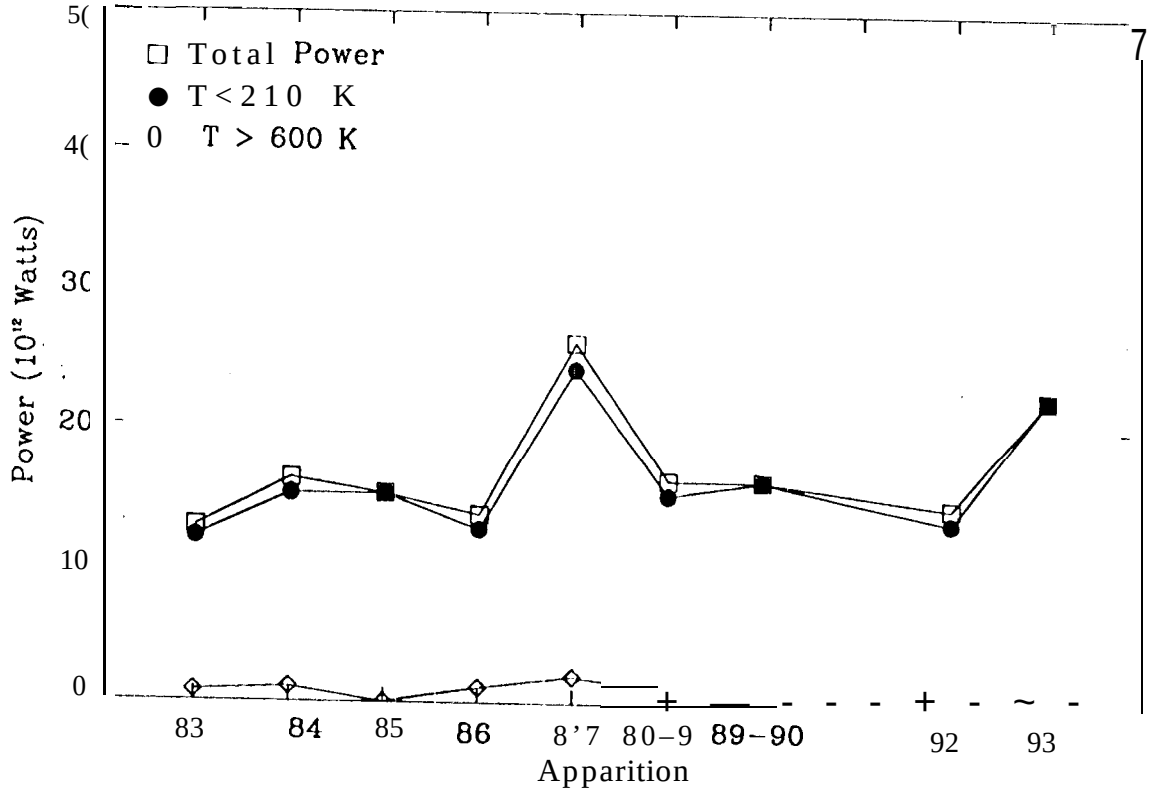
Total Power
T<210 K
T > 600 K
Power (10¹² Watts)
20
10
0
83
84
85
86
8'7
80–9
89–90
92
93
Apparition

Fig. 10a

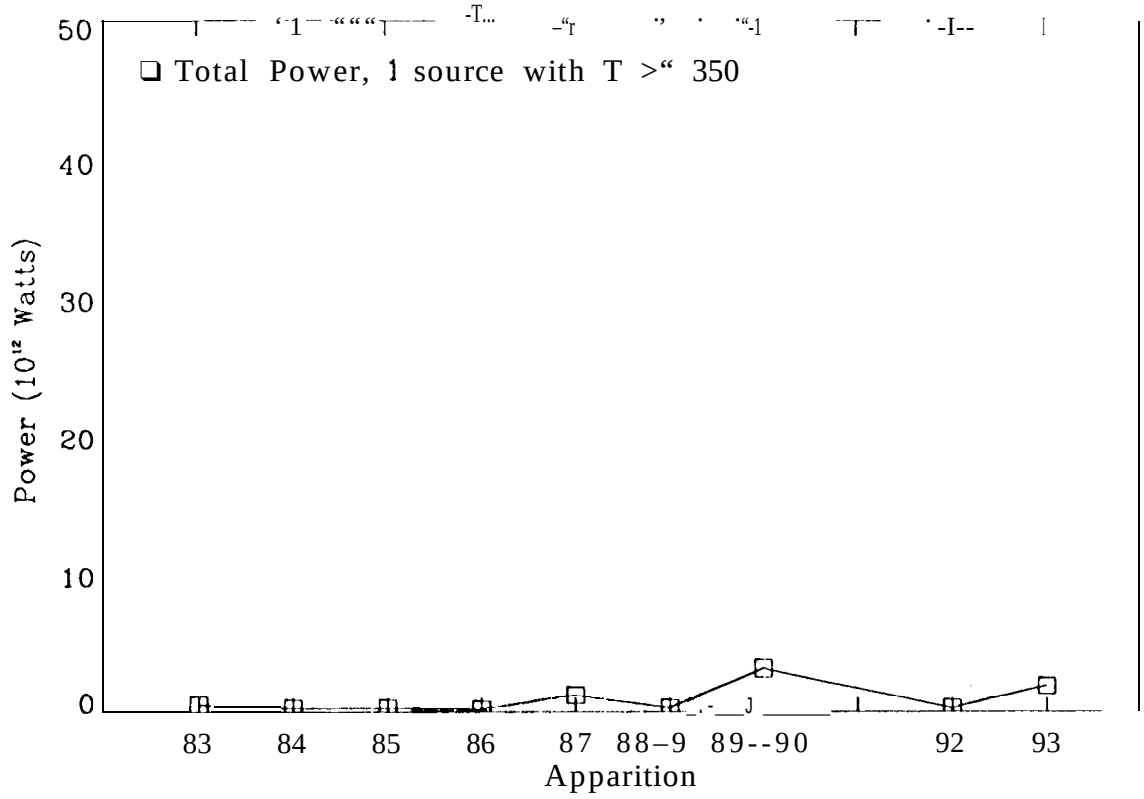
❑ Total Power, 1 source with T >“ 350
Power (10¹² Watts)
50
40
30
20
10
0
83
84
85
86
87
88–9
89--90
92
93
Apparition

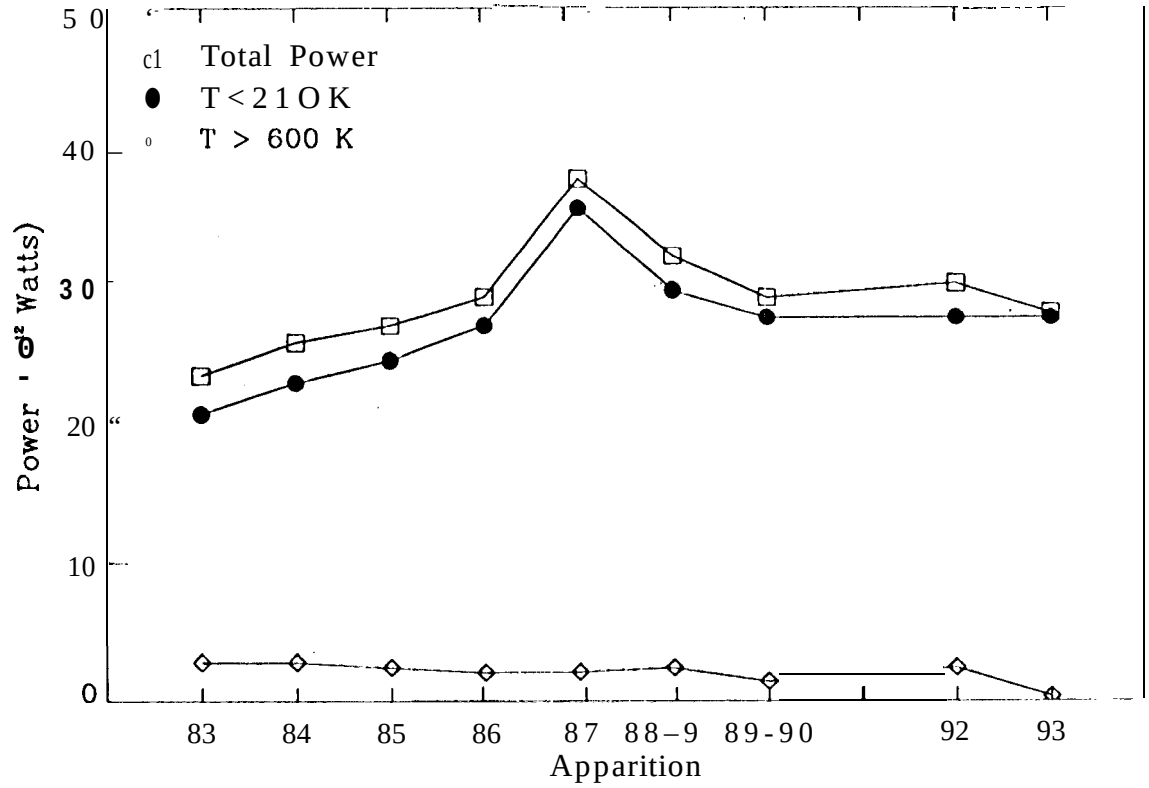
Total Power
T < 21 O K
T > 600 K
Power · σ² Watts)
5 0
40
30
20
10
0
83
84
85
86
87
88–9
89-90
92
93
Apparition

Fig. 10

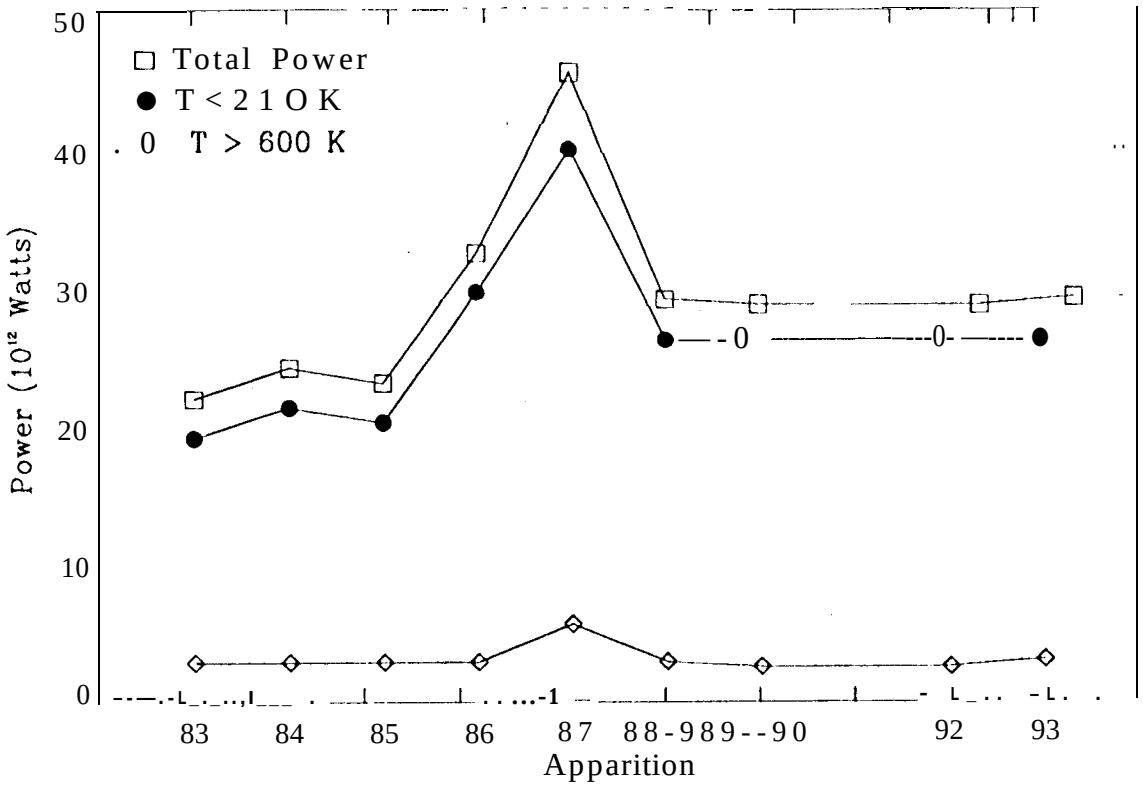
50
40
30
20
10
0
Power (10^{12} Watts)
□ Total Power
● T < 2 1 O K
. 0 T > 600 K
83
84
85
86
87
88-989--90
92
93
Apparition

Fig 10c

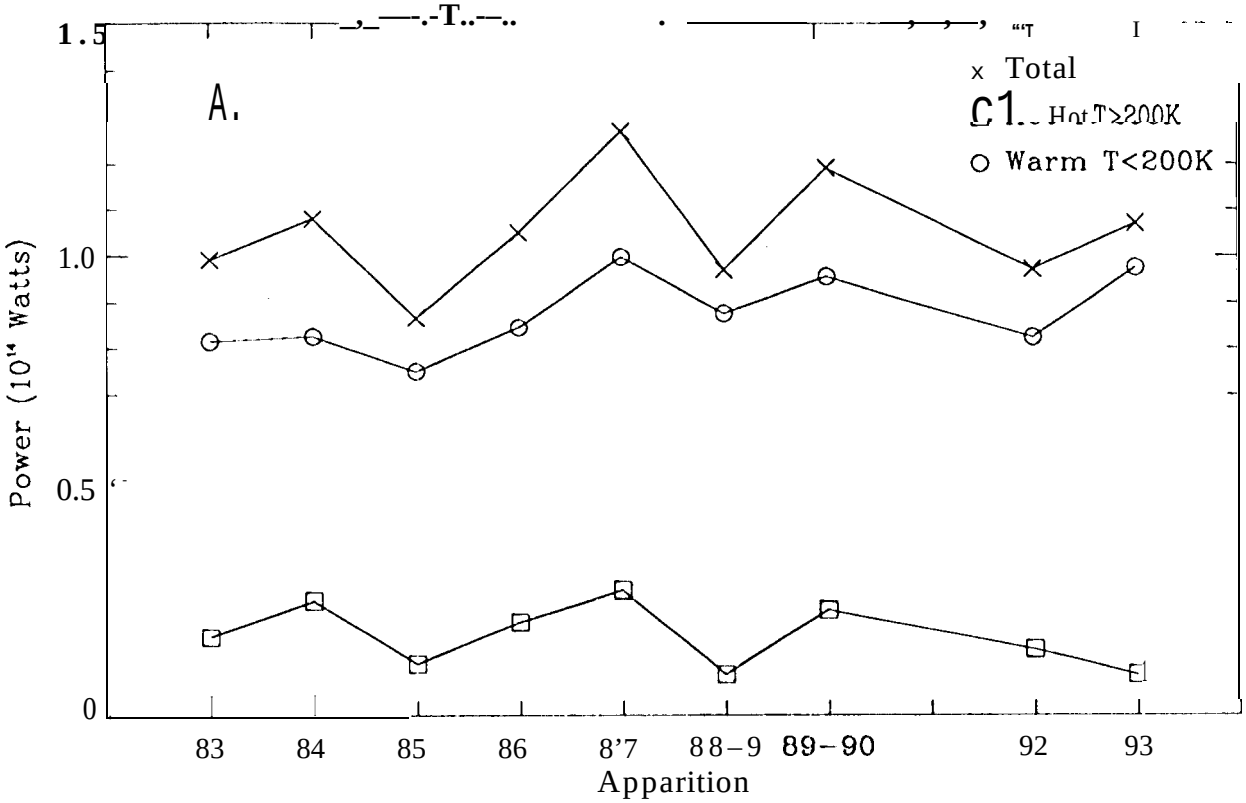
A.
x Total
Hot T≥200K
o Warm T<200K
Power (10¹⁴ Watts)
1.5
1.0
0.5
0
83
84
85
86
8'7
88–9
89–90
92
93
Apparition

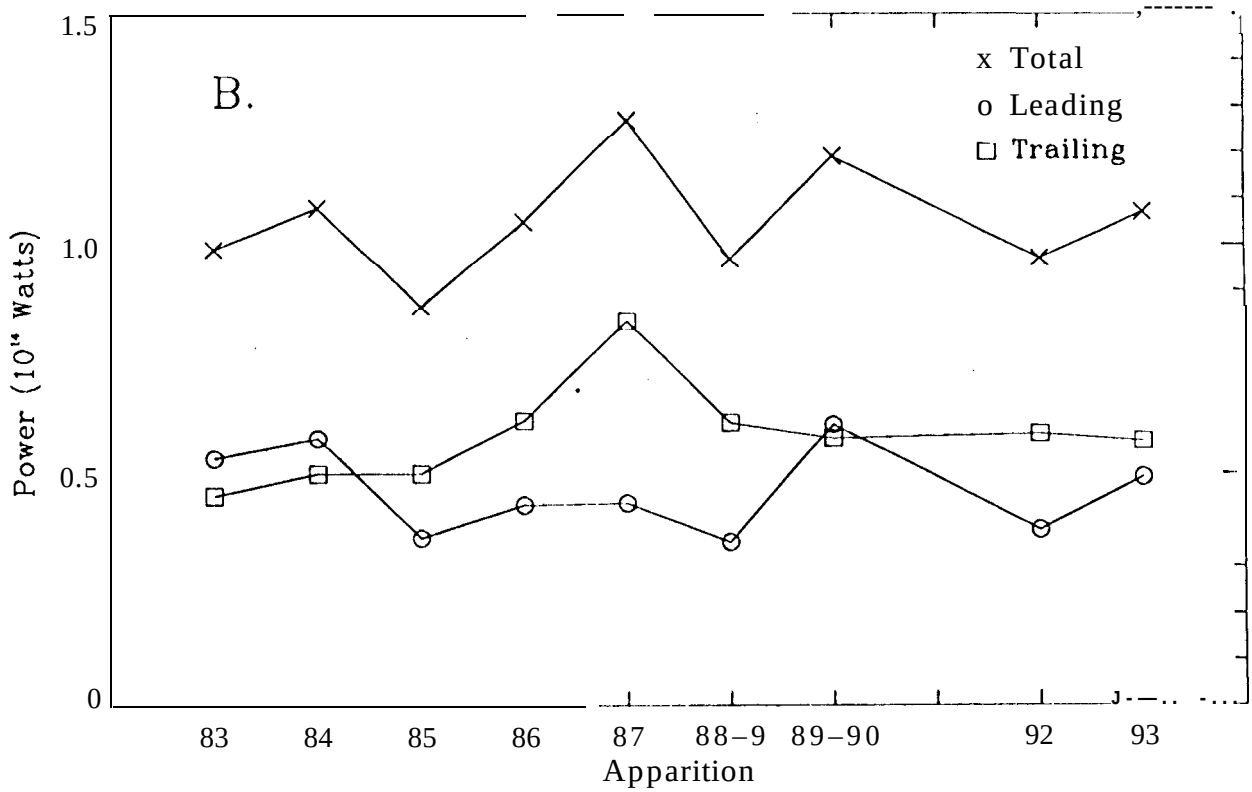
B.
x Total
o Leading
□ Trailing
Power (10¹⁴ Watts)
1.5
1.0
0.5
0
83
84
85
86
87
88–9
89–90
92
93
Apparition

Fig. 11

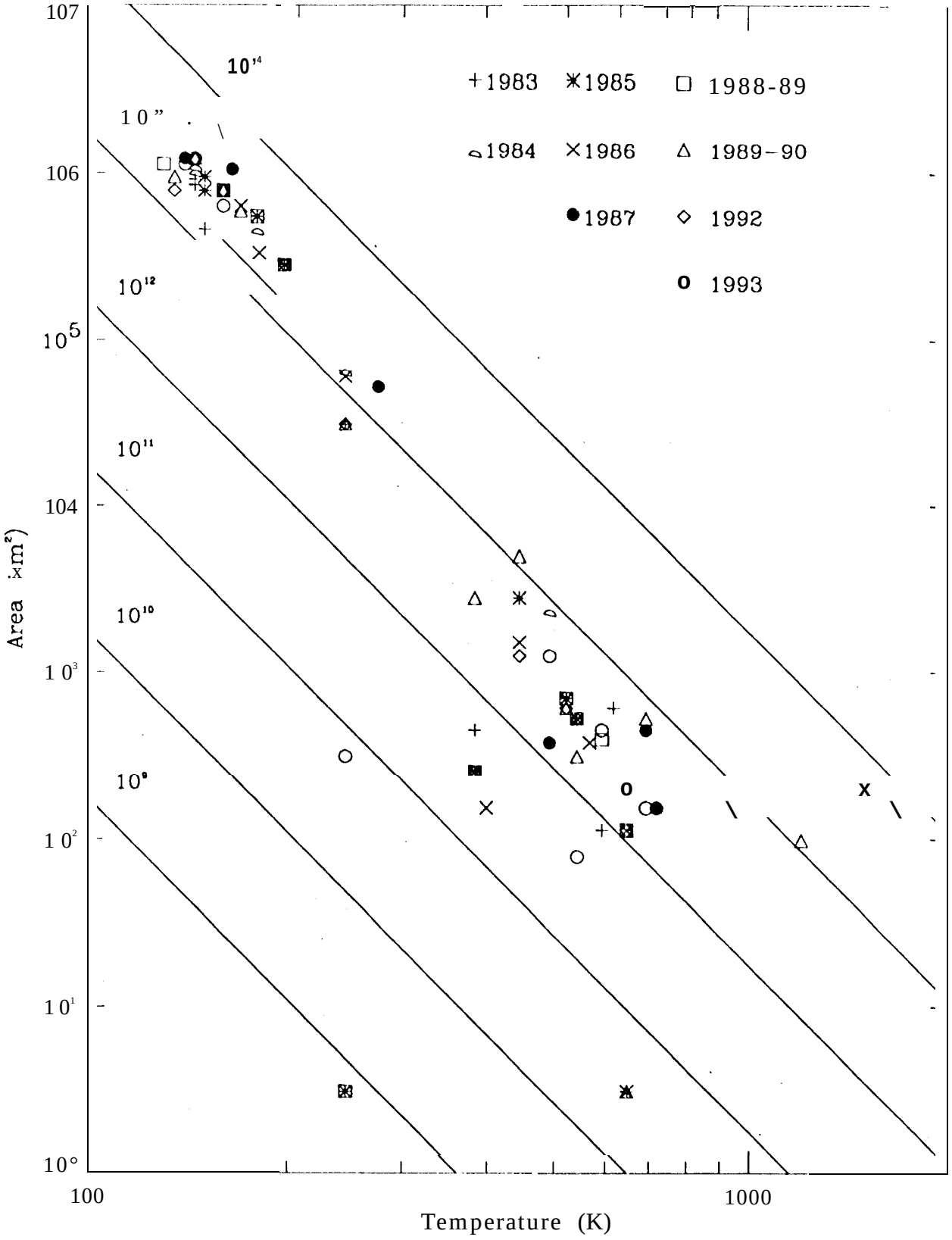
107
106
10^5
104
1 0^3
1 0^2
1 0^1
10°
Area (km²)
100
1000
Temperature (K)
10^14
1 0 "
10^12
10^11
10^10
10^9
+1983
✳1985
□ 1988-89
1984
×1986
△ 1989-90
●1987
◇ 1992
o 1993
o
x

Fig. 12a

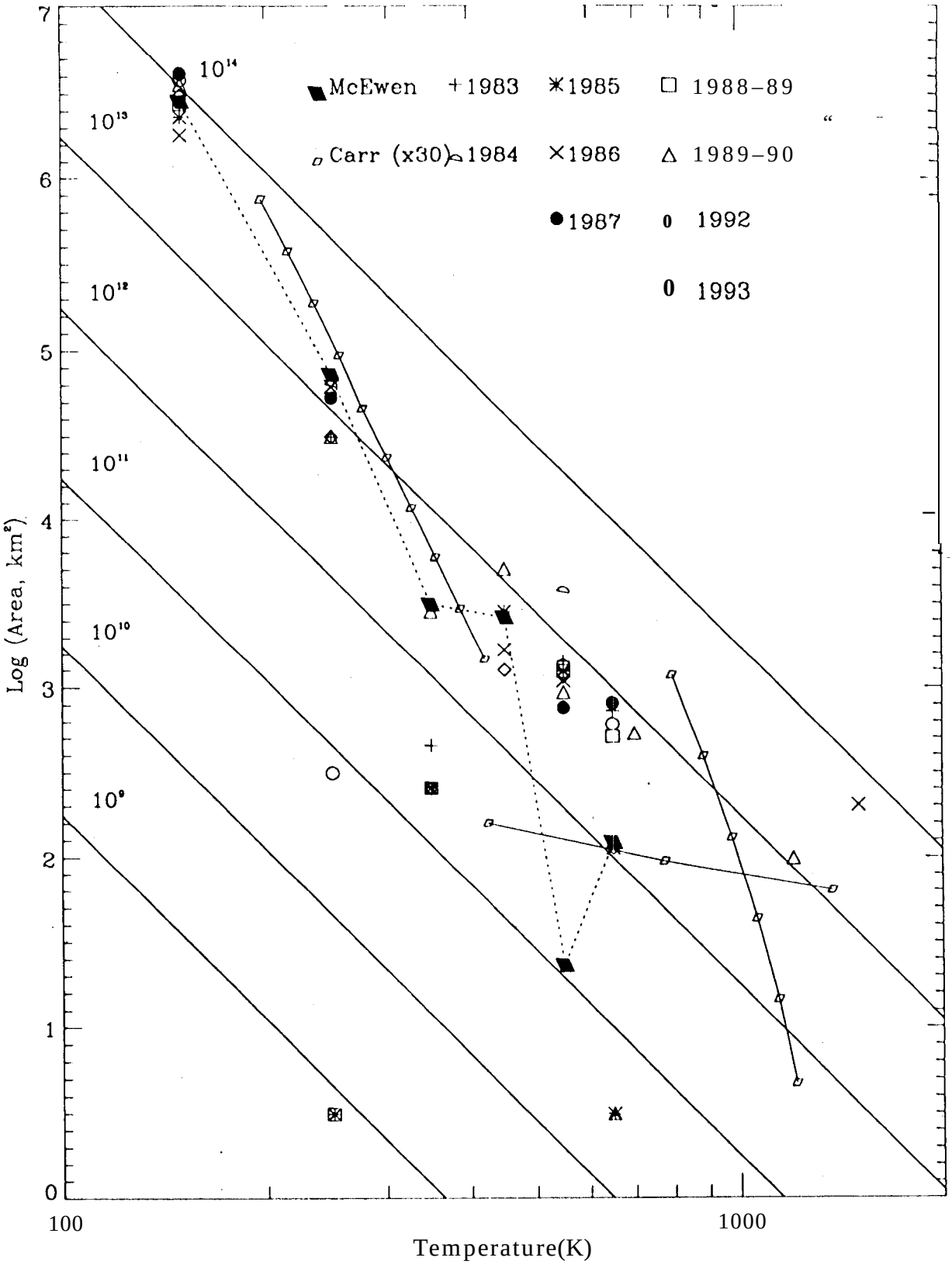
McEwen
Carr (x30)
+1983
1984
✳1985
×1986
□ 1988–89
△ 1989–90
●1987
0 1992
0 1993
10^{14}
10^{13}
10^{12}
10^{11}
10^{10}
10^{9}
Log (Area, km²)
Temperature(K)
100
1000
0
1
2
3
4
5
6
7

Fig12

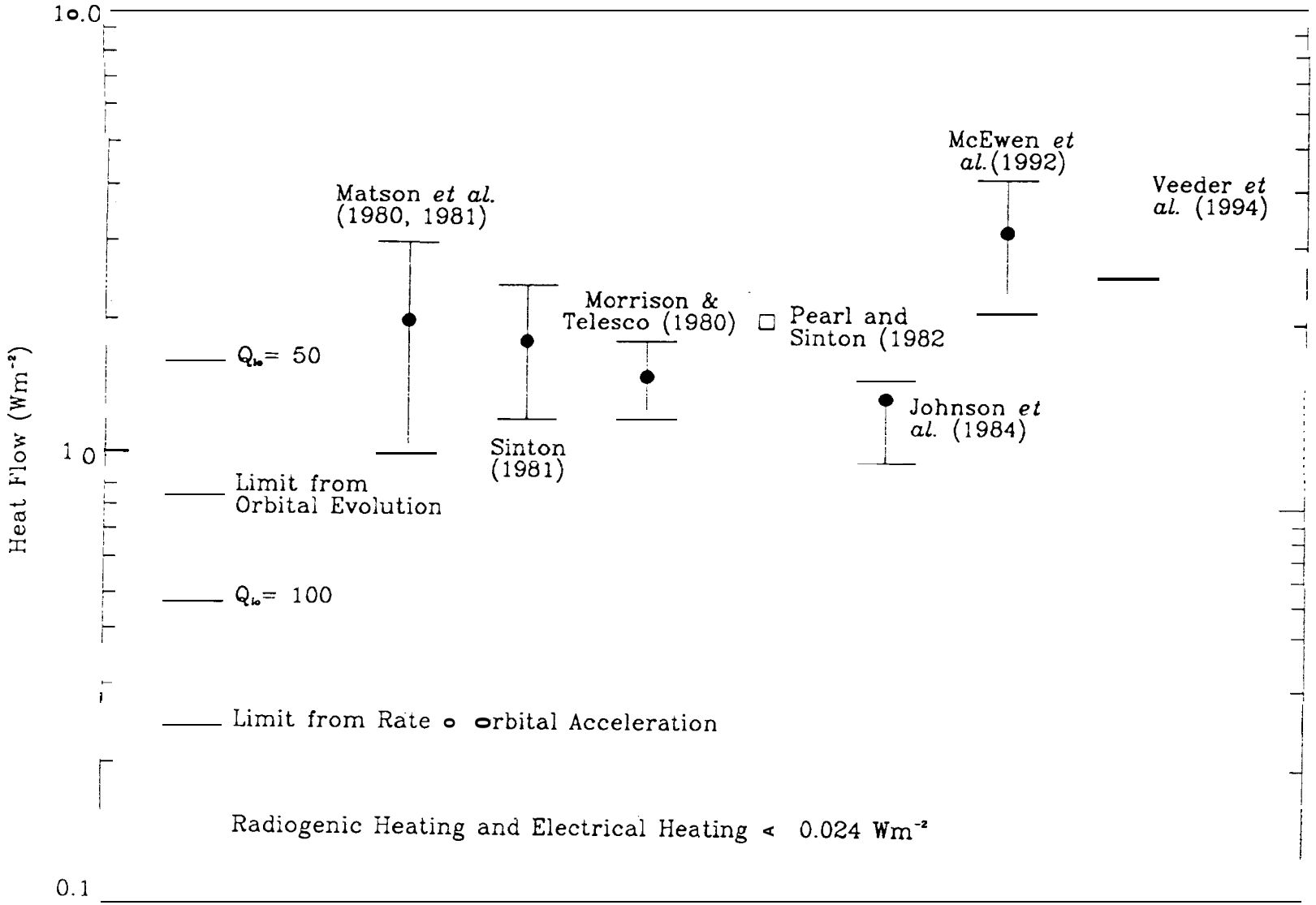
10.0
1 0
0.1
Heat Flow (Wm⁻²)
Matson et al. (1980, 1981)
Sinton (1981)
Morrison & Telesco (1980)
Pearl and Sinton (1982
McEwen et al.(1992)
Johnson et al. (1984)
Veeder et al. (1994)
Q∞= 50
Limit from Orbital Evolution
Q∞= 100
Limit from Rate o orbital Acceleration
Radiogenic Heating and Electrical Heating < 0.024 Wm⁻²

Fig. 13